

*José Carlos Guirado Moreno*

TESIS DOCTORAL

Año 2023

POLÍMEROS INTELIGENTES CON  
APLICACIÓN EN BIOMEDICINA, SEGURIDAD  
CIVIL Y CONTROL ALIMENTARIO.

**Directores:**

**Dr. José Miguel García Pérez**

**Dr. Saúl Vallejos Calzada**



**UNIVERSIDAD  
DE BURGOS**

**Departamento de Química**





## UNIVERSIDAD DE BURGOS

**Departamento de Química**

**D. José Miguel García Pérez**, Catedrático, y **D. Saúl Vallejos Calzada**, Doctor del Área de Química Orgánica del Departamento de Química de la Universidad de Burgos,

**INFORMAN:**

El trabajo que describe esta memoria, titulada **«Polímeros inteligentes con aplicación en biomedicina, seguridad civil y control alimentario»**, se ha realizado en el Departamento de Química de la Universidad de Burgos, bajo su dirección, por **D. José Carlos Guirado Moreno**, y autorizan su presentación para que sea calificada como **TESIS DOCTORAL**.

Burgos, 1 de Junio de 2023

Fdo.: Dr. José Miguel García Pérez      Fdo.: Dr. Saúl Vallejos Calzada



## **Agradecimientos**

*Me gustaría expresar mi profundo agradecimiento a todas las personas que han contribuido de manera significativa a la realización de esta tesis doctoral:*

*En primer lugar, quiero agradecer a mis directores de tesis, José Miguel García y Saúl Vallejos por su orientación, apoyo y experiencia a la hora de desarrollar este trabajo.*

*Al Ministerio de Ciencia, Innovación y Universidades por su financiación mediante la ayuda predoctoral (PRE2018-086240) con referencia del proyecto MAT2017-84501-R.*

*A todos los integrantes del Grupo de Polímeros, por vuestro apoyo y ayuda en el laboratorio tanto a nivel profesional como personal que han hecho posible la realización de este trabajo. También me gustaría agradecer al área de Nutrición y Bromatología por hacerme sentir parte del grupo.*

*A Artur J. M. Valente, a su grupo de investigación y en especial a Gianluca por acogerme y hacerme sentir como en casa durante mi estancia en Coímbra, Portugal.*

*A mi familia y amigos, por haber estado siempre a mi lado, apoyándome en los momentos más duros. A Raúl y Tomás por acogerme y conseguir que sienta el calor de un hogar en esta ciudad. A Susana, Adela y Joanmi por hacerme sentir su cariño aun estando lejos de casa. A Lara, por tu comprensión, tu ayuda y por demostrarme que siempre vas a estar presente, sin ti este camino no hubiera sido posible. A mis hermanos, Javi gracias por enseñarme que hay que luchar por lo que uno quiere y Jorge gracias por apoyarme y ayudarme en esta etapa de mi vida, dentro poco seré yo quien este viéndoos conseguir vuestros objetivos. Por último, gracias a mis padres que siempre han creído en mí y me demuestran su amor día a día.*



**RESUMEN**

<b>CAPÍTULO 1 – Introducción general</b>	<b>1</b>
1.1. <b>Antecedentes históricos de los polímeros</b>	1
1.2. <b>Aplicaciones de los polímeros</b>	3
1.2.1. Polímeros de uso general	4
1.2.2. Polímeros de ingeniería	5
1.2.3. Polímeros de alto valor añadido	7
1.3. <b>Polímeros inteligentes</b>	9
1.4. <b>Polímeros sensores colorimétricos y fluorimétricos</b>	20
1.4.1. Métodos de polimerización	20
1.4.2. Formatos de los polímeros sensores	21
1.4.3. Diseño de polímeros sensores colorimétricos y/o fluorimétricos	25
1.4.4. Estrategias para la preparación de polímeros sensores vinílicos colorimétricos y/o fluorimétricos	28
1.5. <b>Planteamiento de la investigación. Problemas detectados, soluciones propuestas</b>	28
1.5.1. Biomedicina	30
1.5.2. Seguridad civil	30
1.5.3. Control alimentario	31
1.6. <b>Objetivos</b>	32
1.7. <b>Estructura de la Memoria</b>	34
<b>CAPÍTULO 2 – Polímeros sensores en biomedicina.</b>	<b>35</b>
2.1 <b>Introducción</b>	35
2.2 <b>Biosensor polimérico para la detección de SARS-CoV-2</b>	38
2.3 <b>Resultados</b>	40
<i>Lab-on-a-chip for the easy and visual detection of SARS-CoV-2 in saliva based on sensory polymers</i>	43
<b>CAPÍTULO 3 – Polímeros reactivos en seguridad y control documental.</b>	<b>75</b>
3.1 <b>Introducción</b>	75
3.2 <b>Resultados</b>	80
<i>Chromogenic Anticounterfeit and Security Papers: An Easy and Effective Approach</i>	85

<b>CAPÍTULO 4 – Polímeros sensores en el control alimentario</b>	<b>105</b>
4.1 Introducción	105
4.2 Sensor polimérico para la detección y cuantificación de Cu(II) en muestras de vino y/o mosto	107
4.3 Sensor polimérico para la detección y cuantificación de Zn(II) en muestras de pienso animal	111
4.4 Resultados	113
<i>Democratization of copper analysis in grape must following a polymer-based lab-on-a-chip approach.</i>	117
<i>Smart sensory polymer for straightforward Zn(II) detection in pet food samples.</i>	141
<b>CONCLUSIONES Y PERSPECTIVAS</b>	<b>163</b>

---

## RESUMEN

Esta memoria describe el diseño, desarrollo y caracterización de sensores poliméricos con aplicación en biomedicina, seguridad civil y control alimentario. En el ámbito de la biomedicina, se ha llevado a cabo un sensor para el diagnóstico de Covid-19 en muestras de saliva. En seguridad civil, se han descrito polímeros inteligentes como sensores colorimétricos para la lucha contra la falsificación. En el marco del control alimentario se han desarrollado sensores poliméricos para la detección de Zn(II) y Cu(II) en piensos y mostos, respectivamente.

## ABSTRACT

This work describes the design, development, and characterization of polymeric sensors for applications in biomedicine, civil security, and food control. In biomedicine, a sensor has been developed for the diagnosis of COVID-19 in saliva samples. In civil security, intelligent polymers have been described as colorimetric sensors for anticontrol applications. Finally, in the field of food control, polymer sensors have been developed for the detection of Zn(II) in pet food and Cu(II) in grape must.

---



# CAPÍTULO 1

## Introducción general

---

Los polímeros son materiales altamente versátiles, lo que los convierte en un elemento clave en prácticamente todos los ámbitos de nuestra sociedad. A lo largo de más de 100 años de evolución, estos materiales han demostrado una capacidad sin igual para adaptarse a nuevas aplicaciones y necesidades. En el campo de la biomedicina, por ejemplo, han permitido avances significativos en la liberación controlada de fármacos, mientras que en el envasado de alimentos se han desarrollado polímeros antimicrobianos y antioxidantes de última generación. Los avances en esta área han llevado a la creación de polímeros aún más complejos, como los polímeros inteligentes, que ofrecen una multitud de posibilidades, como sensores para la detección de sustancias de interés. En este contexto, el trabajo descrito en esta memoria se centra en el desarrollo de polímeros inteligentes con aplicaciones en campos tan diversos como la biomedicina, la seguridad civil y el control de alimentos.

---

### 1.1. Antecedentes históricos de los polímeros

Los polímeros son materiales que se encuentran presentes en nuestra vida cotidiana. Muchos de los avances tecnológicos de nuestra sociedad provienen de nuevas invenciones en las que se desarrolló una nueva aplicación o se dio a conocer una propiedad de los polímeros.

Los polímeros se definen como macromoléculas que están constituidas por la repetición de distintas subunidades denominadas monómeros que se

---

## 2 | Cap. 1. Introducción general

---

encuentran enlazadas covalentemente entre sí.<sup>1,2</sup>

La historia de los polímeros comienza a principios del s. XX, momento en el cual se desarrolló el primer polímero sintético, la baquelita (sintetizada por Leo Hendrick Baekeland en 1909),<sup>3</sup> esta invención supuso el comienzo hacia el desarrollo de nuevos materiales poliméricos. Aunque, no fue hasta una década después cuando Hermann Staudinger, en 1919, sentó las bases de la polimerización, acuñando por primera vez el término macromolécula. Staudinger fue premiado con el Premio Nobel en 1953 gracias a sus investigaciones que permitieron demostrar que las propiedades de las disoluciones que contienen sustancias poliméricas se debían a la elevada masa molecular de estas. Magda Staudinger, por su parte, realizó estudios del comportamiento de macromoléculas en el ámbito biológico y fue reconocida como colaboradora cuando su marido Hermann Staudinger recibió el Premio Nobel. Además de los trabajos de Staudinger,<sup>4</sup> otros ilustres científicos como Wallace Carothers o Paul Flory realizaron novedosos trabajos en los campos de la policondensación, o en el comportamiento de las moléculas de elevada masa molecular en estado fundido o en disolución.<sup>5,6</sup> Estos avances, de gran repercusión, fueron los que en el año 1974 posicionaron a ambos investigadores para ser premiados con el Premio Nobel.

Con el tiempo, la industria fue capaz de producir polímeros a gran escala, lo que permitió su utilización en una gran variedad de campos. Por ejemplo, algunas empresas del sector alimentario sustituyeron el vidrio como material para el envasado, y empezaron a incorporar secciones de procesado de polímeros (como el poli(tereftalato de etileno), el polietileno, o el polipropileno)

---

<sup>1</sup> F. W. Billmeyer, *Textbook of polymer science*. Wiley, New York, **1984**.

<sup>2</sup> L. H. Sperling, *Introduction to Physical Polymer Science*, Wiley, New York, **2005**.

<sup>3</sup> L. H. Baekeland, *Ind. Eng. Chem.* **1909**, 1, 149-161.

<sup>4</sup> H. Staudinger, *Naturwissenschaften*, **1955**, 42, 221–230.

<sup>5</sup> W. H. Carothers, *J. Am. Soc.* **1929**, 51, 2548; *Chem. Rev.* **1931**, 8, 353; *Collected Papers of Wallace Hume Carothers on High Polymeric Substances*, H. Marck, G.S. Whitby, eds., WileyInterscience, New York, **1926**.

<sup>6</sup> P. J. Flory, *Principles of Polymer Chemistry*, Cornell University Press, **1951**.

para la producción de envases para bebidas y productos lácteos, entre otros.<sup>7</sup> La introducción de los polímeros en este sector supuso una enorme reducción en el peso de los productos, lo que a su vez ha contribuido significativamente a la disminución del consumo energético relacionado con su transporte y producción.

Los polímeros se han vuelto esenciales en una amplia variedad de aplicaciones en las últimas décadas. El PVC ha reemplazado al metal en la fabricación de tuberías, el poli(acrilato de sodio) es el material líder en la producción de pañales y artículos de higiene, mientras que los revestimientos de resinas epoxy solucionaron el problema del botulismo en las latas de conserva. Además, el uso de poliuretanos, poliamidas o poliestireno ha permitido que nuestros vehículos y hogares sean más eficientes, y más respetuosos con el medio ambiente.

En la actualidad, algunos polímeros se han convertido en materiales creados específicamente para aplicaciones altamente exigentes. Un ejemplo notorio es la poli(p-fenilen tereftalamida), conocida por su marca registrada Kevlar®, que se utiliza ampliamente en seguridad civil debido a sus excelentes propiedades mecánicas, superando incluso la tenacidad del acero.<sup>8</sup> Cabe también mencionar a los polímeros inteligentes, que son materiales de alto valor añadido que ofrecen una amplia gama de aplicaciones en diferentes campos.

## 1.2. Aplicaciones de los polímeros

Los materiales poliméricos son un campo de investigación que se mantiene muy activo, y desde el 2015 se han publicado más de 100.000 artículos científicos al año (**Figura 1**). Además, desde el punto de vista de la aplicación práctica, los polímeros pueden clasificarse en función de su uso cotidiano, su empleo como polímeros de ingeniería o su aplicación como polímeros de alto valor añadido.

<sup>7</sup> V. Siracusa, P. Rocculi, S. Romani, M. Dalla Rosa, *Trends Food Sci. Technol.* **2008**, 19, 634-643.

<sup>8</sup> M. Trigo-López, J.M. García, J.A.R. Ruiz, F.C. García, R. Ferrer, Aromatic Polyamides, in: *Encycl. Polym. Sci. Technol.*, John Wiley & Sons, New York, **2018**: pp. 1–51.

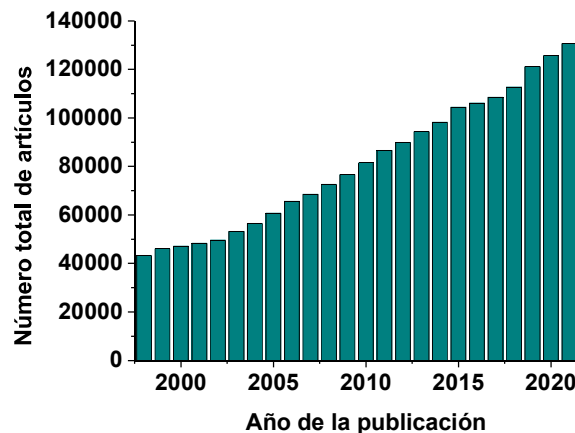


**Figura 1.** Evolución del número total de publicaciones relativas a la ciencia de los polímeros de los últimos 25 años. (Fuente: Web of Science, criterios de búsqueda: «polymer\*» en el título del artículo).

### 1.2.1. Polímeros de uso general

Los hábitos de la sociedad son cambiantes, y parte de estos cambios fueron provocados por la evolución de los polímeros, ya que a medida que se iban desarrollando fueron sustituyendo a los materiales tradicionales. Los polímeros de uso general tienen un intervalo de propiedades amplio que los hacen ideales para multitud de aplicaciones como en el embalaje, envasado o como materiales de construcción, entre muchas otras.

Existen numerosos ejemplos de polímeros de uso común relevantes, entre los que destacan el polietileno, el polipropileno, el policloruro de vinilo, el poli(tereftalato de etileno) y el poliestireno. El polietileno es un polímero semicristalino que se encuentra en diferentes morfologías y se utiliza comúnmente en la fabricación de botellas de plástico, juguetes, contenedores químicos y tuberías.<sup>9,10</sup> El polipropileno, también semicristalino, se utiliza en envases, fibras y recipientes, gracias a su gran resistencia a la tensión y su

<sup>9</sup> L.A. Pruitt, *Load-Bearing Medical Polymers, Compr. Biomater. II*, Elsevier, Oxford, 2017.

<sup>10</sup> S.K. Sen, S. Raut, *J. Environ. Chem. Eng.* **2015**, 3, 462–473.

ligereza.<sup>11</sup> El poli(tereftalato de etileno),<sup>12</sup> otro polímero semicristalino, se utiliza en la fabricación de botellas y también en el sector de la automoción, además de en la industria textil. El poliestireno, por su parte, se utiliza como material amorfó en la construcción y en componentes plásticos de frigoríficos, impresoras y juguetes, por ejemplo.<sup>13</sup> Por último, el policloruro de vinilo es un polímero amorfó que se utiliza, por ejemplo, en la construcción y en la industria médica para materiales de diálisis y blísteres de fármacos.<sup>14</sup>

### 1.2.2. Polímeros de ingeniería

Se denominan polímeros de ingeniería al grupo de polímeros con capacidad de mantener su estabilidad dimensional, mecánica y química cuando las condiciones del entorno son exigentes como, por ejemplo, frente a temperaturas mayores de 100 °C y menores de 0 °C, ambiente corrosivo o elevada presión.<sup>15</sup> El desarrollo de este tipo de polímeros se incrementó después de la segunda guerra mundial, debido a que los materiales existentes no cubrían las necesidades del momento y también por problemas de suministro. Estas problemáticas provocaron un aumento en el interés y en la investigación de nuevos materiales para armamento y en la carrera espacial en la mejora de aeronaves.<sup>16</sup> Al considerar las motivaciones que impulsan el desarrollo de este tipo de materiales, se comprende que las primeras aplicaciones de estos materiales fueran en el sector aeroespacial, el cual catalizó indirectamente mejoras en la industria automotriz y, finalmente, en el sector textil.

Para el desarrollo de material de seguridad en el sector textil, se impulsó la investigación en fibras poliméricas con elevada resistencia mecánica y térmicas. Este desarrollo comenzó a finales de la década de 1930 cuando se

---

<sup>11</sup> J. W. Nicholson, *Chemistry of Polymers*, The Royal Society of Chemistry, **2006**.

<sup>12</sup> D.E. Nikles, M.S. Farahat, *Macromol Mater Eng.* **2005**, 290, 13–30.

<sup>13</sup> C. V Vo, F. Bunge, J. Duffy, L. Hood, *Cell. Polym.* **2011**, 30, 137–156.

<sup>14</sup> R.O. Olekhovich, *Fibers.* **2021**, 9, 12.

<sup>15</sup> A.C. de Leon, Q. Chen, N.B. Palaganas, J.O. Palaganas, J. Manapat, R.C. Advincula, *React. Funct. Polym.* **2016**, 103, 141–155.

<sup>16</sup> H. Dodiuk, *Research and development of high-performance polymeric materials including polyimides and fluoro-polyimides and their industrialized products*, in: *Handb. Thermoset Plast.* William Andrew Publishing, Boston, **2022**.

sintetizó por primera vez la poliamida 6.6 en forma de fibra (Nylon 6.6®). Este material tiene unas excelentes propiedades mecánicas por lo que se utiliza en la fabricación de ropa o de hilos de pescar. El nylon fue un buen punto de partida para que más adelante, a mediados de la década de 1960, se desarrollaran las aramidas, que son poliamidas aromáticas que se utilizaron para la obtención de fibras con elevada resistencia mecánica, térmica y química. Más concretamente, se desarrollaron la poli(*m*-fenilen tereftalamida) y la poli(*p*-fenilen tereftalamida), conocidas por sus nombres comerciales Nomex® y Kevlar®, respectivamente. La estructura química de ambos compuestos (**Figura 2**) es muy similar, aunque en el Kevlar® al tener una distribución 1-4, las cadenas se encuentran alineadas, lo que provoca una mayor resistencia a la tracción que en el Nomex®, razón por la que suele utilizarse para la fabricación de chalecos antibalas. En cambio, El Nomex® presenta mejores propiedades térmicas, por lo que se utiliza en la fabricación de material altamente resistente al fuego, como los uniformes de bomberos. Además, ambos polímeros tienen aplicación en automoción, infraestructuras o la industria aeroespacial.<sup>17</sup>

Otro ejemplo de materiales poliméricos de ingeniería son los policarbonatos. Estos polímeros se caracterizan por sus extraordinarias propiedades ópticas, y su elevada resistencia a la tracción, a los impactos y a la temperatura.<sup>18</sup> Estas propiedades hacen que los policarbonatos tengan importantes aplicaciones en automoción, en construcción o en el desarrollo de materiales de seguridad como cascos.<sup>19</sup> Por otro lado, el politetrafluoroetileno, más conocido por su nombre comercial Teflón®, presenta una alta resistencia a la temperatura, a la adherencia y a la corrosión, propiedades que lo hacen ideal para su aplicación en revestimientos antiadherentes, en el desarrollo de juntas o en aplicaciones médicas, como por ejemplo, en implantes.<sup>20</sup> Otros polímeros que destacan en este campo son las poliimidas (protagonistas en el campo de la electrónica o la industria automotriz), las poliariletercetonas (utilizadas

<sup>17</sup> B. Yang, L. Wang, M. Zhang, J. Luo, Z. Lu, X. Ding, *Adv. Funct. Mater.* **2020**, 30, 2000186.

<sup>18</sup> A. Davis, J.H. Golden, *J. Macromol. Sci. Part C* **1969**, 3, 49–68.

<sup>19</sup> J. Feng, R.-X. Zhuo, X.-Z. Zhang, *Prog. Polym. Sci.* **2012**, 37, 211–236.

<sup>20</sup> E. Dhanumalayan, G.M. Joshi, *Adv. Compos. Hybrid Mater.* **2018** 1, 247–268.

ampliamente en la industria aeroespacial) o las polisulfonas (especialmente en sectores relacionados con la industria médica).<sup>21</sup>

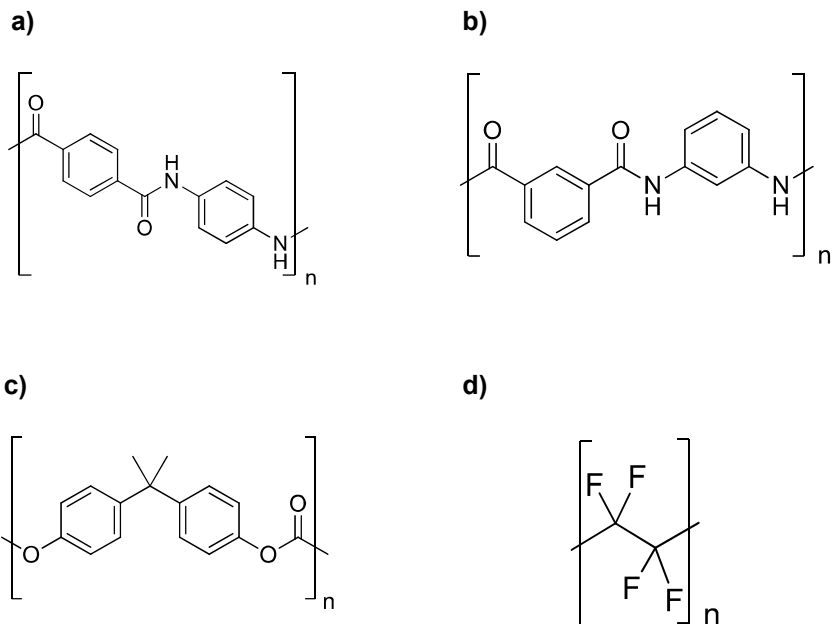


**Figura 2.** Estructuras químicas de: a) Kevlar®; b) Nomex®; c) Polícarbonato formado a partir de bisfenol-A; y d) Teflón®.

### 1.2.3. Polímeros de alto valor añadido

Los polímeros de alto valor añadido son aquellos que se diseñan para una aplicación o finalidad específica y, por eso, su producción anual a nivel mundial es inferior a 1000 toneladas. Entre este tipo de polímeros, destacan los polímeros conductores, antimicrobianos, antioxidantes, inteligentes y los biopolímeros, que se utilizan en aplicaciones como la biomedicina,<sup>22</sup> o en el desarrollo de envases funcionales en la industria alimentaria.<sup>23, 24</sup>

<sup>21</sup> A. Rusli, M.B.H. Othman, K.I. Ku Marsilla, *Plastics in High Heat Resistant Applications, Encycl. Mater. Plast. Polym.*, Elsevier, Oxford, 2022.

<sup>22</sup> R. Rebelo, M. Fernandes, R. Fangueiro, *Procedia Eng.* **2017**, 200, 236–243.

<sup>23</sup> A.M. Díez-Pascual, , *Polymers*. **2020**, 12, 731.

<sup>24</sup> J. Gómez-Estaca, C. López-de-Dicastro, P. Hernández-Muñoz, R. Catalá, R. Gavara, *Trends Food Sci. Technol.* **2014**, 35, 42–51.

Los polímeros conductores son materiales esenciales en la actualidad, impulsados por el crecimiento exponencial de los dispositivos móviles en las últimas dos décadas. Gracias a su estructura química, basada en sistemas conjugados, tienen la capacidad de conducir la electricidad y se han convertido en objeto de gran interés para la investigación y la industria electrónica. Desde la famosa serendipia del poliacetileno como el primer polímero sintético conductor,<sup>25</sup> estos materiales se han establecido como componentes clave en la fabricación de dispositivos solares, baterías y supercondensadores, electrónica flexible y pantallas táctiles.<sup>26</sup>

Otro tipo de polímeros de alto valor añadido son los polímeros inteligentes, que poseen la capacidad de responder con una señal o acción específica ante un estímulo en su entorno, como cambios en la radiación, pH, presión, temperatura o la presencia de analitos específicos.<sup>27</sup> Las aplicaciones de este tipo de materiales van desde la liberación controlada de fármacos, o la regeneración de tejidos,<sup>28,29</sup> hasta el desarrollo de materiales fotodegradables.<sup>30</sup> Además, existen polímeros inteligentes que reaccionan selectivamente frente a un analito concreto (estímulo químico y/o biológico)<sup>31,32</sup> como, por ejemplo, la presencia de metales pesados,<sup>33</sup> moléculas orgánicas<sup>34,35</sup> o incluso virus o bacterias.<sup>36</sup> Esta tesis está relacionada con el desarrollo de este tipo de

- 
- <sup>25</sup> H. Shirakawa, E.J. Louis, A.G. MacDiarmid, C.K. Chiang, A.J. Heeger, *J. Chem. Soc. Chem. Comm.* **1977**, 578–580.
- <sup>26</sup> T.K. Das, S. Prusty, *Polym. Plast. Technol. Eng.* **2012**, 51, 1487–1500.
- <sup>27</sup> J. M. García, F. García, J. Reglero Ruiz, S. Vallejos, M. Trigo-López., *Smart Polymers: Principles and Applications*, De Gruyter, Berlin, Boston, **2022**.
- <sup>28</sup> X. Xiong, A. del Campo, J. Cui, *Smart Polym. Their Appl.* (Second Edition), Woodhead Publishing, Cambridge, **2019**.
- <sup>29</sup> M. V Pereira, A.C. Marques, D. Oliveira, R. Martins, F.T.C. Moreira, M.G.F. Sales, E. Fortunato, *ACS Omega*. **2020**, 5, 12057–12066.
- <sup>30</sup> O. Bertrand, J.-F. Gohy, *Polym. Chem.* **2017**, 8, 52–73.
- <sup>31</sup> J.M. García, J.L. Pablos, F.C. García, F. Serna, *Sensory Polymers for Detecting Explosives and Chemical Warfare Agents, Ind. Appl. Intell. Polym. Coatings*, Springer International Publishing, Cham, **2016**.
- <sup>32</sup> S. Vallejos, M. Trigo-López, A. Arnaiz, A. Miguel, A. Muñoz, A. Mendía, *Polymers*. **2022**, 14, 4954.
- <sup>33</sup> S. Vallejos, A. Muñoz, S. Ibeas, F. Serna, F. C. García, J.M. García, *J. Mater. Chem. A*. **2013**, 1, 15435–15441.
- <sup>34</sup> S. E. Bustamante Fonseca, B. L. Rivas, J. M. García Pérez, S. Vallejos, F. C. García, *J. Appl. Polym. Sci.* **2018**, 135, 46185.
- <sup>35</sup> B. Selvakumar, A. Kathiravan, *Talanta*. **2021**, 235, 122733.
- <sup>36</sup> K. Lee, L.K. Povlich, J. Kim, *Analyst*. **2010**, 135, 2179–2189.

materiales y, en concreto, se enfoca hacia el diseño, síntesis y caracterización de polímeros inteligentes con aplicaciones en biomedicina, seguridad civil y control alimentario.

### 1.3. Polímeros inteligentes

A lo largo de los últimos cien años, aproximadamente, los polímeros han experimentado un crecimiento exponencial en cuanto a la complejidad de su estructura, diseño y aplicaciones. Este desarrollo ha convertido a la versatilidad en una de las características más importantes de los polímeros y ha dado lugar a nuevos avances en el campo de los denominados «polímeros inteligentes» o «*smart polymers*». Estos materiales se pueden clasificar en función del estímulo al que responden, del mecanismo a través del que se genera la respuesta y del tipo de respuesta que presentan (**Figura 3**):



**Figura 3.** Clasificación de los polímeros inteligentes en función del estímulo, el mecanismo que tiene lugar y la respuesta generada.

Atendiendo al tipo de **estímulo**, se diferencian dos grupos de polímeros inteligentes:

- **Estímulos químicos o biológicos:** este tipo de estímulos pueden ser moléculas discretas (en cualquiera de los estados de la materia, es decir,

en forma gaseosa, líquida o sólida), macromoléculas (enzimas, proteínas, etc.), o incluso microorganismos, como virus o bacterias. A estos estímulos se los conoce comúnmente como «dianas», que generalmente están asociados a un problema concreto, y que puede abarcar desde la cuantificación de un metal pesado en aguas de consumo, a la detección de un patógeno en saliva.

- **Estímulos físicos:** existen distintos tipos de estímulos físicos, entre los que destacan la presión (algunos polímeros son piezoelectrónicos por lo que generan una carga eléctrica en respuesta a cambios de presión, lo que les hace útiles como sensores de presión), la temperatura (tienen relevancia tanto en la fabricación de adhesivos como en sistemas de liberación de fármacos) o la luz (dan lugar a los polímeros fotosensibles, los cuales pueden cambiar de forma o degradarse según la radiación que se les irradie), entre otros.

En cuanto a la clasificación de los polímeros inteligentes en función del **mecanismo de interacción**, se diferencian dos grandes grupos, los gobernados por procesos reversibles, y los gobernados por procesos irreversibles. Cada uno de esos procesos viene definido por la naturaleza de la interacción provocada por los estímulos a los receptores. Estos últimos son la parte del polímero capaz de llevar a cabo el reconocimiento molecular o el cambio provocado por un estímulo físico. Los receptores pueden ser simples grupos funcionales, modificaciones de las cadenas laterales del polímero, cadenas peptídicas, etc.

Seguidamente, se detallan las interacciones reversibles de los polímeros sensores según el tipo de mecanismo que presenta:

- **Procesos de desplazamiento:** el receptor del polímero contiene una especie (indicador, medicamento, etc.) que se libera al medio cuando transcurre la interacción con el estímulo. En el caso de un estímulo químico, se puede liberar un analito que actúe como indicador, como ocurre en los ensayos por desplazamiento del indicador (IDAs, de sus siglas en inglés). Por otra parte, en el caso de un estímulo físico, como

la temperatura, esta puede provocar la ruptura de un enlace liberando, por ejemplo, un fármaco como ocurre en los sistemas de liberación de fármacos (DDS, de sus siglas en inglés).

- **Polímeros de impresión molecular (MIPs, de sus siglas en inglés):** estos polímeros presentan una Interacción selectiva causada por «huecos» en el polímero. Estos «huecos» se generan a través de la polimerización del polímero en presencia del analito que posteriormente se elimina.
- **Formación de complejos organometálicos:** interacción reversible que tiene lugar entre los receptores del polímero inteligente y un catión metálico.
- **Procesos electroquímicos:** interacción entre el receptor y el analito que produce una alteración de las propiedades eléctricas del polímero inteligente.

Por lo otro lado, los mecanismos que gobiernan las interacciones irreversibles de los polímeros inteligentes son los siguientes:

- **Polidosímetros:** en este tipo de polímero inteligente se engloban todas las interacciones irreversibles que tienen lugar entre el receptor y el analito. Durante esta interacción se produce una modificación estructural en el polímero inteligente, la cual se traduce en un cambio a nivel macroscópico medible.
- **Polímeros basados en sistemas de transmisión de energía de resonancia de Förster (FRET, de sus siglas en inglés):** estos sistemas contienen un fluoróforo o cromóforo (donador) y, a su vez, un amortiguador «quencher» (aceptor) que hace que el sistema no emita radiación. En presencia de un analito concreto, el sistema FRET se fragmenta lo que provoca un cambio a nivel visual.

La **Tabla 1** muestra esquemáticamente los tipos de mecanismo de interacción

---

de los polímeros inteligentes.

Por último, los polímeros inteligentes también se pueden clasificar en función del **tipo de respuesta** que genera el polímero inteligente, de esta manera se pueden dividir en:

- **Polímeros reactivos:** son polímeros inteligentes que frente a un estímulo externo generan una acción, por lo que se podrían denominar también actuadores basados en polímeros. Un ejemplo de ello es el ácido poliacrílico, el cual exhibe un comportamiento sensible al pH debido a la ionización de su grupo ácido carboxílico en solución acuosa. Por encima de un valor de pH de 4,25 el ácido poliacrílico se encuentra en su forma ionizada, lo que resulta en una fuerte repulsión electrostática entre las cadenas del polímero que da lugar a cambios significativos en sus propiedades físicas y químicas. Es decir, el poliácido acrílico es un polímero reactivo frente al pH ya que su hidrofilia se modifica drásticamente.<sup>37</sup>
- **Polímeros sensores:** son aquellos polímeros inteligentes que responden frente a un estímulo concreto con una alerta en forma de cambio de color,<sup>38</sup> de fluorescencia<sup>39</sup> o de alguna propiedad electroquímica.<sup>40,41</sup> Estas alertas son reacción directa de la interacción entre la especie objetivo y los receptores, y se pueden registrar con equipos como fluorímetro, espectrofotómetros de UV-visible, etc. Este tipo de polímeros inteligentes presentan en su estructura un componente adicional con respecto a los polímeros reactivos, que es la unidad o subunidad indicadora, la cual tiene como función emitir una señal cuando se haya producido la interacción.<sup>42</sup> Estos materiales se aplican en

---

<sup>37</sup> R. Brighenti, Y. Li, F.J. Vernerey, *Front. Mater.* **2020**, 7, 1–18.

<sup>38</sup> S. Seo, J. Lee, M.S. Kwon, D. Seo, J. Kim, *ACS Appl. Mater. Interfaces.* **2015**, 7, 20342–20348.

<sup>39</sup> Q. Xu, S. Lee, Y. Cho, M.H. Kim, *J. Am. Chem. Soc.* **2013** 135, 47, 17751–17754.

<sup>40</sup> A.R. Hanze, T.W. Conger, E.C. Wise, D.I. Weisblat, *J. Am. Chem. Soc.* **1946**, 68, 1389–1392.

<sup>41</sup> Z.J. Li, D. Zhang, K.R. Wu, *Mater. Struct. Constr.* **2001**, 34, 506–512.

<sup>42</sup> M. Y. Chae, A. W. Czarnik, *J. Am. Chem. Soc.* **1992**, 114, 9704.

campos científicos muy diferentes, como la ciencia y tecnología de alimentos,<sup>43</sup> la biomedicina<sup>44</sup> o el control medioambiental.<sup>45,46</sup>

Los polímeros sensores pueden confundirse con las sondas colorimétricas y/o fluorimétrica convencionales, basadas en moléculas discretas. Sin embargo, los polímeros sensores presentan varias ventajas en comparación con estos:<sup>47</sup>

- Las cadenas poliméricas generan un entorno de protección en el que los receptores reaccionan con las especies objetivo de forma más eficaz, tal y como se ha demostrado en diferentes estudios.<sup>48,49,50</sup>
- Las sondas convencionales son generalmente moléculas orgánicas, y su uso como sensores se ve limitado a la utilización de disolventes orgánicos. Los polímeros sensores pueden diseñarse para su utilización en cualquier medio líquido (acuoso, orgánico, o mezclas de ambos), incluso en fase gas.
- No requieren de personal especializado para el análisis.
- Suponen una disminución y/o eliminación del manejo de reactivos, disolventes y equipos de protección individual (EPIs).
- Permiten realizar ensayos *in situ* de forma más simple mediante el uso de sondas sólidas tipo film.<sup>51</sup>

<sup>43</sup> L. Gonzalez-Ceballos, J.C. Guirado-moreno, M. Guembe-garcía, J. Rovira, B. Melero, A. Arnaiz, A. María, M. García, S. Vallejos, *Food Packag. Shelf Life.* **2022**, 33, 100910.

<sup>44</sup> M.Guembe-García, S. Vallejos, I. Carreira-Barral, S. Ibeas, F. C. García, V. Santaolalla-García, J.M. García, *React. Funct. Polym.* **2020**, 154, 104685.

<sup>45</sup> H. El Kaoutit, P. Estévez, F.C. García, F. Serna, J.M. García, *Anal. Methods.* **2013**, *5*, 54–58.

<sup>46</sup> M. Trigo-López, A. Muñoz, S. Ibeas, F.C. García, F. Serna, J.M. García, *Sens. Actuators B Chem.* **2014**, 191, 233–238.

<sup>47</sup> V. Dujols, F. Ford, A. W. Czamik, *J. Am. Chem. Soc.* **1997**, 119, 7386.

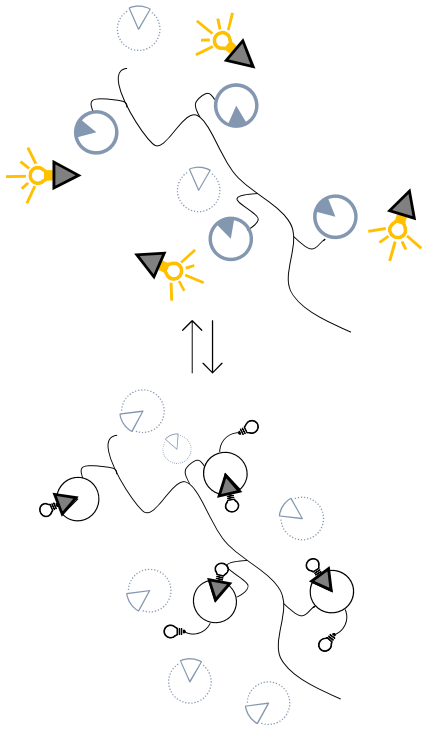
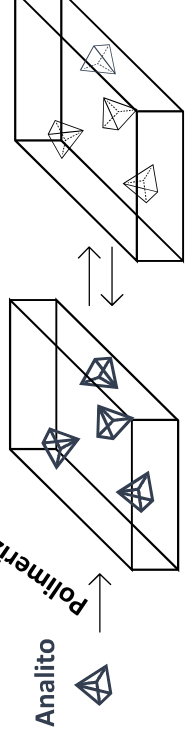
<sup>48</sup> A. Arnaiz, M. Guembe-García, E. Delgado-Pinar, A.J.M. Valente, S. Ibeas, J.M. García, S. Vallejos, *Sci. Rep.* **2022**, 12, 1–12.

<sup>49</sup> S.E. Bustamante, S. Vallejos, B.S. Pascual-Portal, A. Muñoz, A. Mendia, B.L. Rivas, F.C. García, J.M. García, *J. Hazard. Mater.* **2019**, 365, 725–732.

<sup>50</sup> M. Guembe-García, P.D. Peredo-Guzmán, V. Santaolalla-García, N. Moradillo-Renuncio, S. Ibeas, A. Mendia, F.C. García, J.M. García, S. Vallejos, *Polymers.* **2020**, 12, 1249.

<sup>51</sup> S. Vallejos, P. Estévez, F.C. García, F. Serna, J. L. De Peña, J.M. García, *Chem. Comm.* **2010**, 46, 7951–7953.

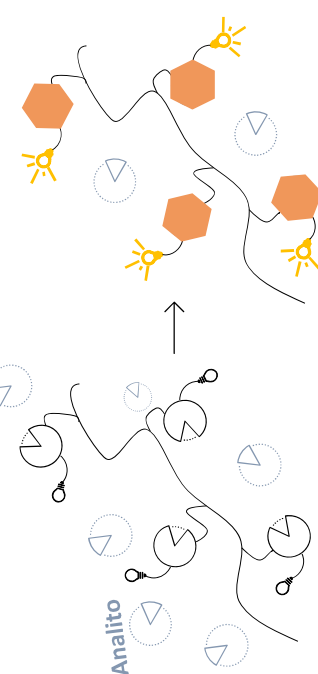
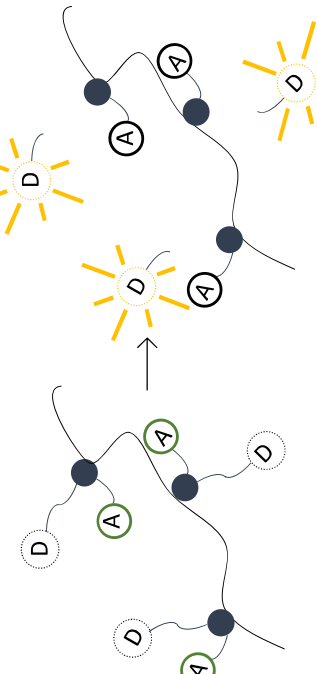
**Tabla 1.** Tipos de mecanismos de interacción de los polímeros inteligentes.

Proceso	Tipo	Esquema
Reversible	IDAs	 <p>Diagram illustrating a reversible interaction mechanism (IDA) involving a polymer chain with photochromic groups (represented by circles with arrows) and guest molecules (represented by triangles). The process shows reversible binding and release between the polymer and the guest molecules.</p>
Reversible	MIPs	 <p>Diagram illustrating a reversible interaction mechanism (MIP) involving a polymer network. The network consists of polymer chains (represented by triangles) cross-linked by functional groups (represented by circles). Guest molecules (represented by triangles) are shown interacting with the polymer chains. An arrow labeled "Análito" points to one of the guest molecules, and an arrow labeled "Polimerización" points to the polymer network.</p>

**Continuación de la tabla 1.** Tipos de mecanismos de interacción de los polímeros inteligentes.

Proceso	Tipo	Esquema
<b>Reversible</b>	Formación de complejos	<p>Diagram illustrating the reversible formation of complexes between receptors and analytes. On the left, a receptor (represented by a circle with a lightning bolt) and an analyte (represented by a circle with a triangle) are shown. An arrow points from the receptor to the analyte, indicating their interaction. On the right, the resulting complex is shown, consisting of the receptor and analyte joined together. A double-headed arrow indicates the reversible nature of this interaction.</p>
<b>Reversible</b>	Procesos electroquímicos	<p>Diagram illustrating reversible electrochemical processes. It shows a receptor (circle with lightning bolt), an analyte (circle with triangle), and an electrode (rectangular box). The receptor and analyte are connected to the electrode. A double-headed arrow labeled <math>\Delta V</math> indicates the reversible nature of the process. The electrode is labeled "Electrodo".</p>

**Continuación de la tabla 1.** Tipos de mecanismos de interacción de los polímeros inteligentes.

Proceso	Tipo	Esquema
<b>Irreversible</b>	Polidosímetros	 <p>Receptor Analito</p>
<b>Irreversible</b>	Polímeros basados en sistemas FRET	 <p>Polímeros basados en sistemas FRET</p>

Los estudios llevados a cabo para la realización de esta tesis doctoral se basan en polímeros inteligentes, concretamente polímeros sensores colorimétricos o fluorimétricos que responden a estímulos químicos y/o biológicos a través de mecanismos de formación de complejos, polidosímetros o sistemas FRET.

Estos dos tipos de polímeros sensores (colorimétricos y fluorimétricos) permiten realizar determinaciones semicuantitativas *in situ* a través de un análisis visual del color (como en las tiras reactivas de pH), y determinaciones cuantitativas utilizando espectrofotómetros de UV-visible y/o fluorímetro. Además, en los últimos años, ha surgido una nueva alternativa impulsada por el implacable crecimiento de los teléfonos inteligentes, y que se resume en la toma de imágenes con la cámara del terminal, seguida del análisis de color digital con diferentes aplicaciones. Esta opción prescinde del uso de equipo sofisticado y no requiere habilidades técnicas para realizar el análisis, ya que los teléfonos móviles están completamente integrados en todas las capas sociales, sin importar la edad o el nivel de formación de los usuarios.

El color de las fotografías digitales se basa en un espacio de color, como por el ejemplo el espacio de color RGB (de sus siglas en inglés rojo, *red* (R), verde, *green* (G) y azul, *blue* (B)).<sup>52,53</sup> Estos espacios definen cada color a través de coordenadas, al igual que un lugar es localizado en un mapa. Por lo tanto, cualquier variación, por pequeña que sea, en alguna de las coordenadas RGB implica un color diferente. Existen más espacios de color además del RGB, y como se observa en la **Figura 4**, y cada uno de ellos presenta una forma diferente (cúbico, esférico, cónico, etc.), dónde los colores se definen por las coordenadas con las que se construye cada espacio. Por ejemplo, en el espacio de color RGB, cada parámetro presenta un rango de 0 hasta 255. Por el contrario, el espacio HSV (de sus siglas en inglés matiz, *hue* (H), saturación, *saturation* (S) y brillo, *value* (V)) utiliza los ejes de brillo y saturación en rangos

<sup>52</sup> S. Vallejos, A. Muñoz, F. C. García, R. Colleoni, R. Biesuz, G. Alberti, J. M. García, *Sens. Actuators B Chem.* **2016**, 233, 120-126.

<sup>53</sup> Y. Fan, J. Li, Y. Guo, L. Xie, G. Zhang, *Measurement*. **2021**, 171, 108829.

de 0 a 1, es decir, tanto por uno de dicho valor. En cambio, el matiz también tiene un rango de 0 a 1 que proviene de la normalización del ángulo que indica el color.<sup>54</sup> Finalmente, otro de los espacios de color más utilizados es el CIE-LAB (Comisión Internacional de la Iluminación; del francés *Commission Internationale d'Éclairage*, LAB). El espacio de color CIELAB fue desarrollado en 1976 como parte del sistema de representación del color por parte de la Comisión Internacional de Iluminación (CIE).

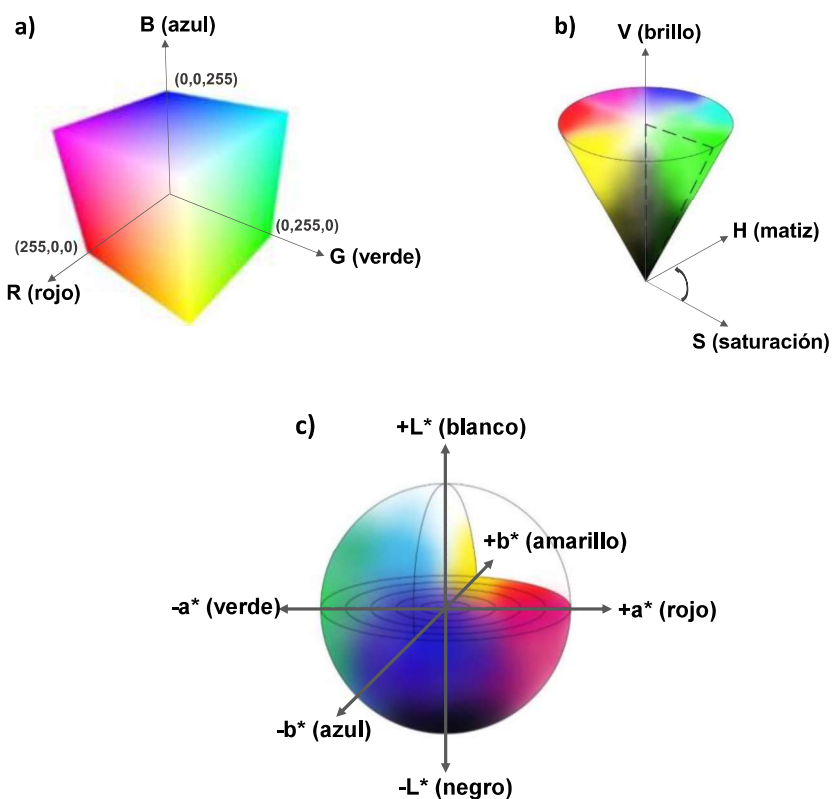


**Figura 4.** Representación de las coordenadas de los espacios de color: a) RGB; b) HSV; y c) CIE-LAB.

En definitiva, los espacios de color permiten transformar una percepción sensorial como el color, en uno o varios números (coordenadas). De esta forma,

<sup>54</sup> P.D. Pawar, S.B. Kale, *Int. J. Sci. Res.* **2014**, 3, 132–137.

si un polímero sensor emite un color verde en presencia de un analito, y es cada vez más verde cuanto más alta es la concentración del analito, se puede representar la variable «G» del espacio de color RGB frente a la concentración del analito y obtener una curva o recta de calibrado. En ocasiones, los colores estudiados no son solo verdes, o solo rojos, sino que las 3 variables RGB ponderan de forma representativa. En estos casos, el número de variables de puede simplificar, y se pueden agrupar en una sola variable a través de un análisis multivariante de componentes principales. Si, además, el método se valida con un método alternativo de referencia, se pueden comparar ambos métodos y determinar si se trata de métodos significativamente diferentes o no (**Figura 5**).

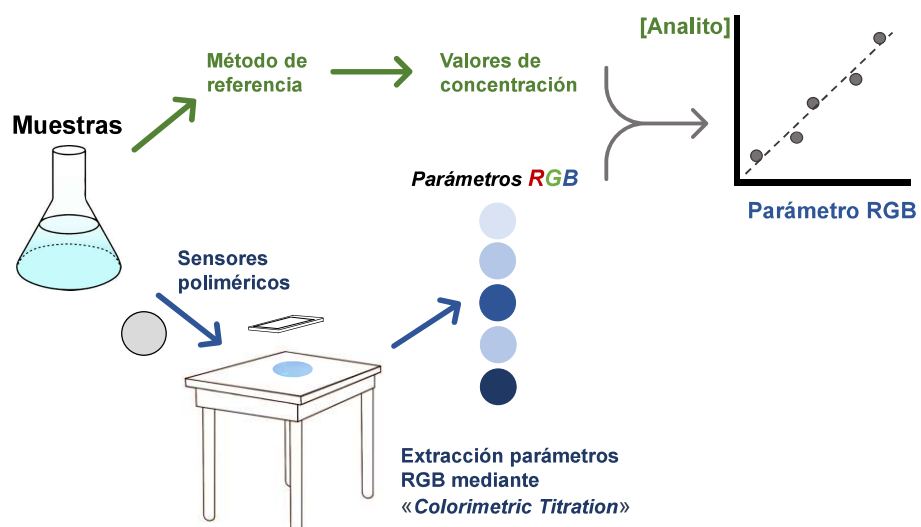


**Figura 5.** Proceso esquemático del método de validación para la detección y determinación de un analito de interés a través del uso de sensores poliméricos colorimétricos o fluorescentes.

Tal es la importancia de este método para el Grupo de Polímeros de la Universidad de Burgos que se decidió desarrollar una aplicación denominada «Colorimetric Titration» para el análisis del color a través de los espacios de color

RGB y HSV.<sup>55,56</sup> Esta aplicación analiza cual es el parámetro que mejor se correlaciona con el cambio de color o fluorescencia que se produce en el polímero sensor.

## 1.4. Polímeros sensores colorimétricos y fluorimétricos

Al emprender la síntesis de un nuevo sensor polimérico, el diseño estructural y las propiedades fisicoquímicas del polímero se encuentran predeterminados por las exigencias específicas de su uso o aplicación final. Por ejemplo, si se requiere un uso en solución, se recomienda utilizar un polímero lineal de baja masa molecular, ya que generalmente suelen ser más solubles. Por el contrario, si el uso final impide el uso de disolventes, un film entrecruzado es una alternativa más adecuada. A continuación, se describen brevemente los métodos de polimerización, formatos y propiedades finales a tener en cuenta a la hora de preparar polímeros sensores.

### 1.4.1. Métodos de polimerización

Los polímeros sensores se llevan a cabo mediante métodos de polimerización convencionales. Los métodos más habituales para el desarrollo de polímeros sensores son la poliadición y la policondensación:

- **Polímeros de adición:** son polímeros que se forman a partir de polimerizaciones en cadena. Este tipo de polimerización requiere de un iniciador, el cual provoca la formación de una especie reactiva que desencadena la formación del polímero. Es decir, los monómeros no presentan grupos funcionales que reaccionen entre sí para dar lugar a la polimerización sin la presencia del iniciador. Esta polimerización presenta 3 etapas (iniciación, propagación y terminación), a su vez, según el tipo de iniciador se realizan polimerizaciones radicalarias

---

<sup>55</sup> S. Vallejos, M. Guembe García, J.M. García Perez, C. Represa Perez, F.C. García García, Colorimetric Titration on the App Store, 2021. <https://apps.apple.com/si/app/colorimetric-titration/id1533793244> (Accedido en 15 de Febrero de 2023).

<sup>56</sup> S. Vallejos, M. Guembe García, J.M. García Perez, C. Represa Perez, F.C. García García, Application for smartphones “Colorimetric Titration”. Software registration BU-122-20 (00/2021/568), 2021. <https://play.google.com/store/apps/details?id=es.inforapps.chameleon&gl=ES> (Accedido en 15 de Febrero de 2023).

---

(térmicas, fotoquímicas o redox) e iónicas (catiónica y aniónica).

- **Polímeros de condensación:** los monómeros que dan lugar a polímeros de condensación presentan grupos funcionales en su estructura que reaccionan entre sí para dar lugar al polímero final. Existen numerosas reacciones químicas entre monómeros que producen polímeros de condensación, como la formación de ésteres o amidas, entre otras. Este tipo de polímeros tienen en común que se producen mediante una polimerización por etapas junto con la liberación de una molécula pequeña (normalmente agua) por cada paso de reacción.

Los polímeros sintetizados para la realización de este trabajo son polímeros de adición que se han obtenido mediante métodos de polimerización radicalarios con iniciador térmico

#### 1.4.2. Formatos de los polímeros sensores

Existen diversos formatos en los que se preparan los polímeros sensores que permiten una adaptación específica al objetivo para el que se sintetiza dicho sensor. Dos formatos especialmente adecuados para el desarrollo de estos polímeros debido a sus ventajas en comparación con las sondas colorimétricas convencionales son los films y los recubrimientos.

Los films son una estructura polimérica formada por una sola capa continua y delgada (normalmente hasta 200 µm de espesor).<sup>57</sup> Pueden estar entrecruzados si contienen un reticulante en su estructura. Mediante este entrecruzamiento se obtienen materiales que se pueden utilizar en medios orgánicos y acuosos sin que se disuelvan. Existen múltiples metodologías para obtener un film como, por ejemplo, mediante:

- **Polimerización en bloque:** es un método de obtención de films a partir de la inyección de los monómeros y el iniciador en un molde. En este método el control del grosor del film viene definido por el molde utilizado.

<sup>57</sup> J.G. Drobny, *Applications of Fluoropolymer Films*, William Andrew, Norwich, 2020.

Si se introduce un monómero reticulante en la formulación se obtiene un film entrecruzado.

- **Disolución-evaporación («casting»):** este método se basa en la deposición de una disolución de los polímeros deseados sobre una superficie lisa para, posteriormente, eliminar por evaporación el disolvente, de manera que los polímeros disueltos quedan en forma de film. En este caso, controlar el espesor de los films es más complicado, pero en función de la cantidad de disolución depositada sobre una misma área de superficie y de la concentración de la disolución inicial se puede obtener resultados razonablemente reproducibles. Para obtener un film entrecruzado a través de esta técnica, es preciso realizar modificaciones sobre el polímero después de su preparación.
- **Electrohilado («electrospinning»):** es un método que permite la obtención de films a partir de una disolución polimérica en presencia de un elevado potencial eléctrico. El proceso genera nanofibras que se acumulan en un soporte, y el espesor de los films se puede controlar variando los tiempos de electrohilado.
- **Inversión de fase:** es un método para la obtención de films poliméricos porosos. Para llevarlo a cabo hay que depositar la disolución del polímero sobre una superficie y sin que haya evaporación del disolvente de la disolución polimérica, se introduce en un baño de coagulación para inducir la inversión de fase. En el baño de coagulación, el disolvente se extrae de la película y se reemplaza por agua. La eliminación de manera rápida del disolvente de la disolución causa la separación de la fase acuosa y la fase polimérica. Este proceso genera films porosos, ya que el disolvente que contenía el polímero sale de la estructura polimérica generando canales que dan lugar a estructuras porosas en el film.<sup>58</sup>

---

<sup>58</sup> J.M. Gohil, R.R. Choudhury, *Chapter 2 - Introduction to Nanostructured and Nano-enhanced Polymeric Membranes: Preparation, Function, and Application for Water Purification*, in: S. Thomas, D. Pasquini, S.-Y. Leu, D.A. Gopakumar (Eds.), *Nanoscale Mater. Water Purif.*, Elsevier, Oxford, **2019**, 25–57.

Por otra parte, existen otras características importantes que se pueden modificar según la aplicación final a la que va dirigida el film. Por ejemplo, se pueden obtener estructuras celulares que tienen relevancia para ciertas aplicaciones<sup>59</sup> como para la detección de oxígeno en forma gaseosa,<sup>60</sup> detección de aniones y cationes,<sup>61</sup> la detección de aminas volátiles,<sup>62</sup> en el desarrollo de sensores de baja presión<sup>63</sup> o la absorción de distintas sustancias de interés medio ambiental.<sup>64</sup>

Finalmente, cabe destacar el uso de films para el desarrollo de polímeros de impresión molecular para la detección, normalmente mediante respuesta electroquímica, de distintos analitos en disolución.<sup>65,66</sup>

Por otra parte, los recubrimientos poliméricos se basan en la formación de una capa polimérica externa sobre una superficie o material. Se debe de tener en cuenta la estructura y naturaleza de la superficie que se quiere cubrir a la hora de desarrollar el material polimérico que va a formar el recubrimiento, ya que la polaridad de ambos materiales (recubrimiento y superficie) deben ser similares para que exista la afinidad adecuada entre ellas, en caso de que no sea así el recubrimiento puede no quedar adherido de manera correcta.

Los sensores poliméricos en forma de recubrimiento tienen multitud de aplicaciones, entre las que destacan, la detección de oxígeno,<sup>67</sup> el recubrimiento de fibras para la detección de explosivos<sup>68,69</sup> detección de aminas biogénas<sup>70</sup> o

<sup>59</sup> A. Kmetty, *J. Appl. Polym. Sci.* **2022**, 139, e51714.

<sup>60</sup> S.-Y. Liu, X.-L. Qi, R.-B. Lin, X.-N. Cheng, P.-Q. Liao, J.-P. Zhang, X.-M. Chen, *Adv. Funct. Mater.* **2014**, 24, 37, 5866–5872.

<sup>61</sup> C.H. Zhang, G.J. Li, J.H. Wang, *Chinese J. Anal. Chem.* **2014**, 42, 607–615.

<sup>62</sup> Y. Wang, G.A. Sotzing, *Chem. Mater.* **2003**, 24, 375–377.

<sup>63</sup> M. Pruvost, *Npj Flex. Electron.* **2019**, 3:7.

<sup>64</sup> Z. Wang, S. Guo, B. Zhang, J. Fang, L. Zhu, *J. Hazard. Mater.* **2020**, 384, 121187.

<sup>65</sup> K. Haupt, K. Mosbach, *Chem. Rev.* **2000**, 100, 2495–2504.

<sup>66</sup> T. Takeuchi, J. Haginaka, *J. Chromatogr. B Biomed. Sci. Appl.* **1999**, 728, 1–20.

<sup>67</sup> W. Waskitoaji, T. Hyakutake, M. Watanabe, H. Nishide, *React. Funct. Polym.* **2010**, 70, 669–673.

<sup>68</sup> R. Aguado, A.R.M.G. Santos, S. Vallejos, A.J.M. Valente, *Molecules* **2022**, 27, 2900.

<sup>69</sup> J.L. Pablos, M. Trigo-López, F. Serna, F.C. García, J.M. García, *RSC Adv.* **2014**, 4, 25562–25568.

<sup>70</sup> J.L. Pablos, S. Vallejos, A. Muñoz, M.J. Rojo, F. Serna, F.C. García, J.M. García, *Chem. Eur. J.* **2015**, 21, 8733–8736.

en el desarrollo de nuevos envases en la industria de la alimentación.<sup>71</sup> Además, existen distintos procesos para realizar recubrimientos poliméricos, entre los que destacan:

- **Recubrimiento por goteo:** es un proceso que se utiliza en la fabricación de productos como microchips o sensores. Para ello, se colocan gotas de la disolución polimérica sobre la superficie de interés y se distribuye uniformemente mediante la tensión superficial y la gravedad de esta forma se obtiene una capa delgada y uniforme de material sólido en la superficie.
- **Recubrimiento con rasqueta:** este tipo de recubrimiento se utiliza en el desarrollo de productos como papel o textiles. Se aplica una capa de polímero disuelto sobre la superficie de interés mediante el uso de una barra de recubrimiento que provoca que la capa del material sea uniforme.
- **Recubrimiento por pulverización:** es un proceso de recubrimiento muy versátil ya que se puede realizar sobre superficies curvas. Para realizarlo hay que pulverizar sobre la superficie una disolución del polímero.
- **Recubrimiento por inmersión:** este tipo de proceso de recubrimiento se realiza sumergiendo el objeto en una disolución del polímero. Posteriormente, se levanta lentamente para permitir que el exceso de disolución gotee y se drene adecuadamente antes de que se seque obteniendo de esta manera una capa uniforme.

En concreto, esta tesis se ha centrado en el desarrollo de polímeros sensores fluorimétricos y colorimétricos en forma de films mediante polimerización en bloque y en forma de recubrimientos sobre celulosa por goteo. Además, todos los polímeros sensores se han sintetizado a través de polimerizaciones radicalarias de monómeros vinílicos.

---

<sup>71</sup> S. Jafarzadeh, A. Salehabadi, A. Mohammadi Nafchi, N. Oladzadabbasabadi, S.M. Jafari, *Trends Food Sci. Technol.* **2021**, 116, 218–231.

### 1.4.3. Diseño de polímeros sensores colorimétricos y/o fluorimétricos

En la **Figura 6** se muestra esquemáticamente la estructura general que presentan los polímeros sensores que se han desarrollado en este trabajo, en la que se diferencian claramente dos partes, la matriz estructural y los grupos receptores, además del entrecruzante. El entrecruzante no es una parte indispensable del polímero sensor, por lo que se añade en función de la aplicación a la que va destinada el material. De manera que, a los films polimerizados por vía radicalaria en bloque, se les añade un entrecruzante en un porcentaje mínimo (habitualmente en un 0,1% molar) para evitar la disolución del material en cualquier disolvente. Por otra parte, no se debe añadir ningún entrecruzante para el desarrollo de polímeros lineales para su aplicación en disolución como, por ejemplo, para la realización de films por disolución-evaporación o recubrimientos.

La matriz estructural se define como la parte que otorga determinadas propiedades al polímero, como la hidrofilia o la manejabilidad. Esta parte del polímero sensor puede estar conformada por un único monómero o por varios según las propiedades que interesen para el material final. La matriz estructural representa, por lo general, más del 95% de la composición de la mezcla de monómeros de la que se va a obtener el polímero sensor, por lo que tiene mucho peso en las propiedades finales del material. Normalmente los receptores representan como máximo un 5% molar de la mezcla de monómeros.

- **Hidrofilia:** es la afinidad que tienen los materiales hacia el agua. Es decir, los polímeros hidrofílicos presentan interacciones favorables con el agua. Por ejemplo, los films poliméricos hidrofílicos son capaces de absorber agua en su estructura, y cuando esto sucede se dice corrientemente que el film está hinchado. Por otra parte, la hidrofilia es una propiedad importante de los polímeros sensores ya que, al introducir agua en su estructura, se favorece la entrada de analitos solubles que pueden reaccionar con los receptores. Es por esto por lo que el tiempo de respuesta del polímero sensor mejora con la hidrofilia. Algunos
-

monómeros que aportan hidrofilia son la *N*-vinipirrolidona, el acrilato de 2-hidroxietilo, la *N,N*-dimetilacrilamida o la acrilamida. En cambio, algunos monómeros que aportan hidrofobia son el metacrilato de metilo, el estireno, el acrilonitrilo o el acrilato de butilo.

- **Propiedades mecánicas:** son las características que describen cómo un polímero se deforma y se rompe cuando está sometido a una fuerza o carga. La resistencia mecánica de los materiales depende de la estructura química de los monómeros que se emplean para desarrollar el material. Así, el metacrilato metilo, de cadena lateral corta, aporta rigidez, mientras que el metacrilato de laurilo, de cadena lateral larga, aporta flexibilidad.

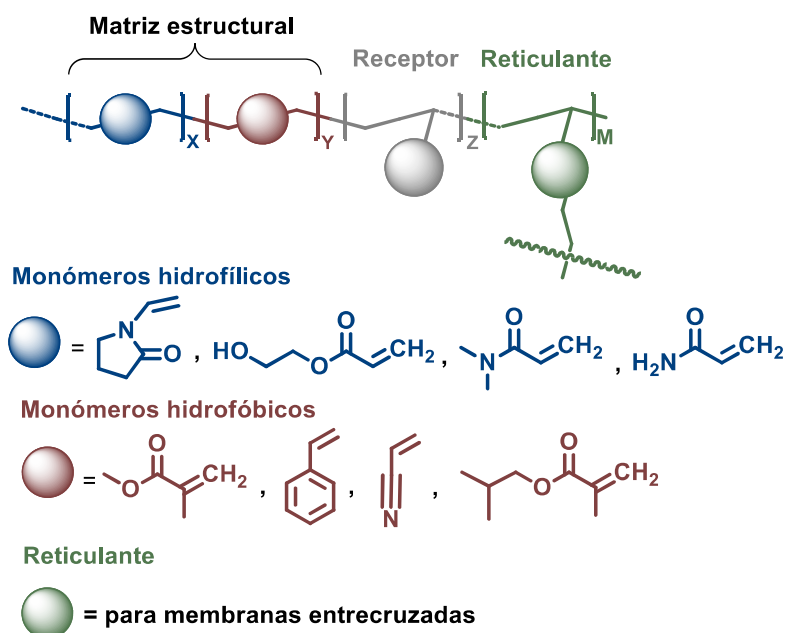


**Figura 6.** Composición de la matriz estructural de los polímeros sensores desarrollados a lo largo de esta tesis doctoral.

No existe relación entre la hidrofilia/hidrofobia y la rigidez/flexibilidad, por lo que existen monómeros hidrofílicos que pueden aportar rigidez, como la *N*-vinipirrolidona, pero también flexibilidad, como el acrilato de 2-hidroxietilo. Por

otro lado, existen monómeros hidrofóbicos que aportan rigidez (metacrilato de metilo), y otros que pueden aportar flexibilidad (acrilato de butilo).

En general, para fabricar un sensor de alta calidad es necesario encontrar el equilibrio adecuado entre la hidrofilia y las propiedades mecánicas del polímero. Aunque es posible mejorar la respuesta del sensor aumentando la proporción de monómeros hidrofílicos, esto puede resultar en un mayor hinchamiento del material en agua y, por lo tanto, en una disminución de sus propiedades mecánicas. Por otro lado, si se incrementa la proporción de monómeros hidrofóbicos, el agua no podrá penetrar en la estructura del material. A pesar de las propiedades mecánicas favorables que pueda tener, no será adecuado para detectar analitos en medio acuoso.

En el marco de esta tesis doctoral se han utilizado matrices estructurales conformadas por mezclas equimolares de *N*-vinilpirrolidona y metacrilato de metilo. La combinación de estos monómeros confiere al material un carácter hidrofílico adecuado para interactuar con los analitos en medios acuosos. Tanto cuando se han desarrollado estos sensores en forma de films, como cuando fueron preparados recubrimientos, esta mezcla proporciona una manejabilidad adecuada en términos de propiedades mecánicas y térmicas para su aplicación en las áreas deseadas.

Además de la matriz estructural, la otra parte indispensable del polímero sensor es el receptor (o subunidad sensora), de los que ya se ha hablado anteriormente. Esta parte es la encargada de responder frente al estímulo provocando un cambio que sea medible macroscópicamente, en lo que a este trabajo se refiere, un cambio de color o fluorescencia. Por la naturaleza de los monómeros que conforman los polímeros sensores preparados (monómeros vinílicos), los receptores deben ser de naturaleza química análoga, por lo que también presentan estructura vinílica.

---

#### **1.4.4. Estrategias para la preparación de polímeros sensores vinílicos colorimétricos y/o fluorimétricos**

Para preparar polímeros sensores con receptores selectivos en su estructura existen dos posibilidades que se detallan en la **Figura 7** y se describen a continuación:

- **Síntesis del monómero sensor y posterior polimerización:** esta metodología se basa en la preparación de un monómero sensor mediante reacciones químicas convencionales. El objetivo de estas modificaciones químicas es el desarrollo de un compuesto con actividad sensora con un receptor selectivo, pero con un grupo polimerizable (concretamente un grupo vinílico). Posteriormente, una vez sintetizado el monómero sensor se copolimeriza con el resto de los monómeros para formar el polímero.
- **Polimerización y posterior modificación mediante reacciones en estado sólido:** en este caso, se inicia el proceso mediante la polimerización de una mezcla de monómeros. Seguidamente, se procede a utilizar la reactividad de uno de los monómeros para modificar su estructura química, generando así los receptores del polímero sensor.

### **1.5. Planteamiento de la investigación. Problemas detectados y soluciones propuestas**

Garantizar la seguridad es uno de los retos que se mantienen a lo largo de nuestra historia como sociedad. Precisamente debido a la complejidad del mundo en el que vivimos cada día aparecen nuevas problemáticas con las que tenemos que lidiar. Estas problemáticas tienen orígenes muy distintos, pueden ser de naturaleza biológica como la pandemia mundial vivida a causa del SARS-CoV-2, o pueden derivar de los malos hábitos humanos individuales o de distintas industrias u organismos. Por otra parte, el control alimentario trata de velar mediante ensayos analíticos la aptitud de los alimentos y, por tanto, en último término, la seguridad de los consumidores. En cuanto a la seguridad civil,

---

la confianza del consumidor frente a los múltiples fraudes existentes está en entredicho, ya que cada año aumenta la producción de falsificaciones y las denuncias de fraude derivadas de la compra fraudulenta. En este contexto, el Grupo de Polímeros de la Universidad de Burgos ha desarrollado multitud de sensores para moléculas discretas (como por ejemplo para la detección de mercurio(II),<sup>72</sup> cromo(VI),<sup>73</sup> o aluminio (III),<sup>74</sup> entre otras), pero en esta tesis se ha desarrollado por primera vez un sensor para biomoléculas (detección de la proteasa principal del SARS-CoV-2). Este cambio implica un aumento en la complejidad del material polimérico, debido entre otros motivos, al aumento del tamaño de la molécula diana, y por consiguiente también el del receptor. Una vez contextualizada la problemática de manera general, a continuación, se detallan los problemas detectados y las soluciones propuestas en cada ámbito concreto.

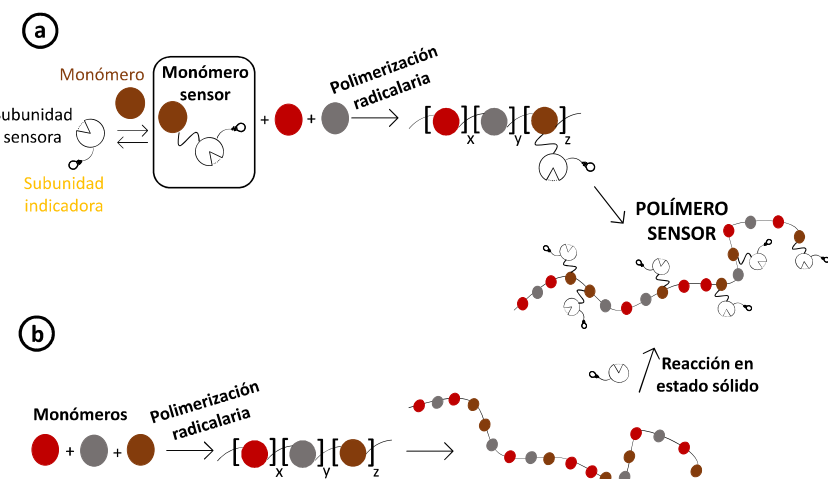


**Figura 7.** Estrategias para el desarrollo de polímeros sensores: a) desarrollo de monómero sensor y posterior polimerización; y b) polimerización para la obtención del material y posterior modificación estructural a través de reacciones en estado sólido.

<sup>72</sup> S. Vallejos, P. Estévez, S. Ibeas, A. Muñoz, F.C. García, F. Serna, J.M. García, *Sens. Actuators B Chem.* **2011**, 157, 686–690.

<sup>73</sup> S. Vallejos, A. Muñoz, F.C. García, F. Serna, S. Ibeas, J.M. García, *J. Hazard. Mater.* **2012**, 227–228, 480–483.

<sup>74</sup> S. Vallejos, A. Muñoz, S. Ibeas, F. Serna, F.C. García, J.M. García, *J. Hazard. Mater.* **2014**, 276 52–57.

### **1.5.1. Biomedicina**

La seguridad sanitaria es un desafío importante en la sociedad actual para mejorar el diagnóstico y tratamiento de enfermedades. Por lo tanto, se requiere una investigación constante y el desarrollo de nuevas técnicas y materiales para detectar enfermedades de manera rápida, sencilla y económica. La pandemia causada por el SARS-CoV-2 puso de manifiesto la necesidad de desarrollar nuevas técnicas y métodos de diagnóstico y detección para enfrentar futuras enfermedades. Si algo aprendimos como sociedad es que las pruebas de diagnóstico son una herramienta fundamental, especialmente en los primeros compases de la pandemia. En el caso de la COVID-19, la toma de muestras tanto de ensayos PCR (de sus siglas en inglés, «*Polymerase chain reaction*») como de test de antígenos implicaba una toma de muestras invasiva con una torunda, algo especialmente complicado cuando los pacientes eran niños, personas de avanzada edad, o personas con necesidades especiales.

En esta tesis doctoral se describe la preparación de una etiqueta sensora basada en un recubrimiento polimérico sobre papel que pueda detectar la presencia del virus de forma sencilla y visible. La elección de un recubrimiento polimérico se debe a las diversas aplicaciones potenciales, como la fabricación de pruebas de diagnóstico, mascarillas sensoras y detección del virus en «superficies altamente expuestas» o «superficies de alto tráfico», como pasamanos de escaleras y agarraderas de autobuses. Este formato es fácil de escalar y mantiene las principales ventajas de los polímeros sensores, como la no necesidad de personal cualificado ni equipamiento específico y el análisis visual y económico.

### **1.5.2. Seguridad civil**

La seguridad civil se puede definir como los mecanismos que la sociedad utiliza para la minimización de los daños y/o problemas para la ciudadanía. En concreto, esta tesis se ha centrado en los problemas relacionados con el envío de paquetes a particulares, o a instituciones (embajadas, ministerios, etc.). La verificación del emisor del paquete implica el conocimiento directo del contenido,

---

y por lo tanto de la seguridad o autenticidad del mismo. La seguridad de los métodos actuales de verificación, como los códigos de barras, queda en entredicho en muchas ocasiones, lo que genera dos grandes riesgos: el fraude del plagio, y el riesgo asociado al envío de paquetes bomba o similares.

En el desarrollo de esta tesis se propuso un método de verificación basado en una reacción química que genera varios colores en la etiqueta de verificación, y que el receptor del paquete puede comprobar con un sencillo rociado de la etiqueta con un espray.

### 1.5.3. Control alimentario

Nunca se ha vivido en una época tan segura como la actual desde el punto de vista de alimentación, en gran parte, gracias a los controles de calidad, seguridad y a la trazabilidad. Unas de las especies más controladas en alimentos y bebidas son los metales pesados. En ocasiones, un exceso de estos metales puede ser perjudicial para salud del consumidor, o para la calidad del alimento. En otras ocasiones, es el defecto de este metal lo que lleva asociado ciertos riesgos.<sup>75,76</sup> Los productores intentan analizar su producto todo lo posible, manteniendo siempre un cierto equilibrio entre el precio y la calidad. Por eso, los métodos de detección de metales pesados que son económicos, y que simplifican en muchas ocasiones tediosos métodos de análisis, han despertado un gran interés en esta industria.

De hecho, en esta tesis se han abordado dos problemas trasladados por parte de dos empresas al Grupo de Polímeros de la Universidad de Burgos, uno relacionado con la detección de cobre en vinos, y otro con la detección de zinc en piensos de mascotas. En esta ocasión, se optó por el formato tipo film, un formato más resistente que los recubrimientos debido a los ambientes industriales y agrícolas a los que estarían potencialmente expuestos en un uso real.

---

<sup>75</sup> W. Maret, *Adv. Nutr.* **2013**, 4, 82–91.

<sup>76</sup> M.G. Lionetto, R. Caricato, M.E. Giordano, T. Schettino, *Int. J. Mol. Sci.* **2016**, 17(1), 127

## 1.6. Objetivos

El trabajo para esta tesis doctoral se ha llevado a cabo en el Grupo de Polímeros, donde se sigue una línea de investigación sobre polímeros sensores. El objetivo general de este trabajo consiste en estudiar estos polímeros que se pueden emplear en la detección de sustancias relevantes para la biomedicina, la seguridad civil y el control alimentario, y mejorar sus características para su aplicación en entornos reales. Para lograr este objetivo, se han establecido objetivos específicos que guían el trabajo:

- Diseñar, desarrollar y caracterizar un sensor polimérico fluorescente para la detección de SARS-CoV-2 en muestras de saliva para el diagnóstico de COVID-19 en pacientes.
- Diseñar, desarrollar y caracterizar un recubrimiento polimérico colorimétrico como método de autenticación de documentos o productos para la lucha contra el fraude, cuya verificación pueda monitorizarse únicamente a través de un teléfono móvil.
- Diseñar, desarrollar y caracterizar un sensor polimérico fluorescente para la detección y cuantificación de Zn(II) en muestras de pienso animal, además de un sensor polimérico colorimétrico para la detección y cuantificación de cobre en mostos.

## 1.7. Estructura de la Memoria

La memoria se divide en cuatro capítulos, siendo el primero una introducción en la que se establecen los objetivos de la tesis doctoral y se explican los conceptos claves y el contexto en el que se desarrolla el estudio. Este capítulo proporciona una visión general de la investigación que se aborda en la memoria y establece las bases para los capítulos siguientes.

En los capítulos siguientes se presenta la metodología empleada para alcanzar los objetivos propuestos. En particular, el Capítulo 2 describe en detalle el desarrollo, la síntesis y la caracterización de un sensor polimérico, así como su evaluación en pacientes como un método alternativo de diagnóstico de la

COVID-19. Además, se presentan los resultados obtenidos durante la prueba de concepto y se analiza su relevancia para el diagnóstico de la enfermedad.

El Capítulo 3 se centra en el desarrollo de un material polimérico con aplicaciones en seguridad civil. En concreto, se describe la creación de un recubrimiento polimérico diseñado para combatir la falsificación y el fraude. Se explican los métodos utilizados para su síntesis y se detallan las pruebas realizadas para demostrar su efectividad en la lucha contra estas prácticas delictivas.

El Capítulo 4 presenta un estudio detallado sobre la síntesis, diseño y caracterización de dos sensores poliméricos para la detección y cuantificación de cationes de interés en la industria alimentaria. El primero de ellos es un sensor fluorogénico que se ha desarrollado para detectar el catión Zn(II) en muestras de pienso animal. Se presenta la síntesis del material polimérico utilizado para este fin, así como los ensayos realizados para evaluar su capacidad de detección y cuantificación en muestras reales. Por otro lado, se describe también el desarrollo de un segundo sensor, basado en la detección de cobre en muestras de mosto de uva.

Es importante señalar que los procedimientos experimentales, resultados, discusión y conclusiones parciales obtenidos en el desarrollo de esta tesis doctoral se han publicado en diversos artículos científicos que se han transscrito íntegramente al final de cada capítulo. Por último, la memoria concluye con una sección de conclusiones en la que se presentan los principales hallazgos obtenidos y se discuten sus implicaciones. Además, se ofrecen perspectivas de futuro para el trabajo realizado, destacando las posibles áreas de investigación y desarrollo en las que se podrían aplicar los resultados obtenidos en esta tesis doctoral.

---



# CAPÍTULO 2

## Polímeros sensores en biomedicina

---

Este capítulo se centra en el desarrollo de un polímero sensor en forma de recubrimiento para la detección del virus SARS-CoV-2. Comienza con una breve introducción sobre la importancia de los polímeros sensores en biomedicina, especialmente en el contexto de la pandemia de COVID-19. A continuación, se detalla la evolución del desarrollo del recubrimiento sensor, incluyendo su diseño, síntesis y caracterización. Por último, el capítulo concluye con la presentación del artículo publicado en *Sensors and Actuators B: Chemical*, donde se detallan con precisión los resultados de la investigación y se discuten sus posibles aplicaciones en el campo de la biomedicina. En general, el capítulo ofrece una visión del desarrollo de este importante avance en la lucha contra la pandemia de COVID-19.

---

### 2.1. Introducción

El SARS-CoV-2 es un virus respiratorio que apareció a finales de 2019, y en solo unas semanas se propagó a lo largo del planeta provocando una de las pandemias más problemáticas que ha vivido la humanidad. Estos años de pandemia nos han enseñado que la prevención debe de mejorar. Es crítico que los métodos de diagnóstico durante los primeros meses, y los tratamientos y vacunas en etapas posteriores, se desarrolle en el menor tiempo posible.

Durante la pandemia, los dos métodos de diagnóstico más populares fueron las pruebas de antígenos y las pruebas de PCR. Sin embargo, ambos presentaban algunas desventajas comunes, como el método invasivo de toma

---

de muestras mediante hisopos de la mucosa de la rinofaringe, lo que resultaba molesto y especialmente complicado en niños, personas mayores y personas con necesidades especiales. Además, los test de antígenos llegaron tarde debido a los ritmos de producción sobrepasados por la situación, incrementando el precio de los mismos y generando interminables colas en farmacias y centros de distribución. Además, las pruebas de PCR eran costosas, con precios que rondaban entre 50 y 100 euros, y los resultados se demoraban en muchas ocasiones hasta 3 días después de la toma de muestras.

El objetivo principal de este capítulo fue abordar los inconvenientes de los métodos de diagnóstico durante la pandemia, como el alto precio, el largo tiempo de respuesta, el tiempo de fabricación y la toma de muestras invasiva. Además, el desarrollo supuso un gran desafío para el grupo de investigación, ya que los polímeros sensores que se habían desarrollado anteriormente estaban dirigidos a objetivos sencillos como moléculas discretas de baja masa molecular (como un polímero sensor para monitorización de heridas crónicas<sup>77</sup> o fibrosis quística)<sup>78</sup>, lo que implicaba el uso de receptores también discretos. Por lo tanto, para poder detectar microorganismos o macromoléculas directamente relacionadas con ellos, era necesario utilizar receptores de gran tamaño.

Llegados a este punto, se plantearon diferentes opciones o estrategias para conseguir un polímero sensor colorimétrico/fluorimétrico del SARS-CoV-2:

- **Polímeros sensores con cadenas laterales peptídicas:** en este caso la especie diana se basaría en una proteasa específica del virus, concretamente la proteasa principal Mpro («*Main protease*» o 3CLpro). El mecanismo de acción de esta propuesta se basa en la introducción de un péptido fluorogénico en la estructura del polímero sensor de manera que esta enzima específica del SARS-CoV-2 reconoce y

<sup>76</sup> A. Arnaiz, M. Guembe-García, E. Delgado-Pinar, A.J.M. Valente, S. Ibeas, J.M. García, S. Vallejos, *Sci. Rep.* **2022**, 12, 1–12.

<sup>77</sup> M. Guembe-García, V. Santaolalla-García, N. Moradillo-Renuncio, S. Ibeas, J.A. Reglero, F.C. García, J. Pacheco, S. Casado, J.M. García, S. Vallejos, *Sens. Actuators, B Chem.* **2021**, 335, 129688.

<sup>78</sup> S. Vallejos, E. Hernando, M. Trigo, F.C. García, M. García-Valverde, D. Iturbe, M.J. Cabero, R. Quesada, J.M. García, *J. Mater. Chem. B* **2018**, 6, 3735–3741.

procede a hidrolizar y, por tanto, se da un proceso «OFF-ON» de la fluorescencia.

- **Polímeros sensores con anticuerpos como receptores:** esta estrategia se basaba en la inmovilización covalente de un anticuerpo capaz de interaccionar con los antígenos correspondientes. Dicho de otra forma, la propuesta se basó en la implementación de la tecnología en la que se basaba un test de antígenos en un material polimérico tipo film.
- **Polímeros sensores con enzimas como receptores:** en este caso, el polímero sensor se basa en el anclaje del receptor ACE2, que es la enzima convertidora de angiotensina II de las células humanas, involucrada directamente en el proceso de detección del virus por parte de nuestras células. Esta estrategia suponía trasladar a un material polimérico el proceso de reconocimiento molecular del que dispone nuestro organismo, basado en una de las interacciones más selectivas que existen, la interacción enzima-sustrato.

De las tres estrategias, la que resultó más prometedora desde el inicio del estudio fue la primera, basada en el anclaje covalente de un sustrato peptídico a un soporte polimérico que ejerce un entorno protector, donde la interacción sustrato-enzima se produce de forma mucho más efectiva.<sup>48</sup>

Atendiendo a los receptores escogidos, es decir, a los sustratos peptídicos específicos para enzimas proteolíticas concretas, éstos suelen estar basados en un par FRET, en una pareja de un amortiguador de fluorescencia «*quencher*» y un fluoróforo incluidos en la misma cadena peptídica (generalmente en los extremos). Se trata de receptores que generan una respuesta fluorimétrica, basada en la transferencia de energía entre el fluoróforo (donador) y el amortiguador (aceptor), tal y como se muestra de forma esquemática en la **Figura 8**. Para que este mecanismo funcione correctamente, el espectro de emisión del donador debe superponerse con el espectro de excitación del acceptor, de tal forma que el péptido en el que se incluyen carece

---

de fluorescencia.<sup>79</sup> Cuando la proteasa corta el péptido, separa donador y aceptor, y se produce una señal fluorescente de tipo encendido «OFF-ON».

Este mecanismo forma parte de un sinfín de biosensores poliméricos, que se aplican en biotecnología, y en biomedicina, como por ejemplo en diagnóstico por imagen «imaging» para el seguimiento de terapias de cáncer,<sup>80</sup> determinación de actividad enzimática,<sup>81</sup> detección de patógenos,<sup>82</sup> etc.

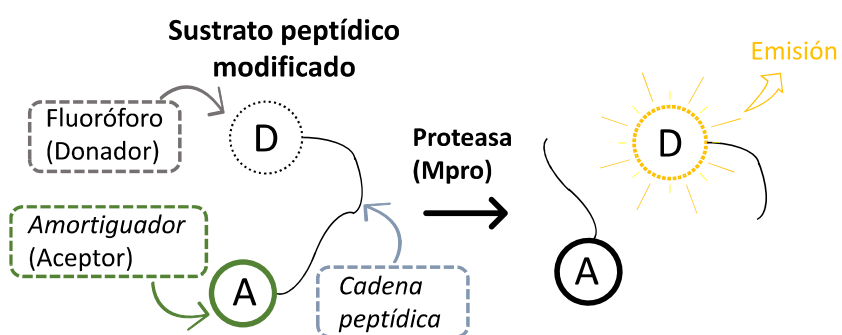


**Figura 8.** Mecanismo de acción del sustrato modificado mediante pares FRET en su estructura química frente a la proteasa Mpro que cataliza la ruptura de los enlaces peptídicos del sustrato.

Lo que se propuso como parte de esta tesis fue la incorporación de este tipo de receptores en soportes poliméricos, mejorando de esta forma la eficiencia de los mismos y dando lugar a sensores de patógenos más manejables y más fáciles de utilizar.

## 2.2. Biosensor polimérico para la detección de SARS-CoV-2

Para el desarrollo de este sensor se sintetizaron polímeros lineales mediante copolimerización radicalaria de *N*-vinilpirrolidona, metacrilato de metilo y 4-aminoestireno, en dos composiciones molares distintas, con el objetivo de evaluar cómo afecta la hidrofilia del material a la eficiencia del sistema sensor.

<sup>79</sup> T. Förster. *Ann. Phys.* **1948**, 437, 55-75.

<sup>80</sup> F. Peng, Y. Su, Y. Zhong, C. Fan, S. T. Lee, Y. He. *Acc. Chem. Res.* **2014**, 47, 612–623.

<sup>81</sup> E. Hutter, D. Maysinger. *Trends Pharmacol. Sci.* **2013**, 34, 497–507.

<sup>82</sup> I. Grabowska, K. Malecka, U. Jarocka, J. Radecki, H. Radecka. *Acta Biochim. ol.* **2014**, 61, 471–478.

Los polímeros se aplicaron como recubrimientos sobre papel con la técnica de recubrimiento por goteo, y finalmente se llevó a cabo la inmovilización del sustrato peptídico a través de la formación de enlaces imina entre grupos amino laterales del material, y grupos amino laterales del sustrato, utilizando glutaraldehído como enlazador (**Figura 9**).

Las etiquetas sensoras se probaron con pacientes reales, a través de un estudio aprobado por la comisión de bioética de la Universidad de Burgos. Además de su capacidad para la detección del virus, también se estudió su citotoxicidad con células epidérmicas y pulmonares. Este trabajo se publicó en la revista *Sensors and Actuators: B: Chemical*.<sup>83</sup>

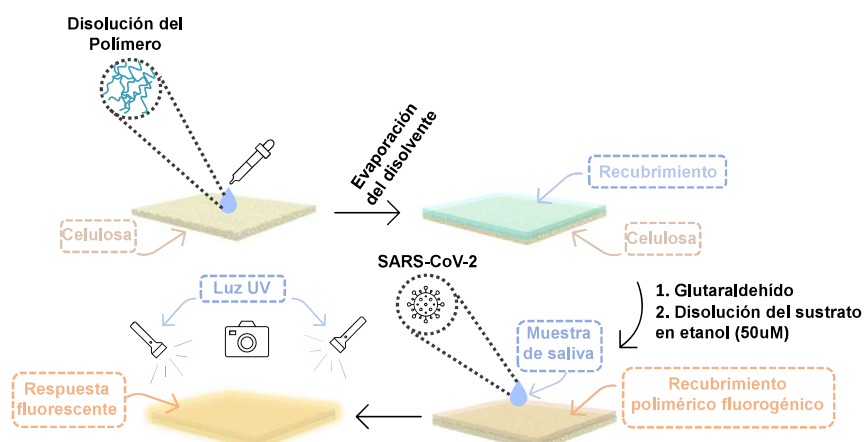


**Figura 9.** Representación esquemática del desarrollo y funcionamiento del polímero sensor en forma de recubrimiento polimérico sobre celulosa.

### 2.3. Resultados

A continuación, se muestran los resultados obtenidos a través de la transcripción íntegra de los trabajos publicados o en proceso de revisión:

- *Lab-on-a-chip for the easy and visual detection of SARS-CoV-2 in saliva based on sensory polymers.*

<sup>83</sup> A. Arnaiz, J.C. Guirado-Moreno, M. Guembe-García, R. Barros, J.A. Tamayo-Ramos, N. Fernández-Pampín, J.M. García, S. Vallejos, *Sensors Actuators B Chem.* **2023**, 379, 133165.



*Lab-on-a-chip for the easy and visual detection of SARS-CoV-2 in saliva  
based on sensory polymers.*



## Lab-on-a-chip for the easy and visual detection of SARS-CoV-2 in saliva based on sensory polymers

Ana Arnaiz<sup>+,a,c</sup>, José Carlos Guirado-Moreno<sup>+,a</sup>, Marta Guembe-García<sup>a</sup>, Rocío Barros<sup>b</sup>, Juan Antonio Tamayo-Ramos<sup>b</sup>, Natalia Fernández-Pampín<sup>b</sup>, José M. García<sup>a</sup>, Saúl Vallejos<sup>a,\*</sup>

<sup>a</sup> Departamento de Química, Facultad de Ciencias, Universidad de Burgos, Plaza de Misael Bañuelos s/n, 09001 Burgos, Spain

<sup>b</sup> International Research Center in Critical Raw Materials for Advanced Industrial Technologies (ICCRAM), R&D Center, Universidad de Burgos, Plaza de Misael Bañuelos s/n, 09001 Burgos, Spain

<sup>c</sup> Universidad Politécnica de Madrid, Calle Ramiro de Maeztu, 7, 28040, Madrid, Spain

<sup>+</sup> These authors contributed equally.

<sup>\*</sup> Corresponding author: Dr. Vallejos ([svallejos@ubu.es](mailto:svallejos@ubu.es))

### Abstract

The initial stages of the pandemic caused by SARS-CoV-2 showed that early detection of the virus in a simple way is the best tool until the development of vaccines. Many different tests are invasive or need the patient to cough up or even drag a sample of mucus from the throat area. Besides, the manufacturing time has proven insufficient in pandemic conditions since they were out of stock in many countries. Here we show a new method of manufacturing virus sensors and a proof of concept with SARS-CoV-2. We found that a fluorogenic peptide substrate of the main protease of the virus (Mpro) can be covalently immobilized in a polymer, with which a cellulose-based material can be coated. These sensory labels fluoresce with a single saliva sample of a positive COVID-19 patient. The results matched with that of the antigen tests in 22 of 26 studied cases (85% success rate).

**Keywords:** Peptide; substrate; fluorimetry; immobilization; COVID-19; paper-supported; coating; pandemics.

*Sensors and Actuators, B: Chemical* **2023**, 379, 133165

## 1. Introduction

At the beginning of 2022, the SARS-CoV-2 virus caused one of the most severe pandemics in the history of humanity and claimed the lives of more than 6 million people [1–3]. After two years of the pandemic, we now know that in the initial stages, where the virus advances rapidly, early detection methods for those infected and the isolation of these people are the most useful tools against the virus's progression [4,5].

Since the pandemic, polymerase chain reaction (PCR) and antigen detection tests have been the most widely used methods for detecting infected people. However, these methods belong to entirely different families, and each of them has advantages and disadvantages concerning the other. The choice of detection method is usually based on the rush for the result (antigens) or the desired precision and sensitivity (PCR).

PCRs belong to the group of nuclear acid-based detection methods, and antigen tests to the group of protein-based detection methods [6]. On the one hand, nuclear acid-based detection methods, such as PCR or Loop-Mediated Isothermal Amplification (LAMP), require an amplification process in which a few DNA strands can be replicated to produce a much larger sample. This amplification process makes the sensitivity of these methods very high. Within this group, we could include aptamer-based detection methods [7]. Unlike DNA, aptamers are single-stranded chains made of 20-80 nucleotides. With them, receptors can be synthesized for specific targets of the coronavirus, such as protein N and protein S [8].

On the other hand, the most relevant protein-based detection methods are called antigen and antibody tests [9]. These systems are composed of a rapid immunoassay kit (Enzyme-Linked ImmunoSorbent, ELISA, or lateral flow kit) in which a protein is detected by antigen-antibody interaction. However, most methods start with taking a sample using a swab, an invasive process that is uncomfortable and unpleasant. Some commercially available kits are non-

---

invasive and work with a saliva sample, but they require a large saliva sample and an additional experimental procedure based on a lateral flow test.

One of the most promising techniques for detecting these types of viruses is a subgroup of the protein-based detection methods called protein function-based detection methods [6,10–13]. They are based on using a peptide substrate to detect an enzyme closely related to the coronavirus, in this case, the Mpro protein [6]. Mpro (also called 3CLpro), is a cysteine hydrolase-like protease essential in viral replication that cleavages polyproteins and generates the corresponding functional proteins necessary for virion formation [14]. This protease has been well characterised for its possible role as a therapeutic target against the SARS-CoV2 virus [15–17]. For example, the peptide substrates designed for Mpro can be chemically modified with fluorophores and quenchers (FRET pairs), so that the interaction with the target enzyme generates a visual response, i.e., an OFF-ON fluorescence change [18]. Furthermore, this response is specific for the Mpro of SARS-CoV-2 and other highly similar Mpro (such as SARS-CoV) [15,16].

Considering all ordinary citizens and children, we believe that developing a non-invasive, visual, and simple detection method for respiratory viruses is worthy, not only for coronavirus but also for other present and future viruses. In this work, we have applied our knowledge in detecting species of interest to develop a polymer that becomes fluorescent in the presence of the Mpro protein, indicative of the presence of SARS-CoV-2. Unlike the published works concerning the detection of this enzyme [10–13], our proposal remains on the synthesis of a linear polymer that can be applied as a coating on a cellulose-based support. The user must only apply a single saliva sample above the smart label and check the fluorescence after the established time with the naked eye or, more precisely, with a smartphone.

---

## 2. Experimental

### 2.1. Materials

All materials and solvents were commercially available and used as received unless otherwise indicated. The following materials and solvents were used: fluorogenic peptide substrate Dabcyl-KTSAVLQSGFRKME-Edans (GenScript, N-Terminus: DABCYL, ≥95.0%, additional information in **SI-Section S1**), methylmethacrylate (MMA) (Merck, 99%), 1-vinyl-2-pyrrolidone (VP) (Acros Organic, 99%), 4-aminostyrene (SNH<sub>2</sub>) (TCI, 98%), glutaraldehyde aqueous solution (VWR, 25%), ethanol (VWR-Prolabo, 99.9%), methanol (VWR-Prolabo, 99.9%), diethyl ether (VWR-Prolabo, 99.9%), dimethylsulfoxide (VWR, 99%), acetonitrile (VWR, 99.9%), dimethylformamide (Supelco, 99.9%) distilled water, acetonitrile (VWR, 99.9%), dimethylsulfoxide-d<sub>6</sub> (VWR, 99.8%), 5-amino-1-naphthalene-1-sulfonic acid (Alfa Aesar, 90%), Mpro 3CL protease from coronavirus SARS-CoV-2 (Sigma), recombinant MERS-CoV 3CL protease, CF (R&D Systems), Trizma (Aldrich, 99.5%), NaCl (VWR, 98%), Ethylenediaminetetraacetic acid (EDTA) (VWR, 99.8%), dithiothreitol (DTT) (TCI, 98%), filter paper in reams (Filter Lab, 73g/m<sup>2</sup>). Azo-bis-isobutyronitrile (AIBN, Aldrich, 98%) was recrystallized twice from methanol.

The tissues and the reagents employed in the *In vitro* EpiDerm™ skin irritation test (EPI-200-SIT) were provided by MatTek In Vitro Life Science Laboratories: EpiDerm™ tissues (EPI-200-SIT), DMEM medium (EPI-100), 5% sodium dodecyl sulfate (SDS) solution (TC-SDS-5%), MTT-100 assay kit (MTT-100), which include the following components: MTT concentrate (MTT-100-CON), MTT diluent (MTT-100-DIL) and extractant solution (MTT-100-EXT). DPBS (Dulbecco's Phosphate-Buffered Saline) was provided by Corning.

### 2.2. Instrumentation and methods

<sup>1</sup>H and <sup>13</sup>C{<sup>1</sup>H} NMR spectra (Avance III HD spectrometer, Bruker Corporation, Billerica, Massachusetts, USA) were recorded at 300 MHz for <sup>1</sup>H and 75 MHz for <sup>13</sup>C using deuterated dimethyl sulfoxide (DMSO-d<sub>6</sub>) at 25°C as solvent.

---

The powder X-ray diffraction (PXRD) patterns were obtained using a diffractometer (D8 Discover Davinci design, Bruker Corporation, Billerica, Massachusetts, USA) operating at 40 kV, using Cu(K $\alpha$ ) as the radiation source, a scan step size of 0.02°, and a scan step time of 2 s.

The polymers thermal characterization was performed by thermogravimetric analysis (Q50 TGA analyzer, TA Instruments, New Castle, DE, USA) with 10–15 mg of sample under synthetic air and nitrogen atmosphere at 10°C·min $^{-1}$ ; and differential scanning calorimetry, with 10–15 mg of the sample under a nitrogen atmosphere at a heating rate of 10°C min $^{-1}$  (Q200 DSC analyzer, TA Instruments, New Castle, DE, USA).

Infrared spectra (FTIR) were recorded with an infrared spectrometer (FT/IR-4200, Jasco, Tokyo, Japan) with an ATR-PRO410-S single reflection accessory.

Enzymatic activity assays were performed using a Synergy HT microplate reader (BioTek®, Winooski, Vermont, USA), measuring fluorescence with 360/40–460/40 nm excitation/emission filters. Digital photographs were taken with a smartphone (Mi 9, Xiaomi, Pekín, China).

Solution fluorescence spectra were recorded using a F-7000 Hitachi Fluorescence spectrophotometer (Hitachi, Tokyo, Japan). A rectangular 10 mm cuvette was used for the fluorescence measurements, measuring all data at 25°C ± 0.1 °C.

### 2.3. Design of sensory polymers

The design of the polymers was carried out thinking about the application as solid sensory material. Our hypothesis relies on the fact that the virus synthesised the protease Mpro when it starts replicating inside infected cells, so, as a respiratory virus, it could be detected in a saliva sample.

First, we believe that a water-soluble polymer does not fit our work for one main reason: the user could inadvertently suck on the sensor tag, ingesting small amounts of polymer. Therefore, the polymer must contain a high enough

---

amount of a hydrophobic monomer, such as methyl methacrylate, so the resulting copolymer is insoluble in water. Second, certain hydrophilicity of the material may favour the interaction between the Mpro enzyme and the substrate, which is why a specific mol% of the hydrophilic monomer 1-vinyl-2-pyrrolidone was included in the formulations. Therefore, two polymers were designed with different hydrophilicity.

Finally, the polymers must have functional groups that serve as anchors for the immobilization of the peptide substrate (Figure 1a, characterization available in **SI-Section S1**). In our case, this immobilization occurs through the aniline side groups provided by the monomer 4-aminostyrene. All the monomers provide polarity to the final copolymers, which we believe is necessary to favour the affinity with the chosen support, i.e., cellulose paper.

#### 2.4. *Synthesis of polymers*

Linear polymers were prepared by radical co-polymerization of the commercially available monomers 1-vinyl-2-pyrrolidone (VP), methyl methacrylate (MMA) and 4-aminostyrene ( $\text{SNH}_2$ ) in different molar ratios, following the experimental procedure described below.

The amounts of each monomer, specified in Table 1, were dissolved in DMF and the solution was added to a round-bottom pressure flask. Subsequently, radical thermal initiator AIBN was added, and the solution was sonicated for 10 min and heated overnight at 60°C, under a nitrogen atmosphere, and without stirring. The solution was then dropwise added to diethyl ether (100 mL) with magnetic stirring, yielding the desired copolymers as whitish precipitates. Finally, polymers were purified in a Soxhlet apparatus with diethyl ether as the washing solvent to eliminate DMF traces. The characterization of polymers can be found in the electronic supporting information (**SI-Section S2**).

Copolymers 3 and 4 were prepared as blanks of copolymers 1 and 2, respectively. These blanks are highly relevant for the storage stability study

---

depicted in **Section 3.2**, and the understanding of the importance of the peptide to be covalently anchored to the copolymers.

**Table 1.** Copolymers' formulations indicating monomers' mol%. The table shows the amounts of monomers, solvent (DMF), and radical thermal initiator (AIBN) used in different copolymerizations.

<b>General formula</b>								
	<b>VP</b>		<b>MMA</b>		<b>SNH<sub>2</sub></b>		<b>AIBN</b>	<b>DMF</b>
	%mol	g	%mol	g	%mol	mg	mg	mL
<b>Copolymer 1</b>	49.75	1.05	49.75	0.94	0.50	11.28	155	9.5
<b>Copolymer 2</b>	4.97	0.11	94.53	1.88	0.50	11.84	163	9.9
<b>Copolymer 3</b>	50.00	1.05	50.00	0.95	0.00	0.00	155	9.5
<b>Copolymer 4</b>	5.00	0.11	95.00	1.89	0.00	0.00	163	9.9

The followed methodology gives rise to polymers with relatively low molecular weight so that the viscosity of coating solutions does not reach high values. These low viscosities can be obtained by carrying out the polymerization with high concentrations of the thermal radical initiator (0.1 M). The resulting copolymers are compatible with coating techniques such as drop-, spray- or dip-coating but incompatible with bar coating.

## 2.5. Preparation of sensory labels

The preparation of the sensory labels by drop coating is schematically shown in Figure 1b. 50 mg of copolymers 1 or 2 were dissolved in acetonitrile (1 mL). Then,

the resulting solution was deposited twice ( $2 \times 10 \mu\text{L}$ ) on the surface of a filter paper disc (6 mm diameter,  $28 \text{ mm}^2$ ), and the solvent was evaporated at  $60^\circ\text{C}$  for 10 min. Analogously, 8 mm disks were prepared specifically for cytotoxicity assays.

After that, the substrate for Mpro was immobilized following two steps. Firstly, the coated paper discs were dipped in an aqueous solution of glutaraldehyde (5%), and left overnight at  $25^\circ\text{C}$ . Then, the discs were washed by dipping them in distilled water for 10 min, and the process was repeated 5 times until the glutaraldehyde odour finally disappeared [19]. Secondly, the discs were dipped in a substrate solution (50  $\mu\text{M}$  in ethanol), and left overnight at  $25^\circ\text{C}$ . Finally, several dip washes were carried out with absolute ethanol ( $3 \times 10$  minutes), 75% ethanol ( $1 \times 10$  min), 50 % ethanol ( $1 \times 10$  min), 25% ethanol ( $1 \times 10$  min), distilled water ( $2 \times 10$  min), and 20 mM Tris-HCl pH 7.3, 100 mM NaCl, 1 mM EDTA, 1 mM DTT buffer ( $2 \times 10$  min). Sensory labels 1 and 2 were air-dried and stored in zip bags. The video included as supporting information (**SI-Video**) explains the complete preparation procedure of the sensory labels.

Additionally, sensory labels (3 and 4) without covalently anchored substrates were also prepared, as depicted in Figure 1c. In this case, the coating solutions contain 0.042 mg of the substrate (50  $\mu\text{M}$ ) and 2.21 mg of copolymer 3 or 4.

#### *2.6. Preliminary enzyme tests and storage stability study*

Measurements were carried out in a microplate reader with 96-well plates, including a 6 mm diameter sensory label at the bottom of each well and 20  $\mu\text{L}$  of a 0.5  $\mu\text{M}$  solution of Mpro in buffer (negative controls were performed with 20  $\mu\text{L}$  of 20 mM Tris-HCl pH 7.3, 100 mM NaCl, 1 mM EDTA, 1 mM DTT buffer). The assay was carried out at the optimum enzyme temperature ( $30^\circ\text{C}$ ), and the fluorescence emission at 460 nm was recorded over time (15, 30, 60, 120, 180, and 240 min). Measuring conditions: excitation slit = 40 nm; emission slit = 40 nm; excitation wavelength = 360 nm.

---

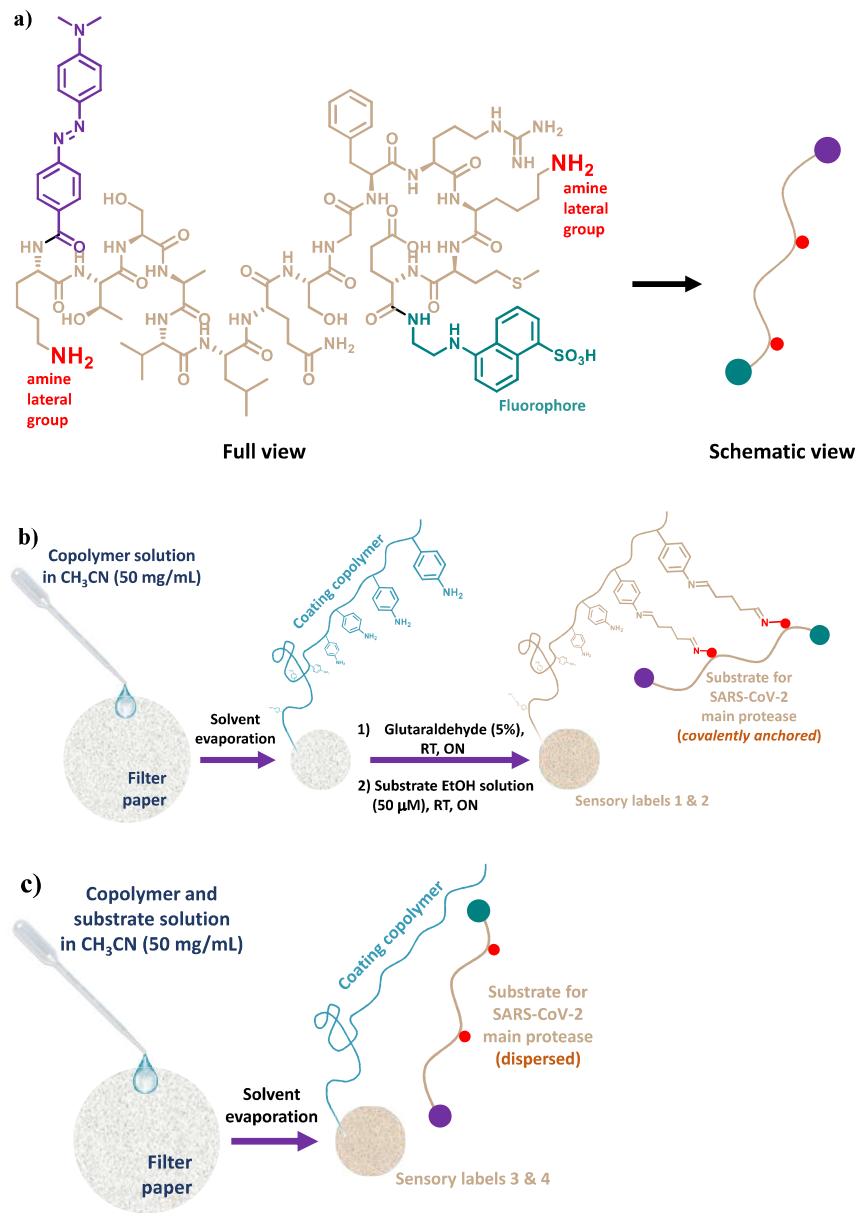


**Figure 1.** Preparation of sensory labels: **a)** chemical structure and schematic view of the fluorogenic peptide substrate for SARS-CoV-2 main protease; **b)** graphical abstract of the sensory labels preparation procedure containing covalently anchored substrates; and **c)** graphical abstract of the sensory labels preparation procedure containing non-covalently anchored substrates.

The stability of sensory labels with and without covalently anchored substrates was studied over time. All labels were room stored in zip bags without more care, and enzyme tests were performed at 1, 7, 14, 28 and 60 days.

The limit of detection (LOD) was estimated *in vitro* for the sensory label 1 and 2 using different concentrations of Mpro enzyme (from 0 to 1 µM) after 1h of incubation with the sensory labels. We estimated the limit of detection (LOD) by the following equation: LOD=3.3xSD/s, where SD is the standard deviation of blank sample and s is the slope of the calibration curve in the region of low Mpro content, respectively.

#### 2.7. *In vitro Skin Irritation Test*

The skin irritation test was performed according to the *in vitro* EpiDerm™ skin irritation test (EPI-200-SIT, MatTek In Vitro Life Science Laboratories, 2020) after confirming the inability of the sensors to interfere with and/or to reduce the MTT following the guideline recommendations.

Upon receipt, the tissues were inspected for damage according to the manufacturer's instructions, transferred to 6-well plates pre-filled with 0.9 mL of assay medium (EPI-100-NMM), and incubated at optimal conditions ( $37^{\circ}\text{C} \pm 1^{\circ}\text{C}$ ,  $5 \pm 1\% \text{ CO}_2$ ,  $90\% \pm 10\% \text{ RH}$ ) for 1 h. Then, the tissues were transferred to a freshly prepared medium and incubated overnight ( $18 \pm 3$  h) at optimal conditions to release transport-stress, after which the tissues were exposed to the sensors for 1 h ( $37^{\circ}\text{C} \pm 1^{\circ}\text{C}$ ,  $5 \pm 1\% \text{ CO}_2$ ,  $90\% \pm 10\% \text{ RH}$ ). As negative and positive controls, the tissues were exposed to DPBS or 5% SDS, respectively. Three tissues were used per test material and controls. After the exposure, tissues were washed 15 times with DPBS, blotted in a sterile blotting paper, dried with a sterile cotton-tipped swab, transferred to a 6-well plate with 0.9 mL culture medium and incubated at optimal conditions for  $24 \pm 2$  h. Finally, the culture medium was removed, fresh medium was added, and the tissues were subsequently incubated again for  $18 \pm 2$  h at optimal conditions.

---

Tissue viability after exposure to the sensors was determined using the MTT viability assay, following procedures described in the OECD guideline Test Nº 439. At the end of the  $18 \pm 2$  h incubation, the tissues were transferred to a 24-well plate containing 0.3 mL of a MTT solution at  $1 \text{ mg mL}^{-1}$ , and incubated for 3 h at optimal conditions. After this step, tissues were rinsed twice with DPBS, and formazan crystals were solubilized by adding 2 mL of isopropanol (MTT-100-EXT) for 2 h at RT with agitation. At the end of the extraction period, tissues were pierced with an injection needle, and the extract ran into the well from which the insert was taken. Afterwards, the tissues were discarded, and the extraction solutions were homogenized and transferred to a 96-well plate. Tissue viability is reported as % of negative control, measuring the OD of each isopropanol extract in duplicate at 570 nm by using a plate reader (BioTek Synergy HT). Isopropanol alone was used as a blank. The viability % of each tissue was calculated relative to negative control using the following equation:

$$\% \text{ Viability tissue} = [\text{ODtissue} / \text{Mean ODNC}] \times 100\% \quad (\text{eq.1})$$

#### *2.8. Tests with subjects. Proof of concept*

The tests with COVID patients and controls were authorized by the bioethics committee of the University of Burgos on April 22, 2022 (Ref. IO 05/2022). All the participants in this study were informed of the entire procedure and signed an informed consent document. Due to the restrictions, and the responsibility we had with a virus as harmful as SARS-CoV-2, we decided the patients themselves would pick up the kit, and carry out the tests at home.

This study was conducted with 26 subjects (14 men and 12 women). Among the participants, there were 15 patients (mild symptoms or asymptomatic patients) and 11 controls confirmed with antigen tests. The age range was from 23 to 69 years, and the tests were performed between 1 and 7 days after the first symptoms, or first positive result with PCR/antigen test.

All tests were performed between 8:00 p.m. and 9:00 p.m., and for security reasons, they were not collected and analyzed until 12 hours later. The

---

participants did not eat, drink or smoke during the 10 min before the test, and they first performed an antigen test on themselves (Boson Biotech, Hotgen, or Deepblue). They then discarded a saliva sample and placed four separate saliva samples over four sensory labels (2 made with copolymer 1, and another 2 with copolymer 2) contained in 2 Petri dishes, so that the discs looked completely covered by saliva. This step was done without forcing a cough, or a tear in the throat, just spitting up naturally. The Petri dishes remained open overnight, and finally, saliva excess was removed with a tissue, and the Petri dishes were sealed with parafilm.

Since the patients kept the tests during the first 12 h, in this case, we could not follow the response of the material with a fluorimeter. However, as it is a visual sensor, photographs of all the sensory labels were taken once received under 365 nm light illumination, always in the same dark room, and always replicating the same lighting conditions, since the photographs were taken on different days. For that, two lamps were placed at 23 cm from the discs and at a 45-degree angle. The smartphone was placed at 20 cm from the disks without tilting. However, from the final user's point of view (1 single photo), it is unnecessary to be so careful with the lighting conditions. It is only required to see the difference in fluorescence between the positive and negative control with the naked eye and take the photo under these conditions.

Each photo contained 3 discs, a positive control, a negative control, and the test disc, and the measurements were carried out by duplicate. G parameter (from RGB digital colour space) were extracted from discs in photographs using the smartphone app "Colorimetric Titration", and the G parameters of the negative and positive control were assigned as 0 and 100 G%, respectively. Thus,  $G_{test}\%$  values were obtained with the following equation:

$$G_{test}\% = (G_{test} - G_{neg}) / (G_{pos} - G_{neg}) \times 100 \quad (\text{eq.2})$$

In this way, values above 55 were considered positive tests for COVID, while values below 45 were considered negative. The range between 45-55 G% was considered borderline and would require a repeat test.

---

### 2.9. Selectivity/specifity study

To study the substrate specificity for Mpro SARS-CoV-2 of our sensory labels two analyses were performed. Similarity matrix percentage and multiple alignments of amino acid sequences from 3CL proteases of different human coronaviruses were performed using MUSCLE program [20], and displayed by ESPript 3.0 web server [21]. In addition, a phylogenetic tree was obtained from Phylogeny.fr software [22]. Amino acid sequences of Mpro or 3CL protease from human coronaviruses were obtained from NCBI database (SARS-CoV: pdb|3V3M|A; SARS-CoV-2: YP\_009742612.1; MERS-CoV: pdb|7D3C|A; HCoV-OC43: YP\_009924323.1; HCoV-HKU1: YP\_009944273.1; HCoV-NL63: pdb|7E6R|A and HCoV-229E: AGT21366.1).

Then, *in vitro* analyses were developed to determine the kinetic parameters of the Mpro 3CL proteases from SARS-CoV-2 and MERS-CoV. These parameters were determined using different substrate concentrations ranging from 2.5 to 40  $\mu$ M and 100 nM of the respective enzyme in a final volume of 100  $\mu$ l. Initial velocities were determined from the linear part of the curve and converted to the amount of hydrolysed substrate per unit of time ( $\mu$ M/min). Kinetic parameters were obtained using the Michaelis-Menten equation in OriginPro Program software. Edans standard curve was performed using known amounts (0-40  $\mu$ M) in reaction buffer 20 mM Tris-HCl pH 7.3, 100 mM NaCl, 1 mM EDTA, 1 mM DTT and the fluorescence was measured at 30 °C using an excitation filter of 360/40 nm and an emission filter of 460/40 nm.

To study the *in vitro* functionality and selectivity, a 6 mm diameter of the sensory labels 1 and 2 discs were placed at the bottom of 96-well plates and 20  $\mu$ l of 0.5  $\mu$ M solution of Mpro from SARS-CoV-2 and MERS-CoV in 20 mM Tris-HCl pH 7.3, 100 mM NaCl, 1 mM EDTA, 1 mM DTT buffer were added. Fluorescence was recorded at 30 and 60 minutes after enzyme addition.

---

### 3. Results and discussion

#### 3.1. Characterization of copolymers

The four synthesized copolymers were characterized by infrared spectroscopy,  $^1\text{H}$  and  $^{13}\text{C}$  nuclear magnetic resonance, thermogravimetric analysis, differential scanning calorimetry, and powder X-ray diffraction. As shown in **SI-Section S2**, copolymers 1 and 2 show aromatic proton signals between 6.2 and 6.8 ppm in the  $^1\text{H-NMR}$  spectra, confirming the presence of aniline side groups in the polymer structure. On the other hand,  $^{13}\text{C-NMR}$  and FT-IR spectra show typical signals of random copolymers prepared with 1-vinyl-2-pyrrolidone and methyl methacrylate. FT-IR spectra of copolymers 2 and 4 (MMA 95 mol%) contain typical peaks of PMMA at  $1718$  and  $1138\text{ cm}^{-1}$ , assigned to C=O stretching and -O-CH<sub>3</sub> stretching vibrations, respectively [23]. Signals related to PVP are only appreciable at FT-IR spectra of copolymer 1 and 3, in which the broad band assigned to the O-H stretching vibration can be shown between  $3060 - 3703\text{ cm}^{-1}$ , probably related to water molecules associated with the copolymer's hydrophilicity [24]. Other characteristic peaks of PVP can also be seen at  $1665\text{ cm}^{-1}$  (carbonyl group), and at  $1021\text{ cm}^{-1}$  (C-N stretching) [25].

The most relevant information came from the PXRD and the polymers' thermal analysis. Thus, the PXRD spectra indicate that the separation between chains is not affected by the introduction of the aniline side groups in the polymer structure since the values of  $2\theta_{\text{MAX}}$  do not vary significantly. In the same way, concerning thermal analysis, copolymers 1 and 3 do not present significant differences in the values of  $T_5$ ,  $T_{10}$  and  $T_g$ . However, copolymer 2 has  $T_5$  and  $T_{10}$  values  $16$  and  $12\text{ }^\circ\text{C}$  higher than copolymer 4, respectively. Therefore, our interpretation is that adding aniline groups improves the interaction between chains through H bonds with the carbonyl groups of the rest of the comonomers, which improves the material's thermal properties. This can also be seen in the behaviour of the  $T_g$ , which increases  $5\text{ }^\circ\text{C}$  when only 0.5% mol of vinylaniline is introduced in the copolymer formulation.

---

### 3.2. Response time and storage stability of sensory labels

Fluorescence emission was measured at a fixed wavelength, and three replicates were performed for each measurement in 96-well plates to obtain statistically robust data, and the fluorescence data were transformed into enzymatic activity data through the following equation:

$$RFUS = F_{\text{sensor+enzyme}} - F_{\text{sensor}} \text{ (eq.3),}$$

where “RFUs” are the relative fluorescence units, and “F” is the emitted fluorescence.

The enzyme tests that were carried out with the sensory labels showed that an OFF-ON fluorescence process occurs when exposed to the Mpro enzyme, as shown in Figure 2a. The system reached equilibrium 180 min after the enzyme addition for all sensory labels except the N°3, in which the response time was 30 min. However, after half an hour, the response is intense enough to be detected with the naked eye. These experiments were performed with an enzyme concentration of 0.5 μM, but the LODs of the sensory labels 1 and 2 are 0.177 μM (6.018 μg/mL) and 0.396 μM (13.4 μg/mL), respectively.

The stability study (Figure 2b) showed that sensory labels with covalently anchored substrates, such as sensory label 1, have a longer shelf-life and remain suitable for at least two months after preparation (black line). However, as we have shown in previous works [26], this stability is not exhibited when using labels with substrate dispersed (not covalently anchored, as sensory label 3), showing the same behaviour as the free peptide substrate (green and pink lines, respectively). Additionally, results for sensory labels 2 and 4 were equivalent. Therefore, our interpretation is that the polymeric chains exert a protective effect only on the covalently anchored substrates. This fact is one of the novel keys of this study since this kind of substrates are usually unstable, so they are not used in the preparation of sensory materials.

### 3.3. Cytotoxicity assays

*In vitro* EpiDerm™ skin irritation test (MatTek) is a test compliant with the OECD

Test Guideline (TG) No. 439 to evaluate the skin irritation potential of the test chemicals in the context of identification and classification of skin irritation hazards according to the EU and Classification Harmonized System of Classification and Labelling Chemicals, GHS, (R38 / Category 2 or no label). Thus, an irritant is predicted if the mean relative tissue viability of three individual tissues exposed to the test substance is reduced below 50% of the mean viability of the negative controls.

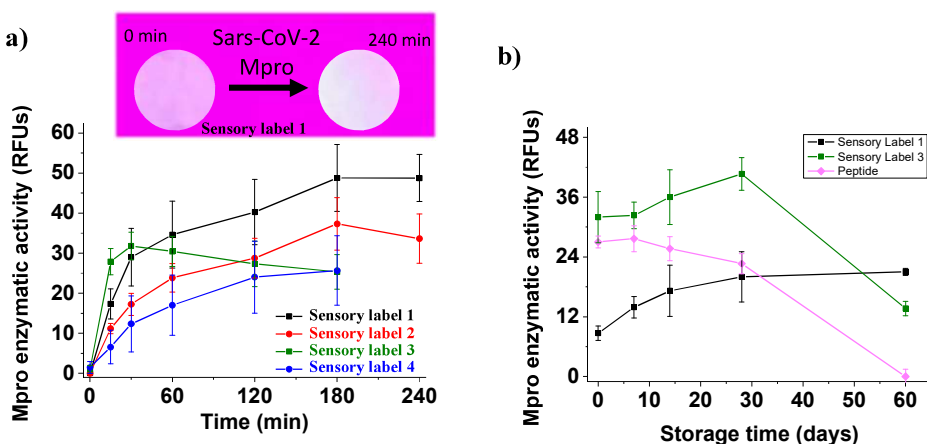


**Figure 2.** Enzyme tests carried out in 96-well plates, including a 6 mm diameter sensory label at the bottom of each well and 20  $\mu$ L of a 0.5  $\mu$ M solution of Mpro in 20 mM Tris-HCl pH 7.3, 100 mM NaCl, 1 mM EDTA, 1 mM DTT buffer. Experimental conditions: temperature = 30°C,  $\lambda_{\text{ex}} = 360$  nm,  $\lambda_{\text{em}} = 460$  nm, excitation slit = 40 nm, emission slit = 40 nm. (a) Response time study of sensory labels 1-4, by monitoring the fluorescence at 15, 30, 60, 120, 180, and 240 min; image of a sensory label 1 before and after interaction with Mpro. (b) Storage stability study of sensory labels 1, 3 and free peptide by measuring the fluorescence response at 60 min after 1, 7, 14, 28 and 60 days of storage using zip bags. Data are means  $\pm$  standard error of 3 independent replicates.

As shown in Figure 3, sensory labels 1 and 2 did not reduce the viability by over 50% when compared with the controls. Therefore, according to the EU and Globally Harmonized System of Classification and Labelling Chemicals, GHS, (R38/ Category 2 or no label), none of them could be considered irritants in the conditions tested.

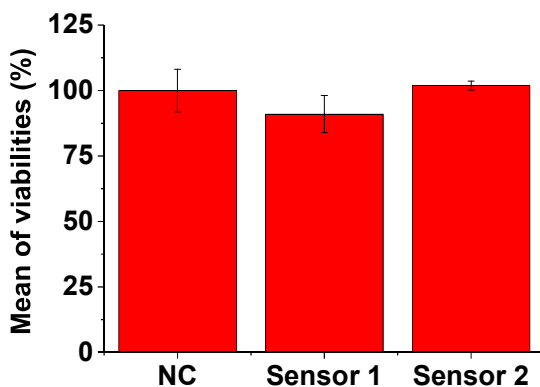


**Figure 3.** EpiDerm™ tissues were exposed to sensory labels 1 and 2 for 1 h. The viability was analysed by MTT assay, and it is expressed as a percentage of negative control. Data represented the mean  $\pm$  standard error of 3 independent replicates. Differences were established using a one-way ANOVA followed by a multiple comparisons test (Tukey test) and considered significant when  $p \leq 0.05$ . The same letter indicates no significant differences between treatments

### 3.4. Selectivity/Specificity of the sensory labels

The most common human respiratory viruses are influenza A and B, syncytial, rhinoviruses, adenoviruses, and coronaviruses. Among them, only rhinoviruses and coronaviruses use their 3C-like proteases to replicate [27]. However, the 3C-like proteases of rhinoviruses only have a 20% homology with the protease studied in this work, they recognize a substantially different peptide sequence (LEVLFQ/GP) than that of the SARS-CoV-2, and their active site is made up of three amino acids instead of two as is the case of coronaviruses [28–30]. Therefore, the specificity and selectivity studies were carried out with viruses from the coronaviruses group.

Seven human coronaviruses (HCoV) have been described until now, the endemic viruses HCoV-OC43, HCoV-229E, HCoV-NL63, HCoV-HKU1 and the epidemic viruses MERS-CoV, SARS-CoV, and SARS-CoV-2. HCoV-OC43 and HCoV-229E are included in the alphacoronaviruses genera, while HCoV-NL63, HCoV-HKU1, MERS-CoV, SARS-CoV, and SARS-CoV-2 are members of the

betacoronaviruses genera [31,32].

To study the specificity of our labels, the encoding amino acid sequences of the 3C-like proteases of these seven coronaviruses were obtained and aligned. Figure S8 (**SI-Section S3**) summarizes the multiple alignment results, showing the highly conserved residues of the catalytic site of the proteases (blue), the strictly equal residues in all the sequences (red), and the residues belonging to the same group of amino acids (yellow). The residues of catalytic site (blue) and those around them (red) are conserved, although their positions are slightly displaced. For instance, while in SARS-CoV and SARS-CoV-2 this catalytic dyad is located at residues Hys41 and Cys145, in MERS-CoV it is located at residues Hys41 and Cys148 [33].

The results of the identity matrix (Table S1, **SI-Section S3**) show that the alpha genera viruses are those with the lowest degree of conservation and, therefore, the lowest similarity with the rest of the coronaviruses. Consequently, on the one hand, we can conclude that the amino acid sequences of the 3C-like protease of SARS-CoV-1 and SARS-CoV-2 are practically identical (96.08% of similarity). On the other hand, the similarity between SARS-CoV-2 and MERS-CoV is quite lower (~50%), and even lower when comparing SARS-CoV-2 with the rest of the coronaviruses as previously reported [12,33]. The phylogenetic tree analysis also supports these results, in which coronaviruses are sorted by genera (**Figure S9, SI-Section S3**). SARS coronaviruses 1 and 2 have evolved separately from the rest of the betacoronaviruses. In fact, the MERS-CoV, HCoV-HKU1 and HCoV-OC43 viruses seem to have the same evolutionary origin, highly influenced by their zoonotic origin (from animals to humans), and definitively they have evolved differently and have adapted to their new niche [32,33].

Accordingly, we performed the enzymatic analyses summarized in Table S2 (**SI-Section S4**), showing the kinetic parameters obtained for Mpro 3CL proteases from SARS-CoV-2 and MERS-CoV using the substrate Dabcyl-KTSAVLQSGFRKME-Edans. As expected,  $K_m$  of the Mpro from SARS-CoV-2 is lower than  $K_m$  of the Mpro from MERS-CoV, i.e.,  $43.02 \pm 3.23 \mu\text{M}$  and  $117.06 \pm$

---

10.61  $\mu$ M values, respectively. This parameter indicates that the Mpro-SARS-CoV-2 presents a higher affinity for the substrate than Mpro-MERS-CoV. In addition, the Mpro-MERS-CoV's enzymatic efficiency (Kcat/KM) is remarkably lower than the Mpro-SARS-CoV-2, confirming our *in silico* studies and previous reports from other authors [12,33,34].

Regarding the tests with sensory labels, the Mpro-SARS-CoV-2 has higher activity than the Mpro-MERS-CoV, which means a higher fluorescence emission when performing fluorescence analysis in the microplate reader, and also higher visual response with the naked eye, as shown in Figure S10.

### *3.5. Proof of concept. Saliva test with 26 subjects (15 patients and 11 controls)*

This study was carried out with 26 subjects, 15 COVID patients, and 11 controls. It is a relatively small number to be considered a medical study, but large enough for a work in which the main claim and novelty is the strategy of preparing these new virus sensors straightforwardly, only anchoring a fluorogenic peptide substrate to a polymer and then using this sensory polymer as a coating for paper.

For example, Figure 4 shows the results of Subject #4 (asymptomatic), who tested positive for COVID with the antigen test and our sensory labels 1 and 2. The figures for the rest of the subjects are included in the **SI-Section S5**.

The COVID patients generated fluorescence in the sensory labels to the naked eye, while the negative cases did not. To assign a numerical value to that response, the digital colour of each label was analysed in two different digital colour spaces (RGB and HSV), and we found G parameter from the RGB colour space was the one that best distinguishes between patients and controls.

Considering the G parameter of the negative control as 0 G%, and the G parameter of the positive control as 100 G%, Subject #4 gave a G% result greater than 55 (75 G% for sensory label 1 and 157 G% for sensory label 2), so the result was positive for COVID in line with the antigen test. Table 2 shows the results for all subjects.

---

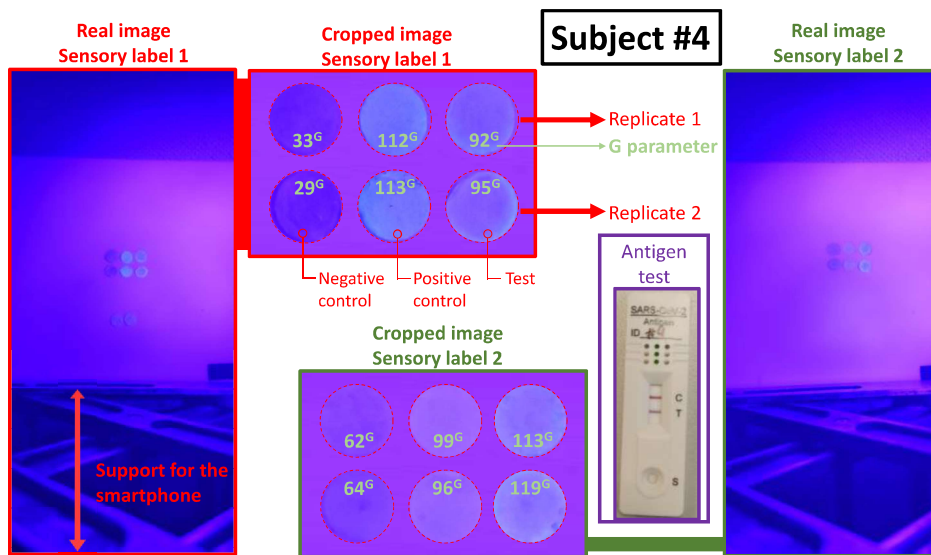


**Figure 4.** Results for Subject #4 testing with sensory label coated with copolymer 1 (sensory label 1), sensory label coated with copolymer 2 (sensory label 2), and antigen test. The image shows the real photograph and the cropped image. Each photo contains 2 negative controls, 2 positive controls, and 2 replicates.

The risk of making a mistake in the experimental procedure was high and difficult to control since all the responsibility lies within the participants. Despite this, our sensory label 1 and the used antigen tests provided the same result in 21 of the 26 cases (81%), which suggests that our proposed idea can be a leading methodology for the industrial production of this type of sensors in the short term. Furthermore, from a comparative point of view, the success rate of self-testing antigen tests is 82.5% [35], very similar to the result obtained with our material.

Sensory label 1 has better results than sensory label 2 (85% match with antigen test versus 65%). Our interpretation is that the greater hydrophilicity of copolymer 1 makes the environment generated for the reaction with the Mpro enzyme more appropriate. Regarding the non-satisfactory results of sensory label 1, we must underline that result for subject #17 is on the borderline, that is, the subject should have repeated the test. The other four unsuccessful cases are one false positive (subject#8) and three false negatives (subjects #13, #14 and

#20). In the case of the false positive, he/she presented symptoms compatible with COVID, and therefore there may be interference with some other rhinovirus. This interference problem can be addressed by increasing the length of the substrate peptide, i.e., making it much more specific for Mpro. Regarding the false negatives, we believe some other substance in the saliva may be quenching the fluorescent signal through deactivation processes. We think that this could be improved by including a tooth and tongue brushing 10 min before the test, but in our case could not be carried out since it is contraindicated in many of the antigen tests.

**Table 2.** Results of the study with 26 subjects, testing COVID with sensory label 1, sensory label 2, and antigen test. The table shows the mean  $\pm$  standard error of 2 replicates of the G% extracted from photographs, and calculated with the equation  $G_{\text{test}}\% = (G_{\text{test}} - G_{\text{neg}}) / (G_{\text{pos}} - G_{\text{neg}}) \times 100$  (eq.3)

Subject	Sensory Label	G parameter (%)	G <sub>test</sub> % [Neg. < 45-55% > Pos.]	Antigen test result	Conclusion
#1	1	6.04 $\pm$ 4.67	NEGATIVE	NEGATIVE	Match
#2		81.04 $\pm$ 6.88	POSITIVE	POSITIVE	Match
#3		97.27 $\pm$ 1.89	POSITIVE	POSITIVE	Match
#4		74.90 $\pm$ 1.26	POSITIVE	POSITIVE	Match
#5		117.76 $\pm$ 5.29	POSITIVE	POSITIVE	Match
#6		59.28 $\pm$ 1.57	POSITIVE	POSITIVE	Match
#7		36.44 $\pm$ 5.33	NEGATIVE	NEGATIVE	Match

Subject	G parameter (%)	G <sub>test</sub> % [Neg. < 45-55% > Pos.]	Antigen test result	Conclusion
#8	66.38 ± 1.31	POSITIVE	NEGATIVE	False positive
#9	85.41 ± 3.22	POSITIVE	POSITIVE	Match
#10	92.59 ± 0.65	POSITIVE	POSITIVE	Match
#11	84.31 ± 2.45	POSITIVE	POSITIVE	Match
#12	90.05 ± 30.33	POSITIVE	POSITIVE	Match
#13	24.12 ± 14.91	NEGATIVE	POSITIVE	False negative
#14	-3.21 ± 30.73	NEGATIVE	POSITIVE	False negative
#15	59.84 ± 3.50	POSITIVE	POSITIVE	Match
#16	17.89 ± 2.44	NEGATIVE	NEGATIVE	Match
#17	49.16 ± 5.87	Borderline	POSITIVE	Repeat test
#18	44.12 ± 0.88	NEGATIVE	NEGATIVE	Match
#19	51.82 ± 3.96	NEGATIVE	NEGATIVE	Match

Subject		G parameter (%)	G <sub>test</sub> % [Neg. < 45-55% > Pos.]	Antigen test result	Conclusion
#20	2	24.92 ± 3.56	NEGATIVE	POSITIVE	False negative
#21		63.64 ± 7.88	POSITIVE	POSITIVE	Match
#22		40.46 ± 2.29	NEGATIVE	NEGATIVE	Match
#23		16.30 ± 6.79	NEGATIVE	NEGATIVE	Match
#24		-7.46 ± 3.59	NEGATIVE	NEGATIVE	Match
#25		-11.05 ± 7.93	NEGATIVE	NEGATIVE	Match
#26		-5.90 ± 7.87	NEGATIVE	NEGATIVE	Match
#1		28.63 ± 1.66	NEGATIVE	NEGATIVE	Match
#2	2	215.94 ± 0.48	POSITIVE	POSITIVE	Match
#3		236.45 ± 13.30	POSITIVE	POSITIVE	Match
#4		156.72 ± 8.96	POSITIVE	POSITIVE	Match
#5		184.54 ± 40.72	POSITIVE	POSITIVE	Match

Subject	G parameter (%)	G <sub>test</sub> % [Neg. < 45-55% > Pos.]	Antigen test result	Conclusion
#6	118.81 ± 1.98	POSITIVE	POSITIVE	Match
#7	121.13 ± 15.77	POSITIVE	NEGATIVE	False positive
#8	132.02 ± 14.20	POSITIVE	NEGATIVE	False positive
#9	153.85 ± 7.69	POSITIVE	POSITIVE	Match
#10	183.84 ± 7.07	POSITIVE	POSITIVE	Match
#11	118.50 ± 10.97	POSITIVE	POSITIVE	Match
#12	81.56 ± 5.00	POSITIVE	POSITIVE	Match
#13	77.62 ± 15.86	POSITIVE	POSITIVE	Match
#14	-3.90 ± 27.80	NEGATIVE	POSITIVE	False negative
#15	56.66 ± 4.64	Borderline	POSITIVE	Repeat test
#16	69.90 ± 1.03	POSITIVE	NEGATIVE	False positive
#17	61.52 ± 0.39	POSITIVE	POSITIVE	Repeat test

Subject	G parameter (%)	G <sub>test</sub> % [Neg. < 45-55% > Pos.]	Antigen test result	Conclusion
#18	-18.88 ± 23.08	NEGATIVE	NEGATIVE	Match
#19	-53.68 ± 2.94	NEGATIVE	NEGATIVE	Match
#20	40.85 ± 13.03	Borderline	POSITIVE	Repeat test
#21	43.16 ± 8.07	NEGATIVE	POSITIVE	False negative
#22	30.87 ± 0.97	NEGATIVE	NEGATIVE	Match
#23	56.15 ± 0.20	Borderline	NEGATIVE	Repeat test
#24	4.66 ± 5.06	NEGATIVE	NEGATIVE	Match
#25	16.19 ± 3.64	NEGATIVE	NEGATIVE	Match
#26	-45.91 ± 6.03	NEGATIVE	NEGATIVE	Match

#### 4. Conclusions

Early detection methods are essential tools against the spread of infectious diseases, as seen in the Severe Acute Respiratory Syndrome Coronavirus 2 (SARS-CoV-2) caused pandemic with the wide spread use of rapid and reliable immunoassay to qualitatively detect antibodies against the virus. Herein, we report on a strategy to prepare an easy-to-use protein function-based detection method using saliva of potentially infected people, based on peptide substrate containing a FRET pair (fluorophore and quencher) to detect the Mpro protein.

Specifically, we have chemically anchored the Mpro substrate to linear polymers with different hydrophilicity, and coated cellulose supports with it to prepare the sensory labels. Results show that the higher hydrophilicity of the copolymer, the higher performance of the sensory labels. Upon contacting the sensor with the saliva (Mpro is present in infected people, as demonstrated), the OFF-ON fluorescence response allows for the qualitative visual detection of the infection (LOD = 0.177 µM for sensory label 1). Moreover, a picture of the sensors provides a quantitative and statistical infection result. The advantages of these sensors are that they can be easily prepared, inexpensively, quickly, and in high quantities. Even more relevant is the proposed methodology that can be applied to detecting saliva or other body fluids and expired air for virus and bacterial infections.

## Open Data

Open Data is available at <https://riubu.udc.es/handle/10259/5684> (Dataset of the work "Lab-on-a-chip for the easy and visual detection of SARS-CoV-2 based on a sensory polymer").

## Supporting Information

Characterization of the fluorogenic peptide substrate for Mpro; characterization of polymers; amino acid sequence analyses of Mpro 3C-like main proteases of human coronaviruses; *in vitro* comparative analysis of Mpro-SARS-CoV-2 and Mpro-MERS-CoV; proof of concept with 26 participants; explanatory video.

The supporting information is available free of charge at:

<https://ars.els-cdn.com/content/image/1-s2.0-S0925400522018081-mmc1.pdf>

## Competing interests

The authors declare no competing interests.

## Acknowledgements

We gratefully acknowledge the financial support provided by all funders. Author

---

Saul Vallejos coordinates the project leading to these results, which has received funding from "La Caixa" Foundation, under agreement LCF/PR/PR18/51130007. This work was supported by the Regional Government of Castilla y León (Junta de Castilla y León) and by the Ministry of Science and Innovation MICIN and the European Union NextGenerationEU PRTR. Author Jose Miguel García received grant PID2020-113264RB-I00 funded by MCIN/AEI/ 10.13039/501100011033 and by "ERDF A way of making Europe". Ana Arnaiz received funding from Ministerio de Universidades-European Union in the frame of NextGenerationEU RD 289/2021 (Universidad Politécnica de Madrid). Finally, all the authors want to thank the support provided by City Hall of Villadiego "Ayuntamiento de Villadiego" when looking for participants for the proof of concept.

## References

- [1] F. Arroyo-Marioli, F. Bullano, S. Kucinskas, C. Rondón-Moreno, Tracking R of COVID-19: A new real-time estimation using the Kalman filter, PLoS One. 16 (2021) e0244474. <https://doi.org/10.1371/JOURNAL.PONE.0244474>.
  - [2] University of Oxford, COVID-19 Data Explorer, (2022). <https://ourworldindata.org/explorers/coronavirus-data-explorer> (accessed March 7, 2022).
  - [3] T. Hale, N. Angrist, R. Goldszmidt, B. Kira, A. Petherick, T. Phillips, S. Webster, E. Cameron-Blake, L. Hallas, S. Majumdar, H. Tatlow, A global panel database of pandemic policies (Oxford COVID-19 Government Response Tracker), Nat. Hum. Behav. 5 (2021) 529–538. <https://doi.org/10.1038/S41562-021-01079-8>.
  - [4] Y. Artik, M.S. Kurtulmus, N.P. Cesur, S.Z. Mart Komurcu, C. Kazezoglu, A. Kocatas, Clinic Evaluation of The Destrovir Spray Effectiveness in SARS-CoV-2 Disease, Electron. J. Gen. Med. 19 (2022) em357. <https://doi.org/10.29333/EJGM/11578>.
  - [5] Q. Fernandes, V.P. Inchakalody, M. Merhi, S. Mestiri, N. Taib, D. Moustafa Abo El-Ella, T. Bedhiafi, A. Raza, L. Al-Zaidan, M.O. Mohsen, M.A. Yousuf Al-Nesf, A.A. Hssain, H.M. Yassine, M.F. Bachmann, S. Uddin, S. Dermime, Emerging COVID-19 variants and their impact on SARS-CoV-2 diagnosis, therapeutics and vaccines, Ann. Med. 54 (2022) 524–540. <https://doi.org/10.1080/07853890.2022.2031274>.
  - [6] M. Diao, L. Lang, J. Feng, R. Li, Molecular detections of coronavirus: current and emerging methodologies, Expert Rev. Anti. Infect. Ther. 20
-

- (2022) 199–210. <https://doi.org/10.1080/14787210.2021.1949986>.
- [7] H. Chen, S.G. Park, N. Choi, H.J. Kwon, T. Kang, M.K. Lee, J. Choo, Sensitive Detection of SARS-CoV-2 Using a SERS-Based Aptasensor, *ACS Sensors.* 6 (2021) 2378–2385. <https://doi.org/10.1021/ACSSENSORS.1C00596>.
- [8] Y. Jiang, M. Hu, A.A. Liu, Y. Lin, L. Liu, B. Yu, X. Zhou, D.W. Pang, Detection of SARS-CoV-2 by CRISPR/Cas12a-Enhanced Colorimetry, *ACS Sensors.* 6 (2021) 1086–1093. <https://doi.org/10.1021/ACSSENSORS.0C02365>.
- [9] A.N. Baker, S.J. Richards, S. Pandey, C.S. Guy, A. Ahmad, M. Hasan, C.I. Biggs, P.G. Georgiou, A.J. Zwetsloot, A. Straube, S. Dedola, R.A. Field, N.R. Anderson, M. Walker, D. Grammatopoulos, M.I. Gibson, Glycan-Based Flow-Through Device for the Detection of SARS-CoV-2, *ACS Sensors.* 6 (2021) 3696–3705. <https://doi.org/10.1021/ACSSENSORS.1C01470>.
- [10] C.J. Kuo, Y.H. Chi, J.T.A. Hsu, P.H. Liang, Characterization of SARS main protease and inhibitor assay using a fluorogenic substrate, *Biochem. Biophys. Res. Commun.* 318 (2004) 862–867. <https://doi.org/10.1016/J.BBRC.2004.04.098>.
- [11] L. Fu, F. Ye, Y. Feng, F. Yu, Q. Wang, Y. Wu, C. Zhao, H. Sun, B. Huang, P. Niu, H. Song, Y. Shi, X. Li, W. Tan, J. Qi, G.F. Gao, Both Boceprevir and GC376 efficaciously inhibit SARS-CoV-2 by targeting its main protease, *Nat. Commun.* 11 (2020) 1–8. <https://doi.org/10.1038/s41467-020-18233-x>.
- [12] C. Ma, M.D. Sacco, B. Hurst, J.A. Townsend, Y. Hu, T. Szeto, X. Zhang, B. Tarbet, M.T. Marty, Y. Chen, J. Wang, Boceprevir, GC-376, and calpain inhibitors II, XII inhibit SARS-CoV-2 viral replication by targeting the viral main protease, *Cell Res.* 30 (2020) 678–692. <https://doi.org/10.1038/s41422-020-0356-z>.
- [13] M.A.T. van de Plassche, M. Barniol-Xicota, S.H.L. Verhelst, Peptidyl Acyloxymethyl Ketones as Activity-Based Probes for the Main Protease of SARS-CoV-2, *ChemBioChem.* 21 (2020) 3383–3388. <https://doi.org/10.1002/CBIC.202000371>.
- [14] Q. Hu, Y. Xiong, G.-H. Zhu, Y.-N. Zhang, Y.-W. Zhang, P. Huang, G.-B. Ge, Y. Xiong contributed equally, The SARS-CoV-2 main protease (Mpro): Structure, function, and emerging therapies for COVID-19, *MedComm.* 3 (2022) e151. <https://doi.org/10.1002/MCO2.151>.
- [15] M.D. Sacco, C. Ma, P. Lagarias, A. Gao, J.A. Townsend, X. Meng, P. Dube, X. Zhang, Y. Hu, N. Kitamura, B. Hurst, B. Tarbet, M.T. Marty, A. Kolocuris, Y. Xiang, Y. Chen, J. Wang, Structure and inhibition of the SARS-CoV-2 main protease reveal strategy for developing dual inhibitors against Mpro and cathepsin L, *Sci. Adv.* 6 (2020).

- [https://doi.org/10.1126/SCIAADV.ABE0751/SUPPL\\_FILE/ABE0751\\_SM.PDF](https://doi.org/10.1126/SCIAADV.ABE0751/SUPPL_FILE/ABE0751_SM.PDF).
- [16] L. Zhang, D. Lin, X. Sun, U. Curth, C. Drosten, L. Sauerhering, S. Becker, K. Rox, R. Hilgenfeld, Crystal structure of SARS-CoV-2 main protease provides a basis for design of improved  $\alpha$ -ketoamide inhibitors, *Science* (80-. ). 368 (2020) 409–412. [https://doi.org/10.1126/SCIENCE.ABB3405/SUPPL\\_FILE/PAPV2.PDF](https://doi.org/10.1126/SCIENCE.ABB3405/SUPPL_FILE/PAPV2.PDF).
- [17] M. Cully, A tale of two antiviral targets - and the COVID-19 drugs that bind them, *Nat. Rev. Drug Discov.* 21 (2022) 3–5. <https://doi.org/10.1038/d41573-021-00202-8>.
- [18] N. Komatsu, K. Aoki, M. Yamada, H. Yukinaga, Y. Fujita, Y. Kamioka, M. Matsuda, Development of an optimized backbone of FRET biosensors for kinases and GTPases, *Mol. Biol. Cell.* 22 (2011) 4647–4656. <https://doi.org/10.1091/mbc.E11-01-0072>.
- [19] R.F.H. Dekker, Immobilization of a lactase onto a magnetic support by covalent attachment to polyethyleneimine-glutaraldehyde-activated magnetite, *Appl. Biochem. Biotechnol.* 22 (1989) 289–310. <https://doi.org/10.1007/BF02921763>.
- [20] R.C. Edgar, MUSCLE: A multiple sequence alignment method with reduced time and space complexity, *BMC Bioinformatics.* 5 (2004) 1–19. <https://doi.org/10.1186/1471-2105-5-113/FIGURES/16>.
- [21] X. Robert, P. Gouet, Deciphering key features in protein structures with the new ENDscript server, *Nucleic Acids Res.* 42 (2014) W320–W324. <https://doi.org/10.1093/NAR/GKU316>.
- [22] A. Dereeper, V. Guignon, G. Blanc, S. Audic, S. Buffet, F. Chevenet, J.F. Dufayard, S. Guindon, V. Lefort, M. Lescot, J.M. Claverie, O. Gascuel, Phylogeny.fr: robust phylogenetic analysis for the non-specialist, *Nucleic Acids Res.* 36 (2008) W465–W469. <https://doi.org/10.1093/NAR/GKN180>.
- [23] S. Ramesh, K.H. Leen, K. Kumutha, A.K. Arof, FTIR studies of PVC/PMMA blend based polymer electrolytes, *Spectrochim. Acta - Part A Mol. Biomol. Spectrosc.* 66 (2007) 1237–1242. <https://doi.org/10.1016/j.saa.2006.06.012>.
- [24] K. Sreekanth, T. Siddaiah, N.O. Gopal, N.K. Jyothi, K.V. Kumar, C. Ramu, Thermal, Structural, Optical and Electrical Conductivity studies of pure and Mn<sup>2+</sup> doped PVP films, *South African J. Chem. Eng.* 36 (2021) 8–16. <https://doi.org/10.1016/j.sajce.2020.09.003>.
- [25] E. Alver, A. Metin, H. Çiftçi, Synthesis and Characterization of Chitosan/Polyvinylpyrrolidone/Zeolite Composite by Solution Blending Method, *J. Inorg. Organomet. Polym. Mater.* 24 (2014) 1048–1054. <https://doi.org/10.1007/s10904-014-0087-z>.

- [26] A. Arnaiz, M. Guembe-García, E. Delgado-Pinar, A.J.M. Valente, S. Ibeas, J.M. García, S. Vallejos, The role of polymeric chains as a protective environment for improving the stability and efficiency of fluorogenic peptide substrates, *Sci. Rep.* 12 (2022) 8818. <https://doi.org/10.1038/s41598-022-12848-4>.
- [27] S. Weston, M.B. Frieman, *Respiratory Viruses, Encycl. Microbiol.* (2019) 85. <https://doi.org/10.1016/B978-0-12-801238-3.66161-5>.
- [28] Q. May Wang, S.-H. Chen, Human Rhinovirus 3C Protease as a Potential Target for the Development of Antiviral Agents, *Curr. Protein Pept. Sci.* 8 (2007) 19–27. <https://doi.org/10.2174/138920307779941523>.
- [29] D.A. Matthews, W.W. Smith, R.A. Ferre, B. Condon, G. Budahazi, W. Slsson, J.E. Villafranca, C.A. Janson, H.E. McElroy, C.L. Grabskov, S. Worland, Structure of human rhinovirus 3C protease reveals a trypsin-like polypeptide fold, RNA-binding site, and means for cleaving precursor polyprotein, *Cell.* 77 (1994) 761–771. [https://doi.org/10.1016/0092-8674\(94\)90059-0](https://doi.org/10.1016/0092-8674(94)90059-0).
- [30] M.G. Cordingley, P.L. Callahan, V. V. Sardana, V.M. Garsky, R.J. Colonna, Substrate requirements of human rhinovirus 3C protease for peptide cleavage in vitro, *J. Biol. Chem.* 265 (1990) 9062–9065. [https://doi.org/10.1016/S0021-9258\(19\)38811-8](https://doi.org/10.1016/S0021-9258(19)38811-8).
- [31] P. Zhou, X. Lou Yang, X.G. Wang, B. Hu, L. Zhang, W. Zhang, H.R. Si, Y. Zhu, B. Li, C.L. Huang, H.D. Chen, J. Chen, Y. Luo, H. Guo, R. Di Jiang, M.Q. Liu, Y. Chen, X.R. Shen, X. Wang, X.S. Zheng, K. Zhao, Q.J. Chen, F. Deng, L.L. Liu, B. Yan, F.X. Zhan, Y.Y. Wang, G.F. Xiao, Z.L. Shi, A pneumonia outbreak associated with a new coronavirus of probable bat origin, *Nature.* 579 (2020) 270–273. <https://doi.org/10.1038/s41586-020-2012-7>.
- [32] V.M. Corman, D. Muth, D. Niemeyer, C. Drosten, Hosts and Sources of Endemic Human Coronaviruses, *Adv. Virus Res.* 100 (2018) 163–188. <https://doi.org/10.1016/BS.AIVIR.2018.01.001>.
- [33] S. Tomar, M.L. Johnston, S.E. St. John, H.L. Osswald, P.R. Nyalapatla, L.N. Paul, A.K. Ghosh, M.R. Denison, A.D. Mesecar, Ligand-induced Dimerization of Middle East Respiratory Syndrome (MERS) Coronavirus nsp5 Protease (3CLpro), *J. Biol. Chem.* 290 (2015) 19403–19422. <https://doi.org/10.1074/jbc.m115.651463>.
- [34] X.Y. Zhang, Y.Y. Zhang, X.G. Zhang, X. Liu, M. Chen, F. Liu, D.Z. Zhang, P.X. Ling, Research progress of new coronavirus SARS-CoV-2 detection technology, *Prog. Biochem. Biophys.* 47 (2020) 275–285. <https://doi.org/10.16476/J.PIBB.2020.0060>.
- [35] A.K. Lindner, O. Nikolai, C. Rohardt, F. Kausch, M. Wintel, M. Gertler, S. Burock, M. Hörig, J. Bernhard, F. Tobian, M. Gaeddert, F. Lainati, V.M. Corman, T.C. Jones, J.A. Sacks, J. Seybold, C.M. Denkinger, F.P.

Mockenhaupt, Diagnostic accuracy and feasibility of patient self-testing with a SARS-CoV-2 antigen-detecting rapid test, *J. Clin. Virol.* 141 (2021) 104874. <https://doi.org/10.1016/J.JCV.2021.104874>.



## CAPÍTULO 3

# Polímeros sensores en seguridad y control documental

---

En este capítulo se describe brevemente las motivaciones que condujeron al desarrollo de un polímero sensor para el control documental, la lucha contra las falsificaciones y el fraude. Seguidamente, se evalúan los requisitos que debe tener el material propuesto para su posible implementación y se describe la composición y funcionamiento del mismo. Finalmente, el capítulo concluye con los resultados obtenidos, que se muestran con la transcripción íntegra del artículo publicado en *ACS Applied Materials and Interfaces* junto con el justificador de solicitud de patente internacional en conjunto con la Universidad de Coimbra y la empresa *The Navigator Company*.

---

### 3.1. Introducción

El número de casos de falsificaciones se está incrementando en los últimos años. De hecho, se estima que la cantidad económica global asciende hasta los 650 mil millones de dólares al año.<sup>84</sup> Este aumento se correlaciona en cierta medida con el ascenso de las compra-ventas digitales. En este tipo de acuerdos normalmente existe una distancia entre el comprador y vendedor y, además, se efectúa el pago con antelación, lo que provoca unas condiciones idóneas para este tipo de fraudes. Por otro lado, pese a que nuestra sociedad cada vez está más digitalizada, la mayoría de los organismos y administraciones públicas

---

<sup>84</sup> N. Katumo, K. Li, B.S. Richards, I.A. Howard, *Sci. Rep.* **2022**, 12, 1–14.

---

siguen recibiendo a diario paquetes que en la mayoría de las ocasiones contienen datos confidenciales. Lamentablemente, delincuentes y diferentes grupos terroristas han aprovechado esta rutina de embajadas, ministerios, subdelegaciones de gobierno, etc., para llevar a cabo ataques en forma de paquetes bomba.

Todas estas circunstancias ponen de manifiesto la necesidad de desarrollar soluciones simples que puedan aplicarse de manera cotidiana y mediante procesos sencillos. Los detectores de metales y las cintas de rayos X, por ejemplo, a menudo son eludidos por los delincuentes, incluso en edificios protegidos. En el caso de los paquetes enviados entre particulares o las compras por internet, el destinatario del paquete no cuenta con más protección que la etiqueta del remitente, que puede falsificarse con facilidad.

En esta sección de la tesis, se detalla el trabajo cuyo objetivo fue el desarrollo de un material inteligente que abordara esta problemática. Antes de proceder con el diseño y la concepción del material, se establecieron los requisitos necesarios que se enumeran a continuación, para que la solución fuera potencialmente aplicable y sin que se viera afectada por un coste económico inalcanzable o por la necesidad de conocimientos técnicos avanzados.

- **Viabilidad en la implementación:** es crucial que la introducción de este material y/o técnica en el mercado sea sencilla y viable. El sector de la paquetería ya cuenta con procesos de fabricación establecidos, y cualquier solución propuesta debe adaptarse a ellos sin implicar grandes cambios.
  - **Bajo coste:** en la industria de la paquetería los márgenes económicos son muy ajustados. El embalaje debe ser una solución de transporte o protección para el contenido real del producto (alimento, artículo, etc.), y no puede incrementar en exceso el coste total. Por tanto, cualquier solución propuesta debe ser asequible y tener un coste razonable.
  - **Sencillez para el usuario:** es fundamental que el nuevo método o
-

tecnología sea fácil de utilizar para el usuario final, ya que de lo contrario podría provocar errores, confusión e incertidumbre.

Teniendo en cuenta todos los requisitos y el objetivo final del material, una opción viable y razonable es el uso de recubrimientos poliméricos inteligentes. Por ejemplo, se pueden incorporar fácilmente en uno de los componentes más comunes de los paquetes: las etiquetas. Estas etiquetas se utilizan para incluir datos y direcciones, y generalmente están hechas de papel. Por lo tanto, es viable realizar un recubrimiento de polímeros inteligentes mediante técnicas como el recubrimiento por goteo o por pulverización. Además, si se utiliza un polímero termoplástico, en las condiciones adecuadas éste podría separarse del papel una vez que se haya utilizado, lo que estaría en línea con facilitar el reciclaje y la economía circular del producto.

En cuanto a la funcionalidad real de este recubrimiento inteligente, la primera opción siempre fue que se produjera un cambio de color en la etiqueta cuando el destinatario recibiera el paquete. Sería algo similar al revelado de una fotografía, en el que la etiqueta tendría varias zonas reactivas que, en presencia de un revelador, cambiarían de color en un orden y posición determinados. En el fondo, esta funcionalidad es muy parecida a la de los polímeros colorimétricos o fluorimétricos, pero al revés. Desde el enfoque de un material sensor, un solo polímero inteligente reacciona ante uno o varios analitos generando colores diferentes. Sin embargo, en nuestra etiqueta, varios polímeros inteligentes reaccionan ante la misma especie produciendo diferentes colores.

De hecho, se diseñaron los polímeros inteligentes en base a un polímero sensor que el Grupo de Polímeros había desarrollado unos años atrás (**Figura 10a**). Este polímero sensor era capaz de detectar 12 compuestos fenólicos distintos, generando colores diferentes con cada uno de ellos.<sup>85</sup> En este caso, se sintetizaron 12 polímeros diferentes, que producían colores diferentes en

---

<sup>85</sup> S.E. Bustamante, S. Vallejos, B.S. Pascual-Portal, A. Muñoz, A. Mendiola, B.L. Rivas, F.C. García, J.M. García, *J. Hazard. Mater.* **2019**, 365, 725–732.

presencia del mismo analito, de tal forma que este actúa como revelador (**Figura 10b**).

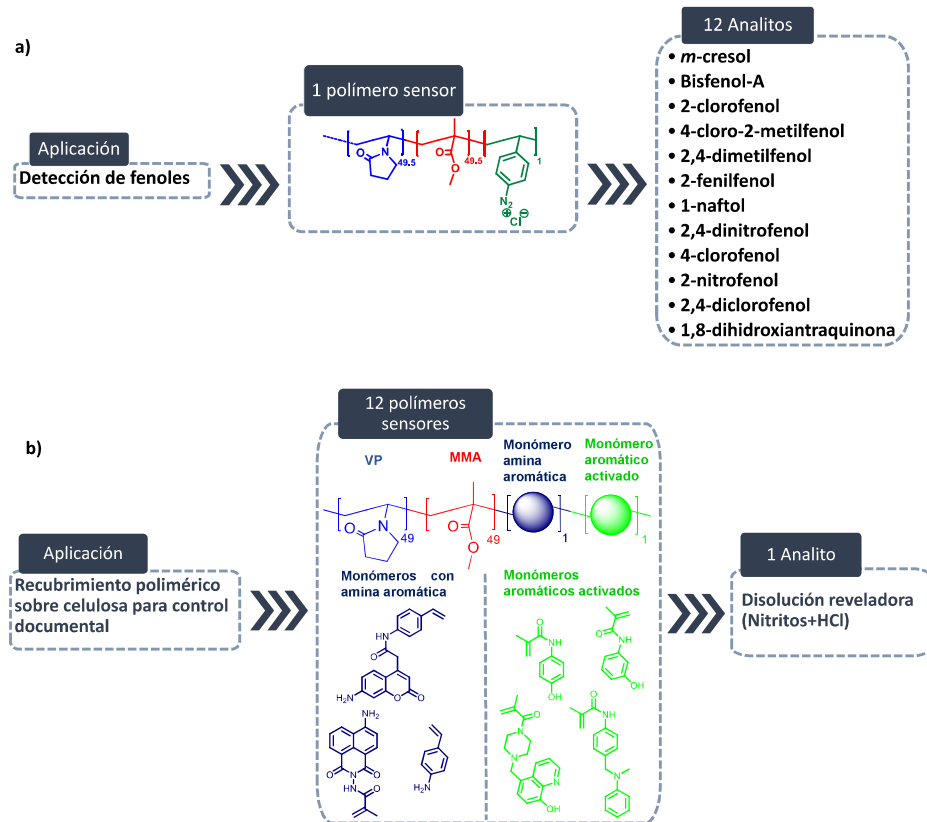


**Figura 10.** a) Planteamiento del funcionamiento del polímero sensor de fenoles (1 polímero sensor para cuantificar 12 analitos); y b) Planteamiento del funcionamiento del polímero sensor para la verificación de productos (12 polímeros sensores para 1 analito).

La química implicada en la solución propuesta es extremadamente sencilla, y se basa en la formación de azocompuestos, conocidos por sus altos coeficientes de extinción molar y muy utilizados en la industria de los colorantes. Los polímeros sensores contienen dos receptores en lugar de uno, como suele ser habitual, y es el nitrito de sodio en medio ácido (revelador) el reactivo que cataliza la reacción entre ambos receptores para que se formen los diferentes azocompuestos. Los receptores son un monómero con un anillo aromático

activado y un monómero con una amina aromática (**Figura 11**). La amina aromática en presencia de nitritos en medio ácido forma una sal de diazonio, que reacciona mediante un acoplamiento diazóico con el monómero con el grupo aromático activado dando lugar al cromóforo (azocompuesto). Por otra parte, debido a la aplicación a la que va dirigido el material, la matriz estructural debe tener afinidad por la celulosa, no ser soluble en agua y presentar cierta hidrofilia (para que la interacción con el analito sea adecuada). Teniendo en mente estos condicionantes, se diseñó la matriz estructural del polímero sensor con una composición molar de un 49% de *N*-vinilpirrolidona y 49% de metacrilato de metilo.

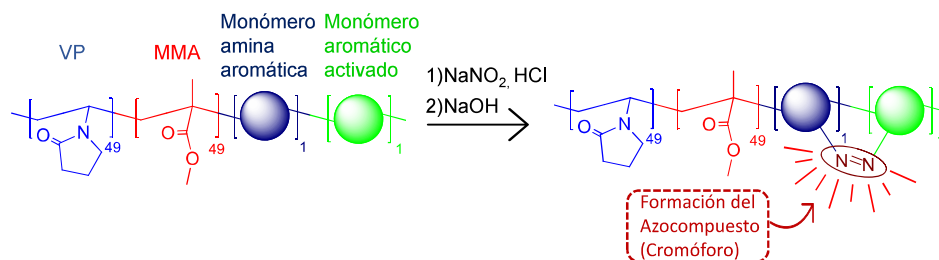


**Figura 11.** Mecanismo de acción del polímero sensor para la obtención del azocompuesto (cromóforo).

El cambio de color producido se puede registrar tras la pulverización de una disolución de nitrito de sodio en medio ácido sobre los papeles recubiertos con los polímeros sensores, y analizar con el uso de la cámara de cualquier teléfono móvil. Precisamente, gracias a este análisis se puede verificar el código de colores obtenidos y comprobar de esta manera la autenticidad del producto. Este mecanismo de acción se muestra de manera esquemática en la **Figura 12**, en la que se utilizan cuatro polímeros sensores diferentes para obtener una secuencia de colores determinada.

Este trabajo el trabajo se desarrolló como parte del proyecto IMPACTUS, en el que participaron diferentes Universidades como la Universidad de Coimbra, y diferentes empresas como el Instituto de Investigaciones Forestales y Papeleras «RAIZ», que es el departamento de investigación de la empresa «The

*Navigator Company*. Gracias a su colaboración, la idea tomó forma, y guiaron todo el proceso de preparación de las etiquetas. El trabajo completo se publicó en la revista *ACS Applied Materials and Interfaces*,<sup>86</sup> y los resultados se protegieron mediante patente PCT, cuya propiedad intelectual se comparte entre la Universidad de Coimbra, la Universidad de Burgos, y RAIZ. (**Figura 13**, número de patente: PCT/IB2021/062484).

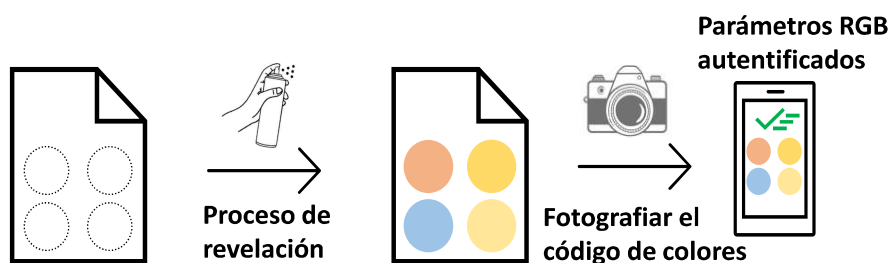


**Figura 12.** Mecanismo de funcionamiento del polímero sensor en forma de recubrimiento para el control de la autenticidad.

### 3.2. Resultados

A continuación, se muestran los resultados obtenidos a través de la transcripción íntegra de los trabajos publicados o en proceso de revisión:

- *Chromogenic Anticounterfeit and Security Papers: An Easy and Effective Approach.*

<sup>86</sup> J.C. Guirado-Moreno, M. Guembe-García, J.M. García, R. Aguado, A.J.M. Valente, S. Vallejos, *ACS Appl. Mater. Interfaces*. **2021**, 13, 50, 60454–60461.

 <b>Receipt of Electronic Submission</b>																					
The Receiving Office (RO/IB) acknowledges the receipt of a PCT International Application filed using ePCT-Filing. An Application Number and Date of Receipt have been automatically assigned (Administrative Instructions, Part 7).																					
Submission Number:	062484																				
Application Number:	PCT/IB2021/062484																				
Date of Receipt:	30 December 2021																				
Receiving Office:	International Bureau of WIPO																				
Your Reference:	ChromoSENSOR																				
Applicant:	RAIZ - INSTITUTO DE INVESTIGAÇÃO DA FLORESTA E PAPEL																				
Number of Applicants:	3																				
Title:	CHROMOGENIC COPOLYMER, METHOD OF PRODUCING THE SAME, PRODUCTS INCORPORATING THE SAME AND METHOD FOR DETECTING COUNTERFEITING AND FOR PRODUCTS AUTHENTICATION																				
Documents Submitted:	<table border="1"> <tr> <td>ChromoSENSOR-appb-000001.pdf (DESCRIPTION.pdf)</td> <td>211180</td> </tr> <tr> <td>ChromoSENSOR-appb-000002.pdf (CLAIMS.pdf)</td> <td>172354</td> </tr> <tr> <td>ChromoSENSOR-appb-000003.pdf (ABSTRACT.pdf)</td> <td>11581</td> </tr> <tr> <td>ChromoSENSOR-appb-000005.pdf (DRAWINGS.pdf)</td> <td>1020100</td> </tr> <tr> <td>ChromoSENSOR-appb.xml</td> <td>887</td> </tr> <tr> <td>ChromoSENSOR-dpcf-000001.zip (pre-conversion files.zip)</td> <td>2217152</td> </tr> <tr> <td>ChromoSENSOR-fees.xml</td> <td>2100</td> </tr> <tr> <td>ChromoSENSOR-requ.xml</td> <td>11563</td> </tr> <tr> <td>ChromoSENSOR-resr-000001.pdf (EarlySearchPT117491 .pdf)</td> <td>95482</td> </tr> <tr> <td>ChromoSENSOR-vlog.xml</td> <td>1925</td> </tr> </table>	ChromoSENSOR-appb-000001.pdf (DESCRIPTION.pdf)	211180	ChromoSENSOR-appb-000002.pdf (CLAIMS.pdf)	172354	ChromoSENSOR-appb-000003.pdf (ABSTRACT.pdf)	11581	ChromoSENSOR-appb-000005.pdf (DRAWINGS.pdf)	1020100	ChromoSENSOR-appb.xml	887	ChromoSENSOR-dpcf-000001.zip (pre-conversion files.zip)	2217152	ChromoSENSOR-fees.xml	2100	ChromoSENSOR-requ.xml	11563	ChromoSENSOR-resr-000001.pdf (EarlySearchPT117491 .pdf)	95482	ChromoSENSOR-vlog.xml	1925
ChromoSENSOR-appb-000001.pdf (DESCRIPTION.pdf)	211180																				
ChromoSENSOR-appb-000002.pdf (CLAIMS.pdf)	172354																				
ChromoSENSOR-appb-000003.pdf (ABSTRACT.pdf)	11581																				
ChromoSENSOR-appb-000005.pdf (DRAWINGS.pdf)	1020100																				
ChromoSENSOR-appb.xml	887																				
ChromoSENSOR-dpcf-000001.zip (pre-conversion files.zip)	2217152																				
ChromoSENSOR-fees.xml	2100																				
ChromoSENSOR-requ.xml	11563																				
ChromoSENSOR-resr-000001.pdf (EarlySearchPT117491 .pdf)	95482																				
ChromoSENSOR-vlog.xml	1925																				
Submitted by:	Mariana Belo Oliveira (Customer ID: user_PT_BELO-OLIVEIRA_MARIANA_1343)																				
Timestamp of Receipt:	30 December 2021 17:55 UTC+1 (CET)																				
Official Digest of Submission:	8B:5D:BA:EF:29:BE:93:B7:45:EB:D9:C5:2F:F3:E4:CE:3D:D1:5E:D3																				
/Geneva, RO/IB/																					

**Figura 13.** Justificante de presentación electrónica de solicitud de patente. Número de solicitud: PCT/IB2021/062484.



*Chromogenic Anticounterfeit and Security Papers: An Easy and Effective Approach.*



## Chromogenic anti-counterfeit and security papers: an easy and effective approach

José Carlos Guirado-Moreno,<sup>a</sup> Marta Guembe-García,<sup>a</sup> José M. García,<sup>a</sup> Roberto Aguado,<sup>b</sup> Artur J.M. Valente,<sup>b,\*</sup> Saúl Vallejos<sup>a,\*</sup>

<sup>a</sup> Departamento de Química, Facultad de Ciencias, Universidad de Burgos, Plaza Misael Bañuelos s/n, 09001 Burgos, Spain

<sup>b</sup> CQC, Department of Chemistry, University of Coimbra, Rua Larga, 3004-535 Coimbra, Portugal.

\*Corresponding author: Dr Valente ([avalente@ci.uc.pt](mailto:avalente@ci.uc.pt)), Dr Vallejos ([svallejos@ubu.es](mailto:svallejos@ubu.es)).

### Abstract

The synthesis and preparation of 12 chromogenic polymers used to build an intelligent label for security paper applications are described. The process involves coating paper sheets with the polymers. Depending on the number of different polymers used in a combinatory way, a maximum of  $12^{12}$  combinations are possible, thus creating a matrix that is practically impossible to counterfeit. Currently, most anti-counterfeiting proposals for paper-based packaging and documents involve some sort of verification under ultraviolet radiation, and the requirement of additional equipment often relegates the end-user to a passive role. In contrast, in our approach, the combination of sensory polymers in an array gives rise to an invisible label, i.e., an owner cryptographic key, which becomes visible upon scattering a nitrite solution (e.g., spraying or using an impregnated foam roller) over the printed label on the security paper. For this purpose, a monomer containing an aromatic primary amino group and another with an activated aromatic ring are covalently bonded to a polymer with high affinity towards paper, consisting essentially of units of methyl methacrylate and 1-vinyl-2-pyrrolidone. Subsequently, the paper samples are coated with the resulting sensory chromogenic polymer.

**Keywords:** Anti-counterfeit, papers, azo-coupling, sensory polymers, colorimetry, RGB parameters.

*ACS applied materials and interfaces, 2021, 13, 50, 60454-60461*

By spraying, painting, or staining an aqueous acid solution of NaNO<sub>2</sub> (at least 1.20 g/L) and the chromogenic polymers, a well-defined color appears, due to the formation of an azo compound. This process provides users with a quick and facile authentication method without additional equipment and without affecting paper strength.

## 1. Introduction

Counterfeiting harms not only many industrial sectors but also different levels of society, from deceived final users to public administrations.<sup>1</sup> Alarmingly, global losses due to this illegal activity are expected to reach between 1.6 and 2.3 trillion USD in 2022,<sup>2</sup> a fair part of that going straight into the coffers of criminal organizations.<sup>3</sup> Faced with such a big threat, anti-counterfeiting techniques have been a widely studied scientific field over the last few decades.

More specifically, in the frame of security papers, most works are based on luminescent security elements, as inks, carbon dots, or markers.<sup>4–10</sup> However, UV-B or UV-C irradiation, rarely at the disposal of the end-user, is often necessary for activating or revealing luminescent materials. Furthermore, the frequent use of metal complexes as fluorophores increases the price of the product and converts the paper into a hybrid product with both organic and inorganic parts, which affects its safety and sustainability. Other proposals require barcode readers or other kinds of scanning, but common smartphones can be used as well, once certain software is installed.<sup>11,12</sup>

A source of inspiration comes from colorimetric sensor arrays, *i.e.*, groups of sensory materials distributed over a substrate in a certain pattern so that each material undergoes a change of color in the presence of a specific target, with more or less selectivity.<sup>13–17</sup> There are a number of well-known possibilities to attain that. For instance, 3,3',5,5'-tetramethylbenzidine changes from colorless to blue upon oxidation,<sup>14</sup> and its immobilization in paper has already been proven successful.<sup>18</sup> Nanoparticles of gold, silver and even copper, whose mechanism of colorimetric detection is surface plasmon resonance, have likewise been used as a coating layer for paper-based immunosensors.<sup>18</sup>

---

However, these and other approaches, such as metalloporphyrins, cobalt(II) chloride or colorimetric Cd-Te quantum dots,<sup>19</sup> generally require heavy metal ions, be it as the analyte that triggers the response, as part of the sensing system itself, or both. Furthermore, the number of possible colors is rather limited in most cases. Likely, the sensor array that resembles our approach the most is Park et al.'s organic solvatochromic system, which results in different combinations of colors when exposed to different organic compounds.<sup>20</sup> With that principle in mind, but shifting the aim from pollutant detection to authentication, azo compounds not only provide a broader range of colors, but also do not require volatile organic solvents to trigger the response.

All considered, we have designed a new verification technique that provides an evident visual response without the need for additional equipment, although a smartphone can aid users in identifying every color with accuracy. First, the dispatcher defines a certain pattern or sequence of colors. This colored code is hidden as colorless and/or yellowish (public-key encryption) by printing, painting, or coating on paper several fully organic copolymers, each containing small proportions of different sensory units. The final user has only to spray a cheap solution, and the array of sensory polymers, comprising the anti-counterfeiting system, changes its color under visible light (private key decryption), making unnecessary any excitation with UV radiation.

The sensory copolymers are mainly based on commercially available 1-vinyl-2-pyrrolidone (VP) and methylmethacrylate (MMA), granting high compatibility with paper and ensuring that there is no elution when the verification solution is applied. These copolymers are chromogenic because of small amounts of both a monomer containing an aromatic amine group (MCN), which is susceptible to forming a derivative of benzene diazonium salt, and an activated ring-containing monomer, e.g., phenols, *N,N*-dimethylaminoanilines, and the like (MCAR). Only when the verification solution (made with reagents available in common hardware stores) is sprayed, painted, or stained over the paper, the azo coupling reaction between both sensory motifs (MCN and MCAR) starts, and the

---

colored azo dye is formed.<sup>21–23</sup> Optionally, applying an alkaline solution (also available in hardware stores prompts the reaction and results in an immediate response. We have prepared 12 different polymers combining 3 MCN and 4 MCAR. The possibility of obtaining different colors, one per polymer, allows the dispatcher to provide customers with numerous chromatic codes.

## 2. Experimental

### 2.1. Materials

All materials and solvents were commercially available and used as received unless otherwise indicated. The following materials and solvents were used: methylmethacrylate (MMA) (Merk, 99%), 1-vinyl-2-pyrrolidone (VP) (Acros Organic, 99%), 4-aminostyrene (SNH<sub>2</sub>) (TCI, 98%), hydrochloric acid (VWR-Prolabo, 37%), sodium hydroxide (VWR-Prolabo, 99%), N,N'-dicyclohexylcarnodiimide (Aldrich, 99%), tetrahydrofuran (VWR-Prolabo, 99.9%), ethanol (VWR-Prolabo, 99.9%), dichloromethane (VWR-Prolabo, 99.9%), 4-amino-1,8-naphtalic anhydride (Merck, 95%), hydrazine monohydrate (Panreac, 80%), triethylamine (VWR, 99%), methacryloyl chloride (Alfa Aesar, 97%), 4-aminobenzyl alcohol (Merck, 98%), ethyl acetate (VWR-Prolabo, 99.9%), methacrylic anhydride (Alfa Aesar, 94%), manganese oxide activated (Fluka, 90%), celite 503 (Merck), aniline (Alfa Aesar, 99%), methanol (VWR-Prolabo, 99.9%), sodium borohydride (Alfa Aesar, 98%), paraformaldehyde (Aldrich, 95%), trifluoroacetic acid (Alfa Aesar, 99.5%), sodium hydroxide (VWR-Prolabo, 99%), sodium chloride (VWR-Prolabo, 98%), 1-boc-piperazine (Merck, 97%), diethyl ether (VWR-Prolabo, 99.9%), 1,4-dioxane (VWR, 99.9%), potassium carbonate (VWR-Prolabo, 99%), sodium sulfate anhydrous (VWR-Prolabo, 99%), hexane (VWR-Prolabo, 98.5%), sodium nitrite (AppliChem Panreac, 99%), filter paper in reams (Filter Lab, 73g/m<sup>2</sup>). Azo-bis-isobutyronitrile (AIBN, Aldrich, 98%) was recrystallized twice from methanol.

### 2.2. Instrumentation

Infrared spectra (FTIR) were recorded with an FT/IR-4200 FT-IR Jasco

---

Spectrometer with an ATR-PRO410-S single reflection accessory. High-resolution electron-impact mass spectrometry (EI-HRMS) was carried out on a Micromass AutoSpec Waters mass spectrometer (ionization energy: 70 eV; mass resolving power: >10 000).  $^1\text{H}$  and  $^{13}\text{C}\{^1\text{H}\}$  NMR spectra were recorded with a Bruker Avance III HD spectrometer operating at 300 MHz for  $^1\text{H}$ , and 75 MHz for  $^{13}\text{C}$ , using deuterated solvents like dimethyl sulfoxide ( $\text{DMSO}-d_6$ ) or deuterated chloroform ( $\text{CDCl}_3$ ) at 25°C.

Materials were also characterized in terms of their thermal and mechanical properties. Thermogravimetric analysis (TGA) was performed on 10–15 mg of sample under synthetic air and nitrogen atmosphere with a TA Instruments Q50 TGA analyzer, setting the heating rate at 10 °C/min. Differential scanning calorimetry (DSC) used 10–15 mg of the sample under a nitrogen atmosphere with a TA Instruments Q200 DSC analyzer, 20 °C/min. Tensile tests were carried out on  $5 \times 9.44 \times 0.10$  mm samples using a Shimadzu EZ Test Compact Table-Top Universal Tester, setting the rate of separation of jaws at 5 mm/min.

Powder X-ray diffraction (PXRD) patterns were obtained using a Bruker D8 Discover (Davinci design) diffractometer operating at 40 kV, using Cu(K $\alpha$ ) as the radiation source, a scan step size of 0.02°, and a scan step time of 2 s.

### 2.3. Choice of main monomers and synthesis of sensory monomers

These kinds of chromogenic copolymers are made up of two parts: the sensory motifs and the main monomers. The latter does not interact directly with the target species but has a fundamental role in attaining selective solubility, adjusting the hydrophilic/hydrophobic balance, and preserving or even improving the mechanical properties.<sup>24</sup> In Supporting Information Section 1 (**SI-S1**), we show the initial tests working with several combinations of commercially available main monomers, including, for instance, hydroxyethyl methacrylate and (2-dimethylamino)ethyl methacrylate. These assays resulted in the choice of VP and MMA. Polymers based on these main monomers in equimolar proportions grant a correct fixation onto paper, and that cannot be eluted by water.

---

On the other hand, the different sensory monomers (MCNs and MCARs) were synthesized from commercially available compounds and with common laboratory equipment. Their synthesis routes and characterization are depicted in **SI-S2**.

#### *2.4. Polymerization*

All the synthesized polymers have the same general structure, which is shown in **Scheme 1**. They were prepared by radical polymerization of the hydrophilic monomer VP, the hydrophobic monomer MMA, MCN, and MCAR in a 49/49/1/1 molar ratio, respectively.

45 mmol of VP, 45 mmol of MMA, 0.94 mmol of MCN, and 0.94 mmol of MCAR were dissolved in DMF (46 mL), and the solution was added to a round-bottom pressure flask. Subsequently, radical thermal initiator AIBN (754 mg, 4.6 mmol) was added, and the solution was sonicated for 10 min; then, it was heated at 60 °C overnight, under a nitrogen atmosphere, and without stirring. After that, the solution was cooled down and dropwise added to diethyl ether (300 mL) with vigorous stirring. All polymers were purified in a Soxhlet apparatus with diethyl ether as the washing solvent.

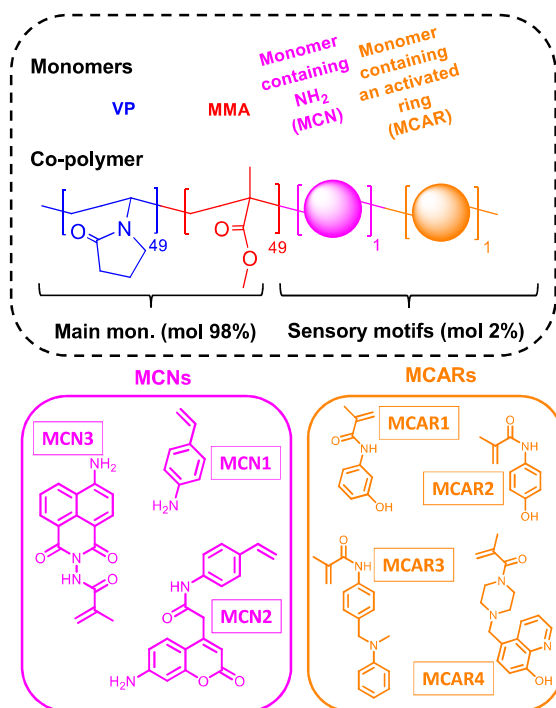
#### *2.5. Paper coating and verification*

100 mg of sensory polymer were dissolved in acetonitrile (1 mL). Then, 50 µL of the resulting solution were deposited on the surface of a filter paper disc (2 cm diameter, 3.14 cm<sup>2</sup>), and the solvent was evaporated at 60 °C for 5 minutes.

In a preliminary titration, the synthesized chromogenic polymers were impregnated with aqueous HCl (3.5% w/w) containing sequential additions of NaNO<sub>2</sub>, to define the minimum concentration of this salt. Once a proper concentration was determined on the basis of titration curves, the same acid solution of NaNO<sub>2</sub> was sprayed over all polymer-coated papers. Then, an aqueous solution of NaOH (1 M) was also pulverized over the discs, immediately revealing an evident color change.

---

All colors were characterized both by UV-Vis spectrophotometry and with a smartphone. For the former, we used an optic fiber accessory for recoding the absorbance spectra. For the latter, more oriented to real use, an iPhone 8 was used for taking a digital photograph and analyzing the RGB parameters (8 bits per channel) with the app "Colorimetric Titration".<sup>25</sup>



**Scheme 1.** The general structure of synthesized polymers, based on two main monomers and two sensory monomers. The copolymer is mainly composed of 1-vinyl-2-pyrrolidone (mol 49%) and methyl methacrylate (mol 49%). The sensory or chromogenic part is based on a monomer containing an amino group (MCN; mol 1%) and a monomer containing an activated ring (MCAR; mol 1%).

### 3. Results and discussion

#### 3.1. Quality and success of synthesis

The relatively high amount of AIBN resulted in low molecular mass polymers, which favors solubility and does not increase viscosity excessively. The yield lay

in all cases between 80% and 85%.

In order to avoid prolixity, the complete characterization of the 12 chromogenic polymers (prepared by combining 3 MCNs and 4 MCARs) can be found in **SI-S3**. **Figure 1** shows an example for one of the polymers, VP:MMA:MCN2:MCAR3 (polymer number 7). After the azo coupling reaction, its strong electronic absorption across the blue and green regions of the visible light spectrum (**Figure 1a**) matches its golden color.

The FTIR spectrum (**Figure 1b**) displays some bands that are common to all polymers, since they are due to MMA and VP, such as the ones at 1623 cm<sup>-1</sup> (VP) and 1726 cm<sup>-1</sup> (MMA). But, in addition, the stretching vibrations of C–C bonds in aromatic rings are also evident around 1500 cm<sup>-1</sup>. Most of the signals owing to the N–H and C–N bonds of sensory monomers are overlapped with that of the main monomers, but the strong bands attributed to N–H wag in the lowest energy region (<900 cm<sup>-1</sup>) allows us to distinguish one combination of monomers from another.

For a more accurate distinction, the <sup>1</sup>H NMR spectrum (**Figure 1c**) displays at the lowest field a singlet corresponding to the hydrogen of the secondary amide of MCN2 and, while the high field region is dominated by the main monomers, the singlet at 3.0 ppm is not common to all polymers. Indeed, it is due to the methyl group attached to the tertiary amino group of MCAR3. Likewise, the carbonyl carbons of MCN2 are highlighted downfield in the <sup>13</sup>C NMR spectrum (**Figure 1d**). In any case, no impurities were detected by NMR spectroscopy.

The thermogram in **Figure 1e** evidences that the material is not stable beyond 327 °C, and the glass transition temperature ( $T_g$ ) of polymer 7 was found to be 141 °C, as shown in **Figure 1f**. We found similar values for the other polymers (**SI-S3**):  $T_5$  ranges from 270 to 339 °C and  $T_g$  ranges from 132 to 153 °C. These values suggest that these polymers show thermal stability for practical purposes.

---

In short, monomer synthesis, polymerization, and purification were proved to be successful. For a more extensive characterization, including X-ray diffraction patterns, the reader is referred to **SI-S3**.

### 3.2. Verification methodology: color changes

The papers' color change is based on the reaction between two sensory monomers (MCN and MCAR) in the presence of nitrite anions. Specifically, nitrite anions react with hydrochloric acid in aqueous media, forming nitrosyl anions. This highly reactive chemical species reacts with MCNs, resulting in the formation of a benzene diazonium salt. Finally, this compound attacks the ring's activated position of MCARs, forming the azo dye (**Figure 4b**).

Revealing the printed discs involves their spraying with an aqueous acid solution of sodium nitrite (25 mL water, 2.5 mL of concentrated HCl, and 100 mg NaNO<sub>2</sub>), followed by the spraying of an aqueous NaOH 1M solution for an instantaneous color change (see **Figure 2a**, and the **Video** provided as electronic supporting information). Depending on the chromogenic monomers of choice (MCN and MCAR), different colors were obtained, as shown in **Figure 2b**.

Different colors were characterized both by UV-Vis spectrophotometry and with a smartphone. For the former, we used an optic fiber accessory for recording the absorbance spectra. For the latter, more oriented to real use, an iPhone 8 was used to take the digital photo and analyze the RGB parameters with the app "*Colorimetric Titration*".<sup>25</sup> In this case, a small piece of plastic was included in the photo as a color reference (see **Figure 2b**). This element is essential to carry out the verification in any lighting condition since it acts as a reference for adjusting digital color curves, and therefore always be able to obtain the depicted color definition RGB parameters as resumed in **Figure 3**. Furthermore, these color codes are unique for each polymer, so the verification system that we propose is a very powerful, low-cost, and easy-to-use tool. Two examples of real hypothetic applications using 4 of the 12 polymers are shown in the Graphical Abstract, but as many as needed could be used (from 1 to 12), in

different positions, different orders, combining various MCNs and MCARs in the same polymer, etc. (see **SI-Video**).

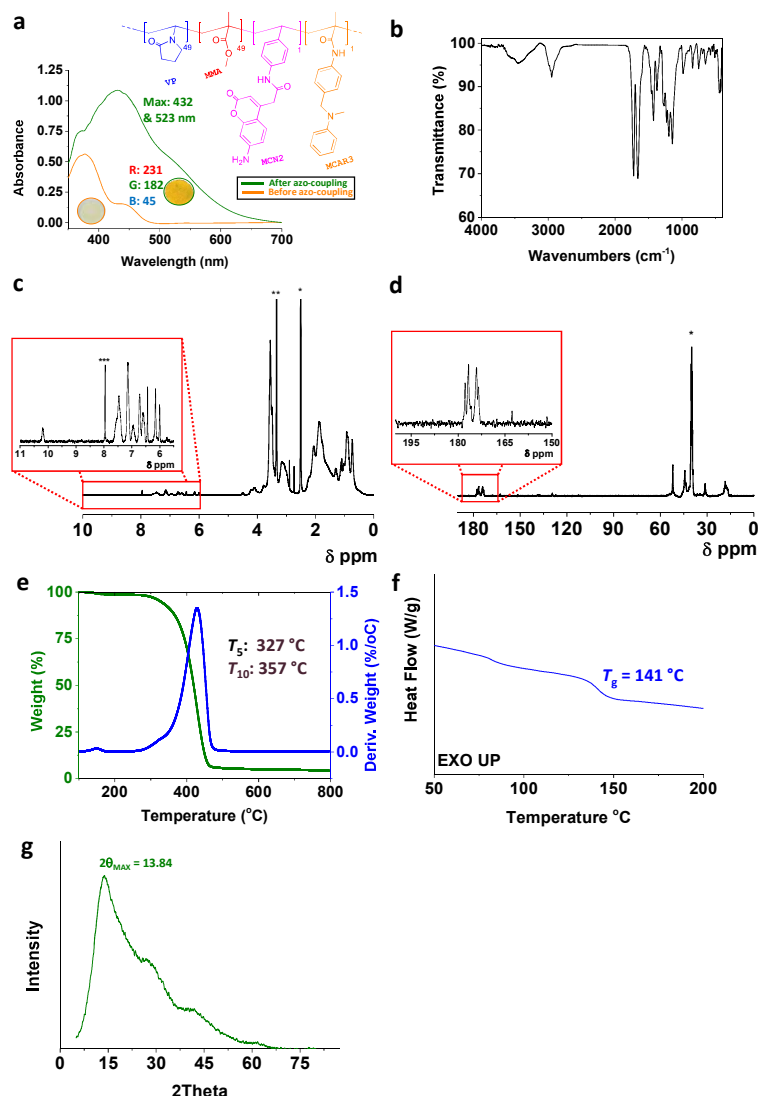


**Figure 1.** Characterization of polymer 7 (golden) by (a) UV-Vis spectrometry, including polymer's formula and real photographs of coated discs; (b) FT-IR spectroscopy; (c) <sup>1</sup>H RMN (\*=DMSO-d<sub>6</sub>, \*\*=H<sub>2</sub>O). (d) <sup>13</sup>C RMN (\*=DMSO-d<sub>6</sub>); (e) Thermogravimetric curve at 10 °C·min<sup>-1</sup> under nitrogen atmosphere, showing  $T_5$  and  $T_{10}$  temperatures; (f) DSC curve at a heating rate of 20°C·min<sup>-1</sup> under nitrogen atmosphere showing  $T_g$  value. (g) PXRD spectra showing  $2\theta_{MAX}$ .

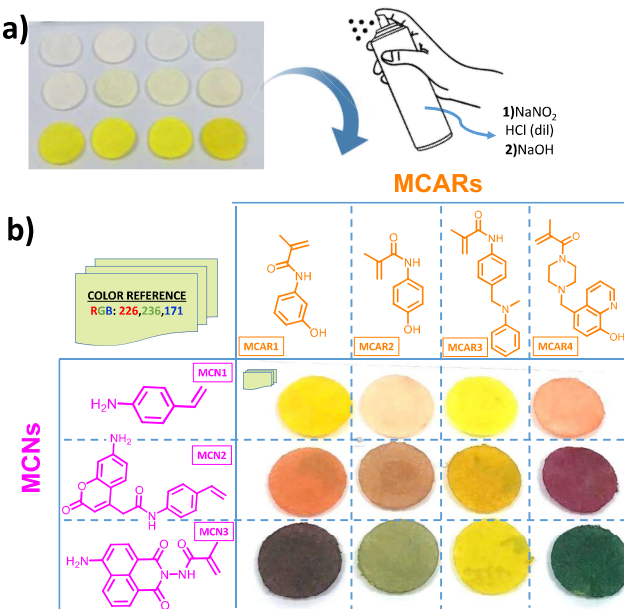


**Figure 2.** Printed and revealed paper discs: a) sensory paper discs; b) revealed discs upon spraying an acid solution of sodium nitrite (0.1 g NaNO<sub>2</sub>, 25 mL water, 2.5 mL HCl 37%) and an aqueous solution of NaOH (1M). The matrix shows the 12 different polymers obtained upon combinations of sensory monomers (MCARs and MCNs, mol 2%, each 1%), which were copolymerized with VP (mol 49%) and MMA (mol 49%).

### 3.3. Study of the minimum required amount of nitrite

From the chemical point of view, this verification system is basically a nitrite anion sensory system. However, related to the application that we propose for these chromogenic polymers, the typically reported properties for sensors, such as the limits of detection and quantification, are trivial. The lower the nitrite concentration of the spray solution, the lower the intensity of the color formed, which is counterproductive for easy authentication.

Nonetheless, there will no longer be an increase in color above a specific concentration since all the sensory motifs will have reacted. For this reason, it is important to define the minimum concentration of nitrites in the spray solution, and below which, the colors could be different and not match the RGB code table depicted in **Figure 3**. Thus, we performed a titration of all chromogenic polymers

with sodium nitrite, and we found 120 mg NaNO<sub>2</sub>/100 mL (17.4 mM) as the minimum concentration for an effective spray solution. **Figure 4a** shows one of the titration curves with one of the polymers as an example (VP:MMA:MCN2:MCAR4 in a 49:49:1:1 molar ratio, respectively), but equivalent results were obtained for the rest of the sensory polymers.



**Figure 3.** (Left) Filter paper discs coated with sensory polymers after spraying an acid solution of sodium nitrite (0.1 g NaNO<sub>2</sub>, 25 mL water, 2.5 mL HCl 37%) and an aqueous solution of NaOH (1M). (Right) RGB color definition parameters for each disc.

### 3.4. Chemical recycling. Separation of the coating and the paper

As we show in **Figure 4c**, the coating can be separated from the paper in a very simple way, simply by treating the paper with a green solvent such as propylene carbonate. In this way, and despite having a minimum amount of polymer (1.6 mg of polymer per cm<sup>2</sup> of paper), our sensory polymer does not imply any paper recycling problem. The copolymers have been specifically designed to be water-resistant for practical applicability of the intelligent labels, but at the same time easily removable with the appropriate green solvent.

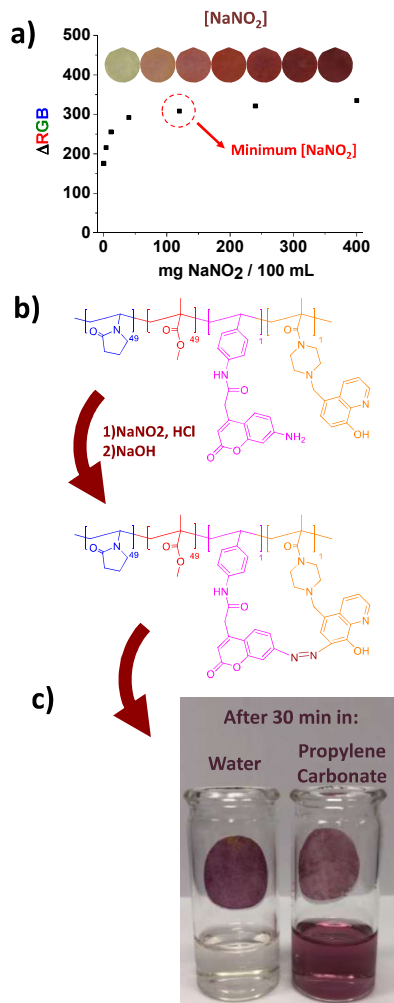


**Figure 4.** (a) Titration of printed paper discs coated with the sensory polymer VP:MMA:MCN2:MCAR4 (molar ratio 49:49:1:1, respectively), with  $\text{NaNO}_2$ . Each 2 cm diameter disc was coated with 50  $\mu\text{L}$  of the sensory polymer solution in acetonitrile (100 mg in 1 mL). The coated paper discs were dipped in different  $\text{NaNO}_2$  acid solutions (0.4/4/12/40/120/240 and 400 mg  $\text{NaNO}_2$ /100 mL) and finally dipped in aqueous  $\text{NaOH}$  (1M). RGB parameters were extracted from the digital photograph, grouped as the unique variable  $\Delta RGB$ <sup>26</sup> and represented against the concentration of  $\text{NaNO}_2$ . (b) Azo-coupling reaction in the chromogenic polymer.<sup>21,22</sup> (c) Colored paper discs after dipping in water and propylene carbonate for 30 minutes. The picture shows the water-resistant character of the polymer and the solubility in propylene carbonate.

### *3.5. Study of the effect of the coating on paper's mechanical properties*

The coating of papers (or specific paper areas) in no case can suppose the loss of properties, reason why a comparative study was carried out analyzing the Young's modulus of the paper without and with coating. Since 98% of the polymers' chemical composition is identical in the 12 examples (mol 49% VP and mol 49% MMA), this study was only carried out with the polymer VP:MMA:MCN2:MCAR4 (molar ratio 49:49:1:1, respectively). The Young's modulus for the paper with and without the coating was 491 and 511 MPa, respectively. Thus, we did not find significant differences between them.

### *3.6. Proof of concept. Encrypting and decrypting*

We are describing a cryptographic system for securing the authenticity of a branded product. This system is partially inspired by the asymmetric public-key/private-key cryptography that secures electronic communications,<sup>22</sup> and we believe a real example would be clarifying for the reader.

In this example, the dispatcher of a branded watch devises a color code, which may be different for every single product, and keeps it private. For instance, we may suggest a simple four-color code: R234/G141/B94 (salmon) – R59/G93/B74 (dark sea green) – R145/G75/B93 (purple) – R231/G182/B45 (golden). This code is then encrypted as an apparently dull label of white/colorless and yellow elements (public key). Encrypting is accomplished by printing or coating up to 12 chromogenic polymers on the paper label, if not on the packaging paper directly, knowing in advance how each of those polymers looks before and after applying a verification solution. We can easily see that the series of polymers required in this example is 5 (MCN2, MCAR 1) – 12 (MCN3, MCAR4) – 8 (MCN2, MCAR4) – 7 (MCN2, MCAR3).

When customers receive the package containing the watch, they can decrypt the code by applying the revealing solution with a two-fold aim: guarantying that the key has not been previously cracked and checking that the code matches the one provided by the manufacturer. Moreover, the dispatcher

---

can send the unique color code electronically only at the moment the purchaser wants, increasing the security of the verification system.

The number of combinations is dependent on the number of polymers, e.g., if the 12 polymers are printed, their permutation without repetition, where the linear order is relevant, gives  $12!$  possibilities ( $V_k(n)$ , where  $n$  and  $k = 12$ ), broadly 479 million of possibilities. Moreover, if the 12 polymers are printed with repetition, the possibilities are  $n^{12}$  ( $V'_k(n)$ , where  $n$  and  $k = 12$ ), broadly 9 trillion possibilities.

#### 4. Conclusions

We have designed an anti-counterfeiting system based on 12 chromogenic polymers applied directly to the paper as coatings. The intelligent colorless label is printed on the paper as an array of printed discs or squares of these polymers in a combination that allows for trillions of possibilities if, for example, the array comprised 12 discs, including repetition of the polymers. The intelligent labels are cryptographic keys belonging to the owner that can be revealed into a color chart for checking the inviolability of the key and the coincidence of the owner key with the revealed label. From a practical viewpoint, the label changes into the color chart of the owner's cryptographic key when sprayed a solution of sodium nitrite in acid medium, followed by a solution of NaOH (1M). This expectation, i.e., that the end-user will handle moderately acidic solutions and alkalis with due safety, is the only drawback of this approach, and hopefully it will be overcome by using impregnated foam rollers or stamps, that could be easily commercialized.

The color change of each sensory polymer depends on the sensory monomers used in the polymer synthesis, and, as mentioned, we have made 12 combinations of chromogenic monomers that generate 12 different colors. For more accurate identification of these colors, the user can quantify the RGB coordinates against a certain reference and compare them with the ones provided by the dispatcher. The integration of the sensory polymers in the paper does not significantly modify the mechanical properties of the paper. While when discrete molecules are used in solution for paper coating, the chemical species are easily

---

eluted from the substrate, the incorporation of the sensory motifs as co-monomers of a VP/MMA-based polymer grants both water resistance and non-migration. At the same time, polymers have been designed to be soluble in the appropriate solvent, so that it is easily removable from the paper for appropriate recycling of both parts.

## Supporting Information

Selection of the best main monomers; synthesis and characterization of MCNs and MCARs; characterization of sensory polymers; proof of concept's video.

The supporting information is available free of charge at:

[https://pubs.acs.org/doi/suppl/10.1021/acسامي.1c19228/suppl\\_file/am1c19228\\_si\\_001.pdf](https://pubs.acs.org/doi/suppl/10.1021/acسامي.1c19228/suppl_file/am1c19228_si_001.pdf)

[https://pubs.acs.org/doi/suppl/10.1021/acسامي.1c19228/suppl\\_file/am1c19228\\_si\\_002.avi](https://pubs.acs.org/doi/suppl/10.1021/acسامي.1c19228/suppl_file/am1c19228_si_002.avi)

## Conflicts of interest

The authors declare that they have no conflict of interest.

## Acknowledgments

We gratefully acknowledge the financial support provided by all funders. Author Saul Vallejos received funding from "La Caixa" Foundation Grant LCF/PR/PR18/51130007. Author Jose Miguel García received funding from "Spanish Agencia Estatal de Investigación" Grant PID2020-113264RB-I00 / AEI / 10.13039/501100011033. Author Artur Valente received funding from Portugal 2020 in the frame of COMPETE 2020 nº246/AXIS II/2017 (Project N.º 21874). We also gratefully acknowledge European Regional Development Fund (ERDF).

## References

- (1) (OECD), T. O. for E. C. and D. The Economic Impact of Counterfeiting and Piracy. *Econ. Impact Counterfeiting Piracy* **2007**, 1–29.
-

- (2) *The Economic Costs of Counterfeiting and Piracy*; 2017.
- (3) Naylor, R. T. *Counterfeit Crime: Criminal Profits, Terror Dollars, and Nonsense*; McGill-Queen's University Press: Quebec City, 2014.
- (4) You, M.; Zhong, J.; Hong, Y.; Duan, Z.; Lin, M.; Xu, F. Inkjet Printing of Upconversion Nanoparticles for Anti-Counterfeit Applications. *Nanoscale* **2015**, 7 (10), 4423–4431. <https://doi.org/10.1039/c4nr06944g>.
- (5) Aguado, R.; Murtinho, D.; Valente, A. J. M. A Broad Overview on Innovative Functionalized Paper Solutions. *Nord. Pulp Pap. Res. J.* **2019**, 34 (4), 395–416. <https://doi.org/10.1515/npprj-2019-0036>.
- (6) Devadas, S.; Suh, E.; Paral, S.; Sowell, R.; Ziola, T.; Khandelwal, V. Design and Implementation of PUF-Based “Unclonable” RFID ICs for Anti-Counterfeiting and Security Applications. *2008 IEEE Int. Conf. RFID (Frequency Identification)* **2008**, 58–64. <https://doi.org/10.1109/RFID.2008.4519377>.
- (7) Andres, J.; Hersch, R. D.; Moser, J. E.; Chauvin, A. S. A New Anti-Counterfeiting Feature Relying on Invisible Luminescent Full Color Images Printed with Lanthanide-Based Inks. *Adv. Funct. Mater.* **2014**, 24 (32), 5029–5036. <https://doi.org/10.1002/adfm.201400298>.
- (8) Guo, J.; Li, H.; Ling, L.; Li, G.; Cheng, R.; Lu, X.; Xie, A.-Q.; Li, Q.; Wang, C.-F.; Chen, S. Green Synthesis of Carbon Dots toward Anti-Counterfeiting. *ACS Sustain. Chem. Eng.* **2020**, 8 (3), 1566–1572. <https://doi.org/10.1021/acssuschemeng.9b06267>.
- (9) Kalytchuk, S.; Wang, Y.; Poláková, K.; Zbořil, R. Carbon Dot Fluorescence-Lifetime-Encoded Anti-Counterfeiting. *ACS Appl. Mater. Interfaces* **2018**, 10 (35), 29902–29908. <https://doi.org/10.1021/acsami.8b11663>.
- (10) Tsai, W. K.; Lai, Y. S.; Tseng, P. J.; Liao, C. H.; Chan, Y. H. Dual Colorimetric and Fluorescent Authentication Based on Semiconducting Polymer Dots for Anticounterfeiting Applications. *ACS Appl. Mater. Interfaces* **2017**, 9 (36), 30918–30924. <https://doi.org/10.1021/ACSAMI.7B08993>.
- (11) Zhou, Y.; Zhao, G.; Bian, J.; Tian, X.; Cheng, X.; Wang, H.; Chen, H. Multiplexed SERS Barcodes for Anti-Counterfeiting. *ACS Appl. Mater. Interfaces* **2020**, 12 (25), 28532–28538. <https://doi.org/10.1021/acsami.0c06272>.
- (12) Wu, B.-H.; Zhang, C.; Zheng, N.; Wu, L.-W.; Xu, Z.-K.; Wan, L.-S. Grain Boundaries of Self-Assembled Porous Polymer Films for Unclonable Anti-Counterfeiting. *ACS Appl. Polym. Mater.* **2019**, 1 (1), 47–53. <https://doi.org/10.1021/acsapm.8b00031>.
- (13) Li, Z.; Askim, J. R.; Suslick, K. S. The Optoelectronic Nose: Colorimetric and Fluorometric Sensor Arrays. *Chem. Rev.* **2019**, 119 (1), 231–292.

- <https://doi.org/10.1021/acs.chemrev.8b00226>.
- (14) Li, X.; Kong, C.; Chen, Z. Colorimetric Sensor Arrays for Antioxidant Discrimination Based on the Inhibition of the Oxidation Reaction between 3,3',5,5'-Tetramethylbenzidine and Hydrogen Peroxides. *ACS Appl. Mater. Interfaces* **2019**, *11* (9), 9504–9509. <https://doi.org/10.1021/acsmi.8b18548>.
- (15) Sun, Z.; Wu, S.; Ma, J.; Shi, H.; Wang, L.; Sheng, A.; Yin, T.; Sun, L.; Li, G. Colorimetric Sensor Array for Human Semen Identification Designed by Coupling Zirconium Metal–Organic Frameworks with DNA-Modified Gold Nanoparticles. *ACS Appl. Mater. Interfaces* **2019**, *11* (40), 36316–36323. <https://doi.org/10.1021/acsmi.9b10729>.
- (16) Annisa, T. N.; Jung, S. H.; Gupta, M.; Bae, J. Y.; Park, J. M.; Lee, H. II. A Reusable Polymeric Film for the Alternating Colorimetric Detection of a Nerve Agent Mimic and Ammonia Vapor with Sub-Parts-per-Million Sensitivity. *ACS Appl. Mater. Interfaces* **2020**, *12* (9), 11055–11062. <https://doi.org/10.1021/ACSAM1.0C00042>.
- (17) Xu, M.; Bunes, B. R.; Zang, L. Paper-Based Vapor Detection of Hydrogen Peroxide: Colorimetric Sensing with Tunable Interface. *ACS Appl. Mater. Interfaces* **2011**, *3* (3), 642–647. <https://doi.org/10.1021/AM1012535>.
- (18) Chen, W.; Fang, X.; Li, H.; Cao, H.; Kong, J. A Simple Paper-Based Colorimetric Device for Rapid Mercury(II) Assay. *Sci. Rep.* **2016**, *6* (1), 1–7. <https://doi.org/10.1038/srep31948>.
- (19) Hu, T.; Xu, K.; Qiu, S.; Han, Y.; Chen, J.; Xu, J.; Chen, K.; Sun, Z.; Yi, H.; Ni, Z. Colorimetric Detection of Urine Glucose Using a C/CdTe QDs–GOx Aerogel Based on a Microfluidic Assay Sensor. *J. Mater. Chem. B* **2020**, *8* (32), 7160–7165. <https://doi.org/10.1039/D0TB00328J>.
- (20) Park, D.-H.; Heo, J.-M.; Jeong, W.; Yoo, Y. H.; Park, B. J.; Kim, J.-M. Smartphone-Based VOC Sensor Using Colorimetric Polydiacetylenes. *ACS Appl. Mater. Interfaces* **2018**, *10* (5), 5014–5021. <https://doi.org/10.1021/ACSAM1.7B18121>.
- (21) Karabiyik, H.; Iskeleli, N. O.; Albayrak, Ç.; Ağar, E. Conformational Analysis and Crystal Structure of (E)-3-Methyl-4-(p-Tolyldiazenyl)Phenol. *Struct. Chem.* **2007**, *18* (1), 87–93. <https://doi.org/10.1007/s11224-006-9130-1>.
- (22) Rathod, K. M.; Thakre, N. S. Synthesis and Antimicrobial Activity of Azo Compounds Containing M-Cresol Moiety. *Chem. Sci. Trans.* **2012**, *2* (1), 25–28. <https://doi.org/10.7598/cst2013.254>.
- (23) Bustamante, S. E.; Vallejos, S.; Pascual-Portal, B. S.; Muñoz, A.; Mendiola, A.; Rivas, B. L.; García, F. C.; García, J. M. Polymer Films Containing Chemically Anchored Diazonium Salts with Long-Term Stability as Colorimetric Sensors. *J. Hazard. Mater.* **2019**, *365*, 725–732.

[https://doi.org/10.1016/j.jhazmat.2018.11.066.](https://doi.org/10.1016/j.jhazmat.2018.11.066)

- (24) Guembe-García, M.; Peredo-Guzmán, P. D.; Santaolalla-García, V.; Moradillo-Renuncio, N.; Ibeas, S.; Mendía, A.; García, F. C.; García, J. M.; Vallejos, S. Why Is the Sensory Response of Organic Probes within a Polymer Film Different in Solution and in the Solid-State? Evidence and Application to the Detection of Amino Acids in Human Chronic Wounds. *Polymers (Basel)*. **2020**, 12 (6), 1249. <https://doi.org/10.3390/polym12061249>.
- (25) The app can be freely downloaded from the App store or the Google Play, IOs and Android, respectively <https://apps.apple.com/gt/app/colorimetric-titration/id1533793244>  
<https://play.google.com/store/apps/details?id=es.inforapps.chameleon&hl=ES> <https://apps.apple.com/gt/app/colorimetric-titration/id1533793244>.
- (26) Ulrich, S.; Moura, S. O.; Diaz, Y.; Clerc, M.; Guex, A. G.; de Alaniz, J. R.; Martins, A.; Neves, N. M.; Rottmar, M.; Rossi, R. M.; Fortunato, G.; Boesel, L. F. Electrospun Colourimetric Sensors for Detecting Volatile Amines. *Sensors Actuators, B Chem.* **2020**, 322, 128570. <https://doi.org/10.1016/j.snb.2020.128570>.



# CAPÍTULO 4

## Polímeros sensores en el control alimentario.

---

Este capítulo comienza con una breve introducción al control alimentario y las posibilidades de implementación de los polímeros sensores. Seguidamente, se definen las problemáticas existentes para la detección de Cu(II) en la industria vinícola y la detección de Zn(II) en piensos para alimentación animal. Finalmente, se muestran los resultados obtenidos en ambos campos mediante la transcripción íntegra de los artículos publicados en *ACS Applied Materials and Interfaces* y en *Spectrochimica Acta Part A: Molecular and Biomolecular Spectroscopy*.

---

### 4.1. Introducción

La seguridad alimentaria es un tema de gran importancia en la sociedad actual, ya que los alimentos son una necesidad básica y su consumo seguro es vital para la salud de las personas. El control alimentario es una herramienta fundamental para garantizar que los alimentos que se consumen sean seguros y estén libres de cualquier tipo de contaminación que pueda poner en riesgo la salud de los consumidores. El control alimentario abarca desde la producción, el procesamiento, el envasado, el transporte y la distribución de los alimentos, hasta su consumo final por parte de los consumidores. En este sentido, es necesario implementar medidas y controles rigurosos para garantizar que los alimentos que se comercializan cumplen con las normativas sanitarias y son

---

seguros para el consumo. Por tanto, la seguridad alimentaria es una responsabilidad compartida entre todos los agentes que intervienen en la cadena alimentaria, desde los productores y fabricantes hasta los consumidores, pasando por las autoridades sanitarias y de control.

En este contexto, es necesario seguir avanzando en la mejora de los sistemas de control alimentario para garantizar que los alimentos que se consumen sean seguros y de alta calidad. Este tipo de controles se suelen realizar a través de técnicas que presentan varios inconvenientes, entre los que se encuentran la necesidad de llevar a cabo el ensayo con personal cualificado. Además, requieren de una elevada inversión económica debido a los gastos de equipamientos, reactivos y de tiempo, y en ocasiones, estas técnicas son demasiado complejas.

La evaluación de estos parámetros varía en función del alimento que se quiere analizar, y existe una gran variabilidad de factores como la carga microbiológica, la evaluación organoléptica, detección de patógenos, contaminantes o parámetros de calidad, entre otros. El desarrollo de nuevas técnicas o métodos de evaluación de estos parámetros de manera rápida, económica y sencilla es de gran interés para la industria alimentaria. Motivado por la creciente necesidad de mejorar la seguridad alimentaria y garantizar la calidad de los productos alimentarios, el Grupo de Polímeros incluyó en los objetivos de esta tesis doctoral el desarrollo de dos sensores poliméricos para la detección y determinación de Zn(II) en muestras de pienso animal, así como para la detección y cuantificación de la concentración de Cu(II) en muestras de vino y/o mosto. Con esta iniciativa, se busca ofrecer soluciones innovadoras y efectivas para el control alimentario y contribuir al bienestar y la salud pública.

---

## 4.2. Sensor polimérico para la detección y cuantificación de Cu(II) en muestras de vino y/o mosto

El vino es un producto muy consumido a nivel mundial,<sup>87</sup> por lo que es esencial controlar y monitorizar su calidad mediante el análisis de diversos parámetros. En este sentido, el Grupo de Polímeros de la Universidad de Burgos ha colaborado con distintas organizaciones para cuantificar algunos elementos relevantes en la industria vinícola, como los polifenoles<sup>88</sup> o el hierro.<sup>89</sup> Fruto de estos trabajos, la compañía francesa «*ICV Groupe (Institut Coopératif du Vin)*» se acercó a nuestro grupo a finales de 2021 con una propuesta relacionada con su día a día: la detección de cobre en los mostos de vino blanco.

A concentraciones elevadas, el cobre puede producir las denominadas «quiebras cúpricas», que generan precipitados en el vino afectando de esta manera a su sabor, aroma y color.<sup>90</sup> Estas cantidades de cobre en el mosto pueden tener diferentes orígenes, aunque se cree que la más influyente son los fungicidas y pesticidas compuestos por cobre, que quedan impregnando la uva, y que a lo largo de los años también se han ido acumulando en los suelos de cultivo.<sup>91</sup>

En la actualidad, la industria utiliza la espectrometría de absorción atómica (FAAS) para determinar la concentración de cobre en el vino. Sin embargo, esta técnica requiere equipos costosos y personal especializado, lo que dificulta su implementación en cada bodega donde se produce el vino. Además, la deslocalización de «*ICV Groupe*» en toda Francia presenta otro desafío para la empresa, ya que analizan el 25% de la producción francesa de vinos con orígenes en diferentes regiones del país. La medida de cobre en los

<sup>87</sup> L. Agnoli, J.F. Outreville, *Appl. Econ. Perspect. Policy*, **2020**, 43, 1101–1124.

<sup>88</sup> S. Vallejos, D. Moreno, S. Ibeas, A. Muñoz, F.C. García, J.M. García, *Food Control*, **2019**, 106, 106684.

<sup>89</sup> S. Vallejos, A. Muñoz, S. Ibeas, F. Serna, F. C. García, J.M. García, *J. Mater. Chem. A*, **2013**, 1, 15435–15441.

<sup>90</sup> Kreitman, G. Y.; Danilewicz, J. C.; Jeffery, D. W.; Elias, R. J. *J. Agric. Food Chem.* **2016**, 64 , 4095–4104.

<sup>91</sup> X. Li, S. Dong, X. Su, *Sci. Rep.* **2018**, 8, 17407.

mostos es puntual y se realiza poco después de la cosecha, lo que significa que la empresa necesita conocer los resultados en un plazo muy corto (24-72 horas). Instalar un equipo de FAAS en cada bodega es una solución, pero resulta inviable desde el punto de vista económico. Por lo tanto, las muestras deben enviarse a diferentes laboratorios de análisis, lo que consume tiempo y en la mayoría de los casos, los resultados no llegan a tiempo.

En este contexto, y a petición de la empresa, se desarrolló un nuevo sensor polimérico en forma de film para la detección y cuantificación de cobre *in situ* en muestras de mosto para la producción de vino. Para la preparación de este material polimérico se sintetizó un monómero sensor basado en la estructura del ácido bicinconínico (BCA), que en presencia de Cu(I), provoca un cambio de color sobre el material final (**Figura 14**). Para la síntesis del monómero sensor, se modificó la estructura química del BCA incluyendo un resto polymerizable (un grupo vinílico), que permite su posterior copolimerización.

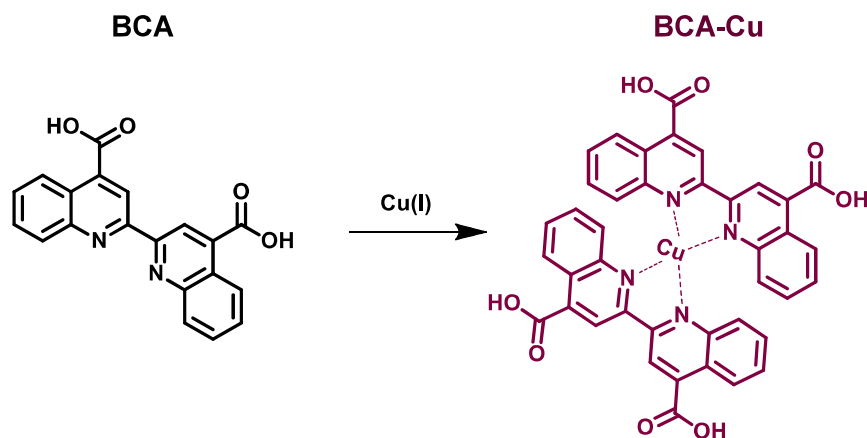


**Figura 14.** Reacción del ácido bicinconínico (BCA) con Cu(II) para la obtención del complejo coloreado. En los vinos está presente Cu(II) el cual se procederá a su reducción por medio de ácido ascórbico.

Una vez diseñado y preparado el monómero sensor, el film sensor se desarrolló mediante copolimerización radicalaria en bloque de *N*-vinilpirrolidona, metacrilato de metilo (como matriz estructural del polímero sensor) y el propio

monómero sensor, en proporciones molares de 49,75;49,75;0,5 respectivamente. Además, se añadió un 0,1 mol% de dimetacrilato de etilenglicol como entrecruzante, algo necesario para evitar la disolución del polímero durante su uso en mostos. Dadas las buenas experiencias con estos monómeros en los trabajos anteriores, de nuevo, decidimos utilizar una mezcla al 50% de metacrilato de metilo y *N*-vinilpirrolidona, aproximadamente, que otorga cierto carácter hidrofílico al film permitiendo así la interacción entre el material y el analito de interés. Esta mezcla de monómeros también se escogió por sus buenas propiedades mecánicas en hinchado, necesarias para el uso potencial de este material en un ambiente agrícola.

La química que sustenta el proceso de detección del cobre en los mostos se conoce desde hace décadas<sup>92</sup> y se emplea en otros ámbitos, como en la detección de proteínas.<sup>93</sup> El complejo organometálico que se forma es altamente específico para el cobre en su estado de oxidación (EO) +1, lo cual implica un proceso de reducción desde el EO más común en la naturaleza para el cobre, que es el EO +2, y es el que se encuentra en los mostos. Esto se superó añadiendo ácido ascórbico como agente reductor en los mostos justo antes de sumergir el polímero sensor en el mosto.

El material fue probado con muestras reales proporcionadas por la compañía, y el estudio completo se ha publicado en la revista *ACS Applied Materials and Interfaces*,<sup>94</sup> además, el material se encuentra patentado (**Figura 15**, Número de solicitud: P202231015).

<sup>92</sup> A.J. Brenner, E.D. Harris, *Anal. Biochem.* **1995**, 226, 80–84.

<sup>93</sup> J.M. Walker, *The Bicinchoninic Acid (BCA) Assay for Protein Quantitation*, in: J.M. Walker (Ed.), *Basic Protein Pept. Protoc.*, Humana Press, Totowa, NJ, **1994**: pp. 5–8.

<sup>94</sup> J.C. Guirado-Moreno, I. Carreira-Barral, S. Ibeas, J.M. García, D. Granès, N. Marchet, S. Vallejos, *ACS Appl. Mater. Interfaces.* **2023**, 15, 12, 16055–16062.



#### Justificante de presentación electrónica de solicitud de patente

Este documento es un justificante de que se ha recibido una solicitud española de patente por vía electrónica utilizando la conexión segura de la O.E.P.M. De acuerdo con lo dispuesto en el art. 16.1 del Reglamento de ejecución de la Ley 24/2015 de Patentes, se han asignado a su solicitud un número de expediente y una fecha de recepción de forma automática. La fecha de presentación de la solicitud a la que se refiere el art. 24 de la Ley le será comunicada posteriormente.

Número de solicitud:	P202231015	
Fecha de recepción:	24 noviembre 2022, 15:14 (CET)	
Oficina receptorá:	OEPM Madrid	
Su referencia:	Ref.2022.09_Conc.Cu	
Solicitante:	Universidad de Burgos	
Número de solicitantes:	1	
País:	ES	
Título:	COPOLÍMERO Y PROCEDIMIENTO PARA DETERMINAR LA CONCENTRACIÓN DE COBRE EN MOSTO O VINO BASADO EN EL MISMO	
Documentos enviados:	Descripción.pdf (19 p.) Resumen.pdf (1 p.) Dibujos.pdf (3 p.) Reivindicaciones.pdf (8 p.) OLF-ARCHIVE.zip	package-data.xml es-request.xml application-body.xml es-fee-sheet.xml feesheet.pdf request.pdf
Enviados por:	CN=SENDINO FERNANDEZ MARTA - 13165048D,SN=SENDINO FERNANDEZ,givenName=MARTA,serialNumber=IDCES-13165048D,C=ES	
Fecha y hora de recepción:	24 noviembre 2022, 15:14 (CET)	
Codificación del envío:	9D:5F:A8:64:4E:23:87:33:48:96:54:5F:A4:FB:5C:D4:7F:D7:52:6C	

**Figura 15.** Justificante de presentación electrónica de solicitud de patente. Número de solicitud: P202231015.

### 4.3. Sensor polimérico para la detección y cuantificación de Zn(II) en muestras de pienso animal

El zinc es un elemento esencial para los seres vivos, ya que está involucrado en una amplia variedad de procesos biológicos.<sup>95</sup> Es un componente estructural de muchas proteínas y enzimas, lo que significa que es necesario para el funcionamiento adecuado de muchas reacciones químicas en el cuerpo. También es importante para el desarrollo y mantenimiento del sistema inmunológico, la síntesis de proteínas, la cicatrización, la regulación del crecimiento y la señalización celular.<sup>96,97,44</sup> Además, el zinc es fundamental para la percepción del gusto y el olfato, y se encuentra en concentraciones altas en los músculos y huesos. La deficiencia de zinc puede causar una amplia gama de problemas de salud, como retraso del crecimiento, pérdida de cabello, inmunidad debilitada, diarrea y problemas de piel.

Como en prácticamente todos los principios activos de medicamentos, alimentos, complementos alimentarios, etc., y tal como indicó Paracelso en el siglo XVI, «*la dosis hace el veneno*». El caso del Zinc (II) no es una excepción, y aunque su ingesta es necesaria para la mayoría de los seres vivos, un exceso de zinc en la dieta implica riesgos para la salud.<sup>98</sup> Desde un punto de vista medioambiental, la presencia de una elevada cantidad de Zn(II) en suelos o aguas subterráneas también lleva asociados numerosos riesgos.<sup>99</sup>

En el año 2014, la EFSA (de sus siglas en inglés, «*European Food Safety Authority*») propuso la reducción del contenido de Zn(II) en los piensos debido a los problemas relativos a su toxicidad en concentraciones elevadas.<sup>100</sup> Aunque las intoxicaciones por Zn(II) de mascotas suelen estar asociadas a la ingesta de

<sup>95</sup> Y. Song, S.W. Leonard, M.G. Traber, E. Ho, *J. Nutr.* **2009**, 139, 1626–1631.

<sup>96</sup> H. Haase, L. Rink, *Immun. Ageing.* **2009**, 6, 1–17.

<sup>97</sup> L. Rink, P. Gabriel, *Proc. Nutr. Soc.* **2000**, 59, 541–552.

<sup>98</sup> M. Guembe-García, S. Vallejos, I. Carreira-Barral, S. Ibeas, F. C. García, V. Santaolalla-García, J.M. García, *React. Funct. Polym.* **2020**, 154, 104685.

<sup>99</sup> S. Hussain, M. Khan, T. Majid, M. Sheikh, M.Z. Mumtaz, T.A. Chohan, S. Shamim, Y. Liu, *Front. Microbiol.* **2022**, 13, 900740.

<sup>100</sup> Z.B. Fard, F. Ghadimi, H. Fattahi, *J. Min. Environ.* **2017**, 8, 35–48.

<sup>100</sup> A.M. Pereira, M.R.G. Maia, A.J.M. Fonseca, A.R.J. Cabrita, *Animals.* **2021**, 11, 978.

un cuerpo extraño, también existen casos de mascotas con una dieta de alto contenido de Zn(II) que ocasiona síntomas como vómitos, diarrea, anemia, ictericia o incluso daños renales o hepáticos.<sup>101</sup> Por lo que, a raíz de esta problemática, la Unión Europea estableció una concentración máxima permitida de 100-150 mg/kg en los piensos destinados a la alimentación animal.<sup>102</sup> El método actual de medida de Zn(II) en piensos se realiza mediante una extracción del catión Zn(II) que posteriormente, se mide por espectrometría de masas por plasma acoplado inductivamente (ICP-MS).<sup>103</sup>

Siguiendo la misma línea de polímeros sensores que se desarrollaron para la detección de cobre en vinos, propusimos una solución para la cuantificación de Zn(II) de forma visual en muestras de pienso. En este caso, escogimos un receptor basado en la estructura de la quinolina para la síntesis del monómero sensor, debido a que han demostrado gran potencial para formar complejos estables con Zn(II), que además presentan fluorescencia.<sup>44,104</sup> Se introdujo un grupo polimerizable en el receptor a través de reacciones de química orgánica simples, lo que permitió obtener el monómero sensor final (**Figura 16**). Para la matriz estructural, se reutilizó la formulación del sensor de cobre en vinos, ya que tanto la aplicación como el procedimiento experimental de cuantificación con el material eran muy similares.

Como en todos los trabajos que se han realizado en el marco de esta tesis, en este caso también se llevó a cabo una prueba de concepto, en la que se probó el material desarrollado en diferentes piensos comerciales para mascotas, principalmente, perros y gatos. En este caso, el Zn(II) de las muestras se extrajo con ácido tricloroacético diluido, se tamponaron, y los materiales simplemente se sumergieron en las disoluciones resultantes. La interacción del material con el Zn(II) generó una respuesta fluorescente, que se registró con

---

<sup>101</sup> J.W. Siow, *Open Vet. J.* **2018**, 8, 458–462.

<sup>102</sup> E. Food, S. Authority, *EFSA J.* **2014**, 12, 1–77.

<sup>103</sup> T. King, R. Sheridan, *J. AOAC Int.* **2019**, 102, 434–444.

<sup>104</sup> X. Sun, Y. Wang, Y. Lei, *Chem. Soc. Rev.* **2015**, 44, 8019–8061.

<sup>44</sup> M. Guembe-García, S. Vallejos, I. Carreira-Barral, S. Ibeas, F. C. García, V. Santaolalla-García, J.M. García, *React. Funct. Polym.* **2020**, 154, 104685.

---

equipos de fluorescencia y también con un teléfono inteligente. Todo el proceso se validó utilizando ICP-MS como técnica de referencia para cuantificar la concentración de Zn(II) en los piensos.

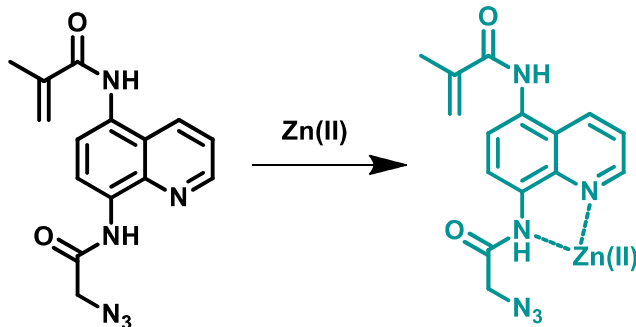


**Figura 16.** Reacción del monómero sensor con Zn(II) para la obtención del complejo fluoróforo.

El estudio completo se publicó en la revista *Spectrochimica Acta Part A: Molecular and Biomolecular Spectroscopy*.<sup>105</sup>

#### 4.4. Resultados

A continuación, se muestran los resultados obtenidos a través de la transcripción íntegra de los trabajos publicados:

- *Democratization of copper analysis in grape must following a polymer-based lab-on-a-chip approach.*
- *Smart sensory polymer for straightforward Zn(II) detection in pet food simples.*

<sup>105</sup> J. C. Guirado-Moreno, I. Carreira-Barral, L. Gonzalez, M.T. Sancho, S. Ibeas, M.A. Fernández-Muiño, *Spectrochim. Acta A Mol. Biomol. Spectrosc.*, **2023**, 284, 0–7.



*Democratization of copper analysis in grape must following a polymer-based lab-on-a-chip approach.*



## **Democratization of copper analysis in grape must following a polymer-based lab-on-a-chip approach**

José Carlos Guirado-Moreno<sup>a</sup>, Israel Carreira-Barral<sup>a</sup>, Saturnino Ibeas<sup>a</sup>, José M. García<sup>a</sup>, Daniel Granes<sup>b</sup>, Nicolas Marchet<sup>b</sup>, Saúl Vallejos<sup>a,\*</sup>

<sup>a</sup> Departamento de Química, Facultad de Ciencias, Universidad de Burgos, Plaza Misael Bañuelos s/n, 09001 Burgos, Spain

<sup>b</sup> Groupe ICV, Direction Générale, La Jasse de Maurin, 34970, Lattes, France.

\* Corresponding author: Dr Vallejos ([svallejos@ubu.es](mailto:svallejos@ubu.es))

### **Abstract**

Quality control in food industry is of the upmost importance from the food safety, and organoleptic and commercial viewpoints. Accordingly, the development of in-situ, rapid and costless analytical tools is a valuable task in which we are working. Regarding this point, the copper content of grape must has to be determined by wineries along the wine production process. For this purpose, grape must samples are sent to laboratories where the copper content is measured usually by flame atomic absorption spectrometry or by inductively coupled plasma mass spectrometry. We herein propose a straightforward, rapid, and inexpensive methodology based both on a film-shaped colorimetric polymer sensor and a smartphone, method that at the same time can be used by unskilled personnel. The sensory polymer films change its color upon dipping it on the grape must and the color evolution is analyzed using the digital color parameters of a picture taken to the film with a smartphone. Furthermore, the analytical procedure is automatically carried out by a smartphone app. The limit of detection of copper of the polymer sensor is 0.08 ppm. Following this approach, 18 production samples coming from the French Groupe ICV company were studied.

**Keywords:** copper detection; grape must; wine industry; sensory polymers; colorimetry; RGB parameters.

*ACS applied materials and Interfaces, 2023, 15, 12, 16055-16062.*

The copper content of the samples was analyzed by the usual procedure carried out by the company (flame atomic absorption spectrometry) and by the method proposed in this work, ranging this content from 0,41 to 6,08 ppm. The statistical study showed that the results of both methos are fully consistent showing that the validity of the propose method for the determination of copper in grape must within the frame of wine production wineries and industries.

## 1. Introduction

Quality control in processed food products is an issue both related to food safety and to the organoleptic perception by the final user. Accordingly, it is gaining increasing relevance yearly, both in final products and in the intermediate production stages.<sup>1-5</sup> For example, a number of analyses are mandatory to pass specific controls and/or to determine the concentration of different markers in beverages such as wine and are related to different organoleptic properties, such as color, flavor, etc.

During the intermediate production processes, grape must contains between 120 and 250 g/L of sugar and between 2.5 and 3.5 g/L of mineral substances.<sup>6-8</sup> Copper is a minority part of the latter, so the amount is quite low.<sup>6</sup> On the one hand, its presence is essential to obtain quality wines since metallic cations such as copper, potassium, magnesium, iron, calcium, cobalt, and zinc are necessary for the proper alcoholic fermentation of sugars. On the other hand, high levels of them could generate problems to the beverage's quality or safety. Metal tanks and pipes used in manufacturing or antifungal treatments in cultivation can increase the concentration of metals such as copper, giving rise to the so-called cupric cracks, which manifest as reddish-brown sediments. The cupric crack is especially important in white wines and is usually avoided by adding bentonite or arabic gum. However, these treatments are not applicable for copper concentrations above 1 mg/L.<sup>9-13</sup>

Among the most common techniques in wineries for copper quantification are flame atomic absorption spectrometry (FAAS) and inductively coupled

---

plasma mass spectrometry (ICP-MS), which imply non-*in-situ* analyses carried out by specialized personnel and with high-cost equipment.<sup>14</sup> Smart polymers can offer more direct and simple solutions to this type of analysis. Smart polymers can respond to a stimulus with an action (reactive polymers) or with an alert (sensory polymers).<sup>15</sup> The latter are based on the same concept as conventional colorimetric probes for anions<sup>16,17</sup> or cations<sup>18–20</sup> but provide great added value by dispensing with the handling of reagents and solvents and being able to work in completely aqueous media.<sup>21–25</sup>

In this work, we propose the democratization of this type of analysis of copper in grape must, by using a film-shaped smart sensory polymer that selectively interacts with copper and generates a color change. Furthermore, our proposal combines the use of the film with a free smartphone application,<sup>3</sup> which analyses the RGB parameters of the formed color. The material is mainly based on commercially available monomers (99.5 mol%), combined with a small amount (0.5 mol%) of a sensory monomer based on the chemical structure of a well-known copper chelating agent as bicinchoninic acid (BCA).<sup>26,27</sup>

## 2. Experimental

### 2.1. Materials

All materials and solvents were commercially available and used as received unless otherwise indicated. The following materials and solvents were used: 1-vinyl-2-pyrrolidone (VP) (99%, Aldrich), methyl methacrylate (MMA) (99%, Aldrich), ethylene glycol dimethacrylate (E) (97.5%, Aldrich), pH 5.00 Citrate Buffer (VWR), acetone (99%, VWR), zinc(II) nitrate hexahydrate (98%, Sigma-Aldrich), iron(III) nitrate nonahydrate (99%, Sigma-Aldrich), manganese(II) nitrate hexahydrate (98+, Alfa Aesar), cobalt(II) nitrate hexahydrate (≥99%, Labkem), calcium nitrate tetrahydrate (≥99%, Sigma-Aldrich), mercury(II) nitrate (98%, Alfa Aesar), cadmium nitrate tetrahydrate (98.5%, Alfa Aesar), potassium nitrate (99+, Sigma-Aldrich), lead(II) nitrate (≥ 99%, Fluka), iron(II) sulphate heptahydrate (99%, Sigma-Aldrich), magnesium nitrate hexahydrate (≥ 99%,

---

Labkem), copper(II) sulphate pentahydrate (98%, Sigma-Aldrich), copper(I) iodide (99%, Riedel-de-Häen), nickel(II) nitrate hexahydrate (98.5%, Sigma-Aldrich), sodium nitrate (99%, LabKem), cesium nitrate ( $\geq$ 99%, Fluka), barium chloride dihydrate (99%, Labkem), ammonium nitrate ( $\geq$ 98%, Sigma-Aldrich), chromium(III) nitrate (98.5%, Alfa Aesar), rubidium nitrate (99.95%, Sigma-Aldrich), dysprosium(III) nitrate (99.9%, Alfa Aesar), lithium chloride ( $\geq$ 99%, Sigma-Aldrich), cerium(III) chloride tetrahydrate ( $\geq$ 99.99%, Sigma-Aldrich), zirconium(IV) chloride (98%, Alfa Aesar), lanthanum(III) nitrate hexahydrate (99.9%, Alfa Aesar), samarium(III) nitrate (99.9%, Alfa Aesar), aluminium(III) nitrate ( $\geq$ 98.9%, Sigma-Aldrich), silver(I) nitrate ( $\geq$ 99.9%, Sigma-Aldrich), neodymium(III) nitrate (99.9%, Alfa Aesar), strontium nitrate (99%, Sigma-Aldrich), potassium hydroxide (99%, VWR-Prolabo), hydrochloric acid (37%, VWR-Prolabo), ethanol ( $\geq$ 99.9%, VWR), methanol ( $\geq$ 99.8%, VWR), tetrahydrofuran ( $\geq$ 99.9%, VWR), ethyl acetate ( $\geq$ 99.9%, VWR), dimethylsulfoxide-*d*<sub>6</sub> (99.9%, VWR), dimethylformamide (99.9%, Supelco), 4-aminostyrene ( $\geq$ 98%, TCI), N,N'-dicyclohexylcarbodiimide (DCC) (99%, Sigma-Aldrich), bicinchoninic acid disodium salt ( $\geq$ 98%, TCI). Azo-bis-isobutyronitrile (AIBN, Aldrich, 98%) was recrystallized twice from methanol.

The grape must samples were provided by the French company “Groupe ICV”, collected in late summer 2021, frozen and sent to the University of Burgos and Groupe ICV-Toulouges, to perform the copper analysis by two methodologies, i.e., using the sensory polymer (proposed method) and FAAS (reference method). Once thawed, sediments can be formed in grape must samples, so they were stabilized with sodium azide (NaN<sub>3</sub>) before the frozen process. More information about grape must samples can be found in the supporting information (**SI**), **Section-S1**.

## 2.2. Instrumentation and methods

<sup>1</sup>H and <sup>13</sup>C{<sup>1</sup>H} NMR spectra (Advance III HD spectrometer, Bruker Corporation, Billerica, Massachusetts, USA) were recorded at 300 MHz for <sup>1</sup>H and 75 MHz for <sup>13</sup>C using deuterated dimethylsulfoxide (DMSO-*d*<sub>6</sub>) at 25°C as solvent.

---

The polymers' thermal and mechanical characterization was performed by: a) thermogravimetric analysis (Q50 TGA analyzer, TA Instruments, New Castle, DE, USA) with 10–15 mg of sample under synthetic air and nitrogen atmosphere at  $10^{\circ}\text{C}\cdot\text{min}^{-1}$ ; b) differential scanning calorimetry, with 10–15 mg of the sample under a nitrogen atmosphere at a heating rate of  $10^{\circ}\text{C}\cdot\text{min}^{-1}$  (Q200 DSC analyzer, TA Instruments, New Castle, DE, USA), and c) tensile properties analysis of the samples ( $5 \times 9.44 \times 0.122$  mm at  $1 \text{ mm}\cdot\text{min}^{-1}$ ) (Shimadzu EZ Test Compact Table-Top Universal Tester, Shimadzu, Kyoto, Japan).

Infrared spectra (FTIR) were recorded with an infrared spectrometer (FT/IR-4200, Jasco, Tokyo, Japan) with an ATR-PRO410-S single reflection accessory.

FAAS was performed with an atomic absorption spectrophotometer (GBC 933 AA, Gbc Scientific, Braeside, Australia).

Ultraviolet visible spectroscopy (UV/Vis) spectra were recorded using a spectrophotometer (Hitachi U-3900, Hitachi, Tokyo, Japan). A rectangular 10 mm cuvette was used for the measurements, which were all conducted at  $25^{\circ}\text{C} \pm 0.1^{\circ}\text{C}$ .

The weight percentage of water taken up by the films upon soaking in pure water at  $20^{\circ}\text{C}$  until reaching equilibrium (water-swelling percentage, WSP) was obtained from the weight of a dry sample film ( $\omega_d$ ) and its water-swelled weight ( $\omega_s$ ) using the following expression:  $\text{WSP} = 100 \times [(\omega_s - \omega_d)/\omega_d]$ .

High-resolution mass spectrometry (HRMS) was carried out on an Agilent 1260 HPLC-Infinity coupled with a 6545 ESI-Q-TOF/MS system (Agilent Technologies, Palo Alto, CA, USA).

Digital photographs were taken with a Huawei p30 pro (Huawei, Shenzhen, China), placing the films within a homemade lightbox to reproduce always the same lighting conditions.<sup>28</sup> The distance between the object and the smartphone was 13 cm. G parameter of digital photographs was extracted using the smartphone app "Colorimetric Titration".<sup>29,30</sup>

---

### 2.3. Synthesis of the sensory monomer **Mono-BCA**

We prepared the sensory monomer **Mono-BCA** using bicinchoninic acid disodium salt as reactant. The reactions are depicted in **Figure 1a**, and the complete description of the synthetic procedure and the full characterization of intermediates and monomer can be found in the Supporting Information (**SI-Section S2**).

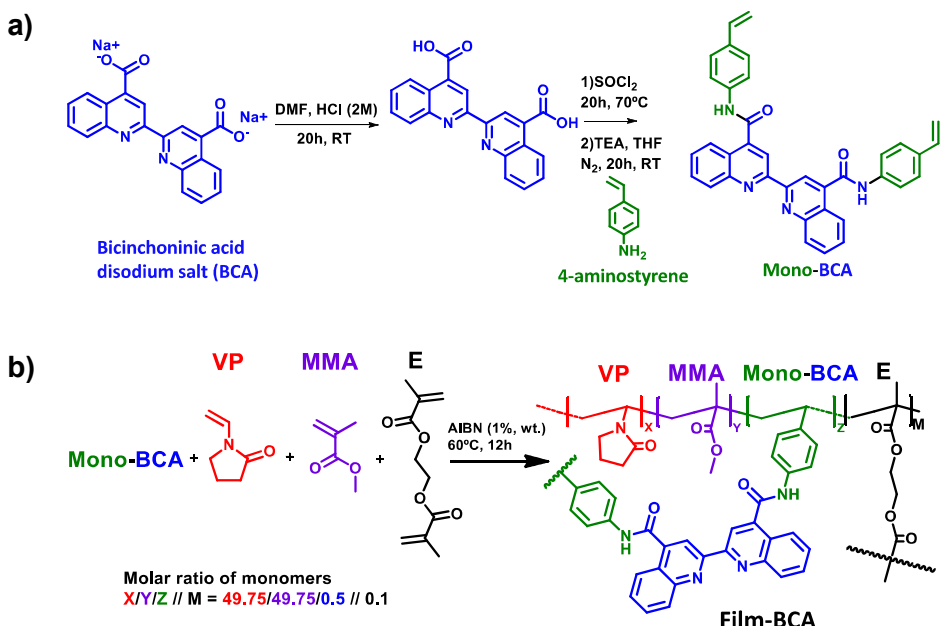


**Figure 1.** Synthetic route for: a) the sensory monomer **Mono-BCA**; and b) the film-shaped sensory polymer **Film-BCA**.

### 2.4. Preparation of the sensory polymer synthesis **Film-BCA**

We prepared the sensory film **Film-BCA** by thermally initiated bulk radical polymerization.<sup>31</sup> In a vial, two commercial monomers (VP and MMA), a crosslinker (ethylene glycol dimethacrylate, E), the synthesized sensory monomer (**Mono-BCA**) and DMSO (same volume as the sum of monomers) were mixed in a molar ratio of 49.75/49.75/0.5//0.1 (VP/MMA/**Mono-BCA**//E). Additionally, we added AIBN (1%, wt.) as the radical thermal initiator. We injected

the mixture into a mold (200  $\mu\text{m}$  thickness) comprised of two sealed silanized glasses and heated it overnight at 60 °C, where the polymerization took place under an oxygen-free atmosphere. Finally, we washed the resultant film-shaped material with water and methanol and cut it into 8 mm side squares with plastic scissors. The sensory material was stored in zip bags to keep it moist, and to prevent it from drying out and cracking. Plastic or glass materials were used throughout the process to avoid contamination with copper. The FTIR, TGA, DSC, and PXRD patterns can be found in **SI-Section S3**.

#### *2.5. Preparation of the solution to record the mass spectrum of the 2:1 and 1:1 **Mono-BCA:Cu(I)** complexes*

Firstly, a  $10^{-4}$  M solution of **Mono-BCA** in DMSO was prepared. Secondly, a DMSO solution containing  $\text{CuSO}_4 \cdot 5\text{H}_2\text{O}$  ( $10^{-3}$  M) and ascorbic acid ( $3.3 \times 10^{-3}$  M) was prepared; ascorbic acid was required to reduce Cu(II) to Cu(I). Subsequently, 1.4 mL of the latter were added to 2.0 mL of the former while stirring. In this way, the solution contains an excess of Cu(I) (6.7 eq.), thus ensuring the formation of the complex. An aliquot of this solution was taken, and its mass spectrum (+ESI) recorded. The spectrum and the magnification of the peaks corresponding to the 2:1 and 1:1 **Mono-BCA:Cu(I)** complexes are displayed in **SI-Section S4**.

#### *2.6. Selectivity study*

We conducted a selectivity study to evaluate the colorimetric response of **Film-BCA** with 30 different cations. Sensory squares were dipped into aqueous solutions of cations ( $5 \times 10^{-3}$  M, distilled water) for 12 hours. Finally, sensory squares were washed with water and methanol and were photographed together under the same light conditions.

#### *2.7. Titration by UV-Vis of Cu(I) with **Mono-BCA***

A  $\text{CuSO}_4 \cdot 5\text{H}_2\text{O}$  solution ( $1 \times 10^{-3}$  M, DMSO) was titrated with a solution of **Mono-BCA** ( $1.04 \times 10^{-4}$  M, DMSO), and the spectra were recorded at final copper concentrations ranging from  $4.9 \times 10^{-6}$  M to  $4.1 \times 10^{-4}$  M, DMSO. The copper solution included 0.06 mg/mL of ascorbic acid, necessary to reduce Cu(II) to

Cu(I). The UV-Vis spectra were recorded at  $25\text{ C} \pm 0.1\text{ }^{\circ}\text{C}$  using the following conditions: slit width = 2 nm; scan speed = 600 nm/min; step = 0.5 nm.

#### *2.8. Titration of Cu(I) with **Film-BCA***

We carried out the experiment by immersing for 12 hours **Film-BCA** sensory squares (8 mm side) in solutions containing 50  $\mu\text{L}$  of a pH 5 buffered aqueous solution of ascorbic acid (0.08 g/mL), and 2 mL of a pH 5 buffered aqueous solution of Cu(II) solutions ranging from 0.5 to 10 ppm. After that, sensory squares were washed with water and photographed with the smartphone. The measurements were carried out in duplicate.

#### *2.9. Detection and quantification of copper in grape musts with **FILM-BCA***

Similarly, to the procedure described in Section 2.8, eighteen grape must samples from the French company Groupe ICV were measured in duplicate by mixing 2 mL of grape must with 50  $\mu\text{L}$  of an aqueous solution of ascorbic acid (0.08 g/mL) buffered at pH 5. The sensory squares (8 mm side) were finally dipped in this solution for 12 hours, washed with water (10 mL for 15 minutes) and methanol (10 mL for 15 minutes), and washed again with water (10 mL for 15 minutes). Afterward, we photographed the sensory squares and extracted the G parameter from the digital images. This parameter was correlated with the results obtained from Groupe ICV by FAAS. **Figure 2** shows the procedure schematically.

#### *2.10. Limits of detection (LOD) and quantification (LOQ)*

The limit of detection (LOD) and the limit of quantification (LOQ) of our sensory system was calculated by the following equations:  $\text{LOD} = 3.3 \times SD/s$  and  $\text{LOQ} = 10 \times SD/s$ , respectively, where “SD” is the standard deviation of the blank sample and “s” is the slope of a calibration curve in the region of low analyte content, from 0.25 to 1 ppm. The calibration curve and the fitted equation is shown in **Figure S6, SI-Section S5**.

---

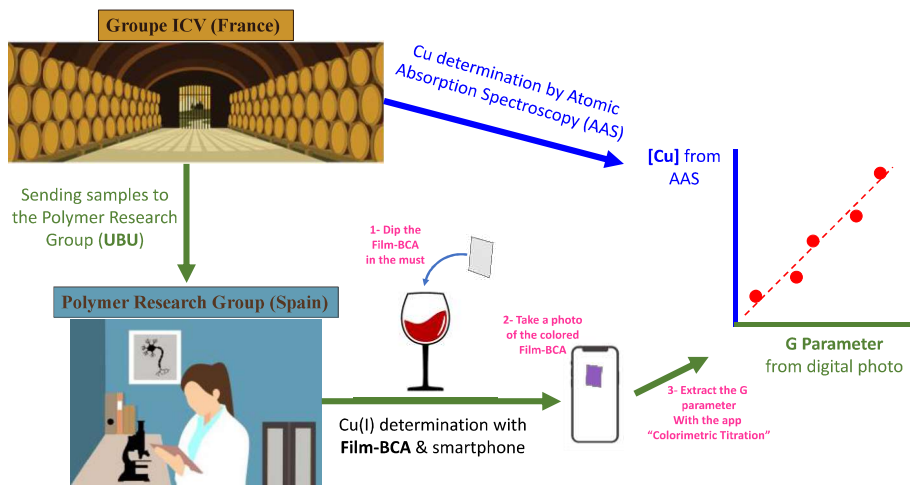


**Figure 2.** Graphical abstract of the experimental procedure carried out for the quantification of copper in grape must samples by FAAS and by using Film-BCA.

### 3. Results and discussion

In this work, we report on a new way to measure copper in the pre-fermentation stage of wine production. The process is carried out with a smart film-shaped sensory polymeric material able to interact with Cu(I), signaling this interaction by providing a color change. Below we will briefly describe the design of the material, the interaction with Cu(I), and the proof of concept carried out with 18 grape musts.

#### 3.1. Design of the film-shaped smart sensory polymer

The study stems from the need expressed by the French company "Groupe ICV" to create an alternative method to FAAS as the most common method for measuring total copper in grape musts. Installing a flame photometer within each winery is an economically unfeasible strategy for highly delocalized companies such as "Groupe ICV", which analyzes samples from branches distributed throughout the French territory. In addition, not all wineries have the appropriate facilities and specialized personnel to carry out copper quantification using the methods described in the literature,<sup>27</sup> which require advanced equipment and

handling of reagents/solvents. Therefore, we proposed simplifying the analysis as much as possible for this study, using a sensory polymer and a smartphone.

The material is oriented to *in-situ* field-tests, and probably to be used by non-specialized personnel, so we designed a material resistant to careless handling containing a high mol% of MMA (49.75 mol%), a monomer that provides great rigidity to the material. On the other hand, the material needs to absorb the grape must sample (aqueous medium), so it also requires certain hydrophilicity, which in this case is provided by the VP monomer (49.75 mol%). Finally, the chemical modification of a molecule widely known in the field of copper detection, BCA, was proposed.<sup>27</sup> This molecule cannot be chemically anchored to a polyacrylic material since it is not a monomer, so a polymerizable group was introduced into the chemical structure, as graphically depicted in **Figure 1a**. A small amount (0.5 mol%) of the resulting sensory monomer was copolymerized with VP and MMA, but enough for a visual color change of the material in the presence of Cu(I).

The designed films are thermostable materials, chemically crosslinked with ethyleneglycol dimethacrylate (**Figure 1b**). The nominal crosslinking ratio of the material is 167, which is directly related to the water swelling percentage of the material (75%), as seen analogously in previous works.<sup>32</sup> **Film-BCA** had a glass transition temperature of 142 °C, a thermal resistance, in terms of 5% and 10% weight loss of 351 and 370 °C, respectively, and a Young's modulus of 299 MPa.

### 3.2. Study of the interaction of the sensory monomer **Mono-BCA** with Cu(I)

The stoichiometry of the **Mono-BCA**:Cu(I) complex was studied by mass spectrometry and UV-Vis spectrophotometry, and the measurements were carried out by using DMSO as solvent, due to the low solubility of Mono-BCA both in water and water:organic solvent mixtures.

In the results from mass spectrometry, we found two different peaks related to two complexes with stoichiometries 1:1 and 2:1 (**Mono-BCA**:Cu(I)),

---

being the 2:1 stoichiometry the most expected one as described in similar studies carried out with BCA and Cu(I) (see **Figure S4** in **SI-Section S4**).<sup>26</sup>

Concerning UV-Vis spectrophotometry, we focused on the band centered at 566 nm, corresponding to the formation of the colored complex, as shown in **Figure 3a**. Fitting of the titration profile provides a high complex formation constant,  $3.6 \times 10^6$  M, and the Job's plot representation shows a maximum at Mono-BCA's molar ratio of 0.5, which means a 1:1 stoichiometry (**Figure 3b**).

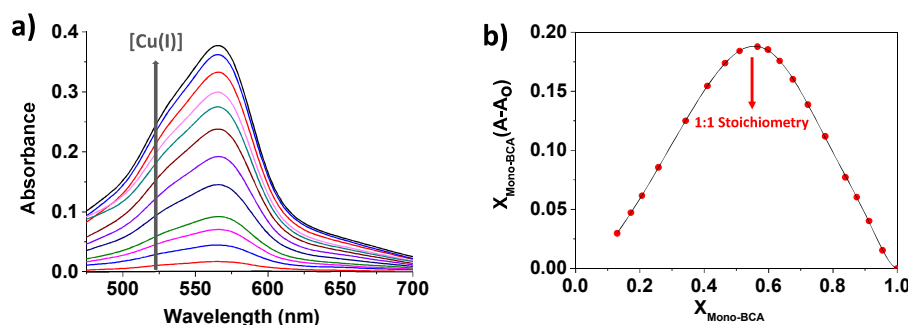


**Figure 3.** **a)** Titration of Cu(I) with **Mono-BCA** in DMSO. The concentration of Cu(I) in the cuvette was increased from  $4.9 \times 10^{-6}$  M to  $4.1 \times 10^{-4}$  M and the initial concentration of **Mono-BCA** was  $8.6 \times 10^{-5}$  M. **b)** Job's Plot diagram, which represents  $X_{\text{Mono-BCA}}(A-A_0)$  versus the molar fraction of **Mono-BCA**. " $A_0$ " is the initial absorbance at 566 nm ( $[\text{Cu(I)}]=0$  M), and "A" is the absorbance at 566 nm for each point of the titration.

The experimental conditions, especially the solvent (DMSO), do not correspond to the real measurement conditions in grape musts (aqueous medium). Nevertheless, the results indicate a great affinity between **Mono-BCA** and Cu(I), so we extrapolate this behavior when working with **Film-BCA**.

### 3.3. Selectivity study of **Film-BCA** with 30 cations

As shown in **Figure 4a**, **Film-BCA** only changes color in the presence of Cu(I) and Ag(I). Therefore, **Film-BCA** does not change color with the most abundant cations in wine, such as Na(I) or K(I), which is a great advantage. In addition,

$\text{Ag(I)}$  concentrations in wine are negligible,<sup>33,34</sup> so we consider **Film-BCA** does not present interferences to quantify copper in grape musts.

### 3.4. Preliminary experiments. Copper quantification in aqueous solutions using **Film-BCA**

After dipping squares of **Film-BCA** in  $\text{Cu(II)}$  solutions with concentrations ranging from 0.5 to 10 ppm, and after taking a photograph of the films, the G parameter was extracted and represented against the copper concentration. The trend is linear in this concentration range, as shown in **Figure 4b**, and the obtained limits of detection (LOD) and quantification (LOQ) were 0.08 and 0.25 ppm, respectively (more info in **SI-Section S5**). Therefore, these limits are suitable for this application, where the most found copper concentrations range is 0.2-6 ppm.

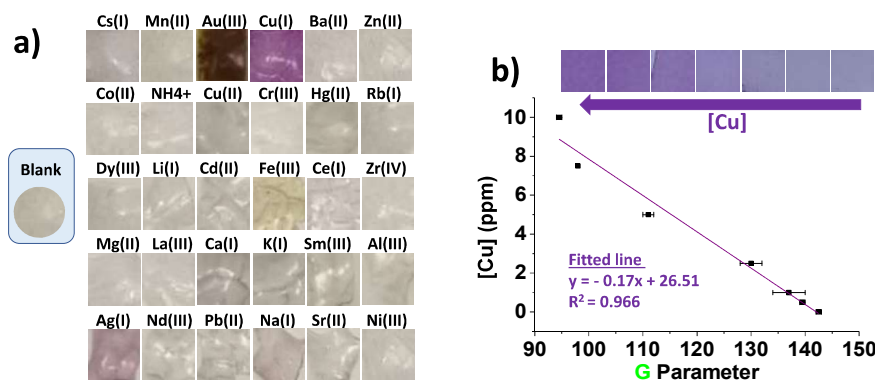


**Figure 4.** a) Photograph of the qualitative experiment for testing the colorimetric response of **Film-BCA** with 30 cations. Experimental conditions: Cation concentration ( $5 \times 10^{-3}$  M) in pH 5 aqueous buffer; volume = 2 mL, dipping time = overnight. b) Sensory squares (8 mm side) of **Film-BCA** were dipped for 12 hours in aqueous solutions containing 2 mL of pH 5 buffered aqueous  $\text{Cu(II)}$  solutions (concentrations ranging from 0.5 to 10 ppm) and 50  $\mu\text{L}$  of pH 5 buffered aqueous solution of ascorbic acid (0.08 g/mL). The graph shows the representation of the copper concentration vs the G parameter from the photographed squares (mean  $\pm$  standard error of 2 replicates).

### 3.5. Proof of Concept. Copper quantification in grape musts using **Film-BCA**

After validating the operation of **Film-BCA** in preliminary tests, we set out to carry out a proof of concept using real samples of grape must from the wine industry. The copper concentration results obtained by Groupe ICV in France were used

as a reference (FAAS), so the color obtained in the **Film-BCA** sensor squares was plotted against those reference data. The result of this fitting is shown in **Figure 5**. Finally, if the G parameter of each sample is reintroduced in that fitted equation, the copper concentration data shown in **Table 1** are obtained and these results can be compared with the reference method.

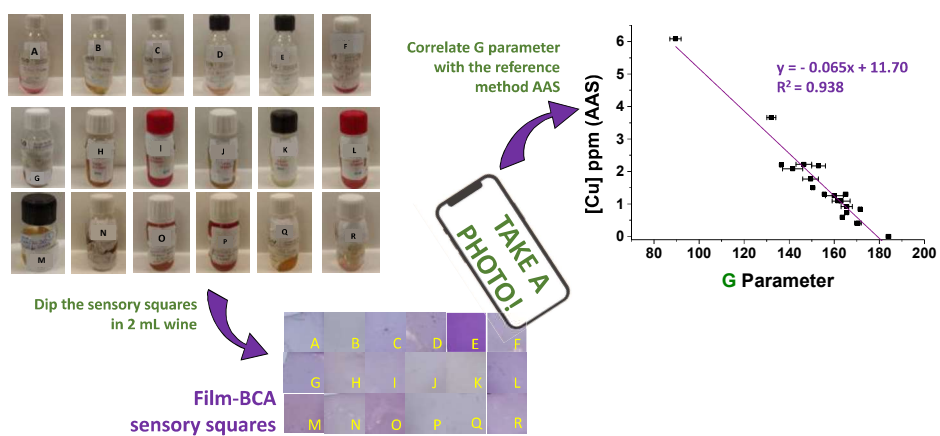


**Figure 5.** Graphical abstract of the proof of concept, including the representation of the Cu concentration obtained by the reference method (FAAS) against the G parameter obtained from the photographs (**Film-BCA**, data are means  $\pm$  standard error of 2 replicates).

The data shown in Table 1 have been statistically analyzed with a Mann-Whitney independent samples t-test (non-parametric test, **SI-Section S6**), and we can affirm that there is no significant difference between the means of the two methods.

Samples B and J require special mention, since the FAAS method indicates that sample J has more copper, and method B indicates that sample B is the most concentrated. Our interpretation is that there was some contamination when carrying out the FAAS sample preparation, something relatively acceptable in an agricultural environment.

**Table 1.** Cu(I) concentration of measured grape musts obtained by the reference method (FAAS) and the proposed method, based on the use of **Film-BCA** and a smartphone. Cu concentration data from **Film-Cu** method are means of  $\pm$  standard errors of 2 replicates.

Sample ID	Geographical origin	Concentration (ppm)	
		FAAS	Film-Cu
A	Trèbes	0.73	0.89 $\pm$ 0.03
B	Trèbes	0.59	1.02 $\pm$ 0.03
C	Trèbes	1.3	1.54 $\pm$ 0.03
D	Provence	2.08	2.45 $\pm$ 0.29
E	Provence	6.08	5.85 $\pm$ 0.16
F	Provence	1.09	1.05 $\pm$ 0.26
G	Toulouges	1.5	1.87 $\pm$ 0.03
H	Beaumes	1.25	1.25 $\pm$ 0.26
I	Beaumes	2.17	1.70 $\pm$ 0.20
J	Beaumes	0.84	0.49 $\pm$ 0.03
K	Beaumes	0.41	0.56 $\pm$ 0.10
L	Beaumes	2.22	2.13 $\pm$ 0.23
M	Maurin	3.66	3.08 $\pm$ 0.13
N	Toulouges	1.1	1.15 $\pm$ 0.03
O	Nîmes	2.2	2.78 $\pm$ 0.03
P	Nîmes	0.92	0.89 $\pm$ 0.16
Q	Toulouges	1.3	0.93 $\pm$ 0.07
R	Narbonne	1.77	1.93 $\pm$ 0.23

In short, our proposed material can be easily used at wineries to analyze copper in grape musts. This could represent a significant advance for wineries since the timeouts and sample transport are reduced, increasing productivity, and reducing the risk of cupric cracks, with the only technical requirement of having a smartphone. Comparatively, Table 2 shows the most used methods for the quantification of copper, especially in wineries, emphasizing the possibility of

carrying out an *in-situ* detection, with the required equipment, and the detection limits.

**Table 2.** Figure of merits showing the advantages and disadvantages of the proposed methodology for the quantification of Cu in grape musts/wines against the most used ones.

Detection method	In situ measure	Quantification in wine/grape must	Equipment required	LOD	Ref.
<b>FAAS</b>	No	Yes	Flame atomic absorption spectrometer	0.40 µg/L	35
	No	No	ICP-Mass spectrometer	2.0 µg/g	36
	No	Yes	ICP-Mass spectrometer	-	37
<b>ICP-MS</b>	No	Yes	ICP-Mass spectrometer	0.04 µg/L	38
	No	Yes	ICP-Mass spectrometer	0.6 µg/L	39
	No	No	Fluorimeter	-	40
<b>Fluorimetry probes in solution</b>	No	Yes	Fluorimeter	8.2 µg/L	41
<b>Total reflection X-ray fluorescence</b>	No	Yes	TXRF spectrometer	0.1 mg/L	42
<b>Colorimetric probes in solution</b>	No	Yes	UV/Vis spectrophotometer	0.01 mg/L	43
	No	No	UV/Vis spectrophotometer	0.5 nM	44
<b>Colorimetric chemosensor nanofibrous hydrogel</b>	Yes	No	UV/Vis spectrophotometer	0.01 mg/L	45
<b>Colorimetric film (Film-BCA)</b>	Yes	Yes	Smartphone	0.08 mg/L	This Work

#### 4. Conclusions

In-situ and inexpensive detection methods and methodologies are a tool that is in great demand by companies dedicated to laboratory analysis, especially when results are needed quickly and sample sending is ruled out. In collaboration with the company Groupe ICV, dedicated to chemical analysis in the wine industry, we have jointly developed a film-shaped smart sensory polymer for the quantification of copper in grape must, the novelty of which is that it does not require specialized personnel, reagents or specialized equipment. The material is an excellent tool for this type of company, which has wineries all over the country and cannot afford the installation and maintenance of expensive and advanced equipment for quantifying a key parameter in wine production, such as copper concentration. It is a robust system that we have tested with real samples of grape musts provided by the mentioned company, which are also from different growing areas, such as Narbonne, Nîmes, Maurin, Beaumes, Toulouges, Provence, and Trèbes. For this publication, we have worked with dipping times of 12 hours since it is important to reach the system's equilibrium to draw solid conclusions. However, this time can be reduced and adapted to the needs of the industry. The limits of detection (LOD) and quantification (LOQ) offered by the material are 0.08 and 0.25 ppm, respectively, which makes it suitable for this specific application. The sensory material, methodology, and necessary equipment have been easily oriented for use by non-specialized personnel, and therefore the only device needed for copper quantification is a smartphone.

#### Supporting Information

Information about grape must samples; synthesis and characterization of Mono-BCA; characterization of the sensory polymer Film-BCA; high-resolution mass spectra of the 2:1 and 1:1 Mono-BCA:Cu(I) complexes; information about the limit of detection (LOD) and limit of quantification (LOQ); statistical analysis.

The supporting information is available free of charge at:

---

[https://pubs.acs.org/doi/suppl/10.1021/acسامي.3c00395/suppl\\_file/am3c00395\\_si\\_001.pdf](https://pubs.acs.org/doi/suppl/10.1021/acسامي.3c00395/suppl_file/am3c00395_si_001.pdf)

## Open Data

Open Data is available at <https://riubu.ubu.es/handle/10259/5684> under the name “Democratization of copper analysis in grape must following a polymer-based lab-on-a-chip approach”.

## Conflicts of interest

The authors declare that they have no conflicts of interest.

## Acknowledgments

We gratefully acknowledge the financial support provided by all funders. This work was supported by the Regional Government of Castilla y León (Junta de Castilla y León) and by the Ministry of Science and Innovation MICIN and the European Union *NextGenerationEU* PRTR. Author Jose Miguel García received grant PID2020-113264RB-I00 funded by MCIN/AEI/ 10.13039/501100011033 and by “ERDF A way of making Europe”.

## References

- (1) Budzik, G.; Woźniak, J.; Paszkiewicz, A.; Przeszłowski, Ł.; Dziubek, T.; Dębski, M. Methodology for the Quality Control Process of Additive Manufacturing Products Made of Polymer Materials. *Materials (Basel)*. **2021**, *14* (9), 2202. <https://doi.org/10.3390/MA14092202>.
- (2) Hemamalini, V.; Rajarajeswari, S.; Nachiyappan, S.; Sambath, M.; Devi, T.; Singh, B. K.; Raghuvanshi, A. Food Quality Inspection and Grading Using Efficient Image Segmentation and Machine Learning-Based System. *J. Food Qual.* **2022**, *2022*, 5262294. <https://doi.org/10.1155/2022/5262294>.
- (3) Guembe-García, M.; González-Ceballos, L.; Arnaiz, A.; Fernández-Muiño, M. A.; Sancho, M. T.; Osés, S. M.; Ibeas, S.; Rovira, J.; Melero, B.; Represa, C.; García, J. M.; Vallejos, S. Easy Nitrite Analysis of Processed Meat with Colorimetric Polymer Sensors and a Smartphone App. *ACS Appl. Mater. Interfaces* **2022**, *14*, 37051–37058. <https://doi.org/10.1021/acسامي.2c09467>.

- (4) González-Ceballos, L.; Fernández-Muiño, M. A.; Osés, S. M.; Sancho, M. T.; Ibeas, S.; Reglero-Ruiz, J. A.; Vallejos, S. Polymer Film as Starch Azure Container for the Easy Diastase Activity Determination in Honey. *Food Chem.* **2021**, 355, 129629. <https://doi.org/10.1016/j.foodchem.2021.129629>.
- (5) González-Ceballos, L.; Cavia, M. del M.; Fernández-Muiño, M. A.; Osés, S. M.; Sancho, M. T.; Ibeas, S.; García, F. C.; García, J. M.; Vallejos, S. A Simple One-Pot Determination of Both Total Phenolic Content and Antioxidant Activity of Honey by Polymer Chemosensors. *Food Chem.* **2021**, 342, 12830. <https://doi.org/10.1016/j.foodchem.2020.128300>.
- (6) Puig-Deu, M.; Lamuela-Raventós, R. M.; Buxaderas, S.; Torre-Boronat, C. Determination of Copper and Iron in Must: Comparison of Wet and Dry Ashing. *Am. J. Enol. Vitic.* **1994**, 45 (1), 25–28.
- (7) Amerine, M. A.; Winkler, A. J. Composition and Quality of Musts and Wines of California Grapes. *Hilgardia* **1944**, 15 (6), 493–675. <https://doi.org/10.3733/HILG.V15N06P493>.
- (8) Llauradó, J.; Rozès, N.; Bobet, R.; Mas, A.; Constantí, M. Low Temperature Alcoholic Fermentations in High Sugar Concentration Grape Musts. *J. Food Sci.* **2002**, 67 (1), 268–273. <https://doi.org/10.1111/J.1365-2621.2002.TB11396.X>.
- (9) Sun, X.; Ma, T.; Yu, J.; Huang, W.; Fang, Y.; Zhan, J. Investigation of the Copper Contents in Vineyard Soil, Grape Must and Wine and the Relationship among Them in the Huaizhuo Basin Region, China: A Preliminary Study. *Food Chem.* **2018**, 241, 40–50. <https://doi.org/10.1016/J.FOODCHEM.2017.08.074>.
- (10) Kreitman, G. Y.; Danilewicz, J. C.; Jeffery, D. W.; Elias, R. J. Reaction Mechanisms of Metals with Hydrogen Sulfide and Thiols in Model Wine. Part 1: Copper-Catalyzed Oxidation. *J. Agric. Food Chem.* **2016**, 64 (20), 4095–4104. [https://doi.org/10.1021/ACS.JAFC.6B00641/ASSET/IMAGES/LARGE/JF-2016-006417\\_0015.JPG](https://doi.org/10.1021/ACS.JAFC.6B00641/ASSET/IMAGES/LARGE/JF-2016-006417_0015.JPG).
- (11) Kontoudakis, N.; Guo, A.; Scollary, G. R.; Clark, A. C. The Impact of Aging Wine in High and Low Oxygen Conditions on the Fractionation of Cu and Fe in Chardonnay Wine. *Food Chem.* **2017**, 229, 319–328. <https://doi.org/10.1016/J.FOODCHEM.2017.02.065>.
- (12) Sánchez Misiego, A.; García-Moncó Carra, R. M.; Ambel Carracedo, M. P.; Guerra Sánchez-Simón, M. T. Electroanalytical Determination and Fractionation of Copper in Wine. *J. Agric. Food Chem.* **2004**, 52 (17), 5316–5321. <https://doi.org/10.1021/JF049562I/ASSET/IMAGES/LARGE/JF049562IF00004.JPG>.
- (13) Wu, X.; Wang, H.; Yang, S.; Tian, H.; Liu, Y.; Sun, B. A Novel Coumarin-

- Based Fluorescent Probe for Sensitive Detection of Copper(II) in Wine. *Food Chem.* **2019**, *284*, 23–27. <https://doi.org/10.1016/J.FOODCHEM.2019.01.090>.
- (14) Guirard, G.; Vecino Soto, C. *Bases Científicas y Tecnológicas de La Enología*, 1st ed.; Editorial Acribia, 2004.
- (15) García Pérez, J. M.; García García, F. C.; Vallejos, S.; Trigo, M.; Reglero-Ruiz, J. A. Sensory Polymers. In *Smart Polymers. Principles and Applications*; De Gruyter: Berlin/Boston, 2021; p 12.
- (16) Norton, A. E.; Sharma, M.; Cashen, C.; Dourges, M. A.; Toupance, T.; Krause, J. A.; Motkuri, R. K.; Connick, W. B.; Chatterjee, S. PH-Mediated Colorimetric and Luminescent Sensing of Aqueous Nitrate Anions by a Platinum(II) Luminophore@Mesoporous Silica Composite. *ACS Appl. Mater. Interfaces* **2021**, *13* (14), 16197–16209. <https://doi.org/10.1021/acsami.0c20821>.
- (17) Cheng, X.; Zhou, Y.; Qin, J.; Li, Z. Reaction-Based Colorimetric Cyanide Chemosensors: Rapid Naked-Eye Detection and High Selectivity. *ACS Appl. Mater. Interfaces* **2012**, *4* (4), 2133–2138. <https://doi.org/10.1021/am3001083>.
- (18) Wu, X.; Guo, Z.; Wu, Y.; Zhu, S.; James, T. D.; Zhu, W. Near-Infrared Colorimetric and Fluorescent Cu<sup>2+</sup> Sensors Based on Indoline-Benzothiadiazole Derivatives via Formation of Radical Cations. *ACS Appl. Mater. Interfaces* **2013**, *5* (22), 12215–12220. <https://doi.org/10.1021/am404491f>.
- (19) Kim, Y. R.; Mahajan, R. K.; Kim, J. S.; Kim, H. Highly Sensitive Gold Nanoparticle-Based Colorimetric Sensing of Mercury(II) through Simple Ligand Exchange Reaction in Aqueous Media. *ACS Appl. Mater. Interfaces* **2010**, *2* (1), 292–295. <https://doi.org/10.1021/am9006963>.
- (20) Şener, G.; Denizli, A. Colorimetric Sensor Array Based on Amino Acid-Modified Gold Nanoparticles for Toxic Metal Ion Detection in Water. *Methods Mol. Biol.* **2019**, *2027*, 75–80. [https://doi.org/10.1007/978-1-4939-9616-2\\_6](https://doi.org/10.1007/978-1-4939-9616-2_6).
- (21) Vallejos, S.; Estévez, P.; García, F. C.; Serna, F.; De La Peña, J. L.; García, J. M. Putting to Work Organic Sensing Molecules in Aqueous Media: Fluorene Derivative-Containing Polymers as Sensory Materials for the Colorimetric Sensing of Cyanide in Water. *Chem. Commun.* **2010**, *46* (42), 7951–7953. <https://doi.org/10.1039/c0cc02143a>.
- (22) Vallejos, S.; Estévez, P.; Ibeas, S.; Muñoz, A.; García, F. C.; Serna, F.; García, J. M. A Selective and Highly Sensitive Fluorescent Probe of Hg<sup>2+</sup> in Organic and Aqueous Media: The Role of a Polymer Network in Extending the Sensing Phenomena to Water Environments. *Sensors Actuators, B Chem.* **2011**, *157* (2), 686–690. <https://doi.org/10.1016/j.snb.2011.05.041>.

- (23) Vallejos, S.; Muñoz, A.; Ibeas, S.; Serna, F.; García, F. C.; García, J. M. Solid Sensory Polymer Substrates for the Quantification of Iron in Blood, Wine and Water by a Scalable RGB Technique. *J. Mater. Chem. A* **2013**, 1 (48), 15435–15441. <https://doi.org/10.1039/c3ta12703f>.
- (24) Vallejos, S.; Reglero, J. A.; García, F. C.; García, J. M. Direct Visual Detection and Quantification of Mercury in Fresh Fish Meat Using Facilely Prepared Polymeric Sensory Labels. *J. Mater. Chem. A* **2017**, 5 (26), 13710–13716. <https://doi.org/10.1039/c7ta03902f>.
- (25) Guembe-García, M.; Peredo-Guzmán, P. D.; Santaolalla-García, V.; Moradillo-Renuncio, N.; Ibeas, S.; Mendía, A.; García, F. C.; García, J. M.; Vallejos, S. Why Is the Sensory Response of Organic Probes within a Polymer Film Different in Solution and in the Solid-State? Evidence and Application to the Detection of Amino Acids in Human Chronic Wounds. *Polymers (Basel)*. **2020**, 12 (6), 1249. <https://doi.org/10.3390/polym12061249>.
- (26) Smith, P. K.; Krohn, R. I.; Hermanson, G. T.; Mallia, A. K.; Gartner, F. H.; Provenzano, M. D.; Fujimoto, E. K.; Goeke, N. M.; Olson, B. J.; Klenk, D. C. Measurement of Protein Using Bicinchoninic Acid. *Anal. Biochem.* **1985**, 150 (1), 76–85. [https://doi.org/10.1016/0003-2697\(85\)90442-7](https://doi.org/10.1016/0003-2697(85)90442-7).
- (27) Clark, A.; Kodoudakis, N.; Smith, M.; Smith, P. A.; Wilkes, E. N. The Determination of Total Cu in White Wine by BCA Colorimetric Analysis. *Natl. Wine Grape Ind. Cent.* **2018**, 1, 1–4.
- (28) Vallejos, S.; Reglero, J. A.; García, F. C.; García, J. M. Direct Visual Detection and Quantification of Mercury in Fresh Fish Meat Using Facilely Prepared Polymeric Sensory Labels. *J. Mater. Chem. A* **2017**, 5 (26), 13710–13716. <https://doi.org/10.1039/c7ta03902f>.
- (29) Vallejos, S.; Guembe García, M.; García Pérez, J. M.; Represa Pérez, C.; García García, F. C. *Colorimetric Titration on the App Store*. <https://apps.apple.com/si/app/colorimetric-titration/id1533793244> (accessed 2021-08-07).
- (30) Vallejos, S.; Guembe García, M.; García Pérez, J. M.; Represa Pérez, C.; García García, F. C. *Application for smartphones “Colorimetric Titration”*. Software registration BU-122-20 (00/2021/568). <https://play.google.com/store/apps/details?id=es.inforapps.chameleon&hl=ES> (accessed 2021-08-07).
- (31) Trigo-íñiguez, M.; Mu, A.; Ibeas, S.; Serna, F.; García, F. C.; García, J. M. Sensors and Actuators B: Chemical Colorimetric Detection and Determination of Fe (III), Co (II), Cu (II) and Sn (II) in Aqueous Media by Acrylic Polymers with Pendant Terpyridine Motifs. *Sensors Actuators B Chem.* **2016**, 226, 118–126. <https://doi.org/10.1016/j.snb.2015.11.116>.
- (32) Guirado-Moreno, J. C.; González-Ceballos, L.; Carreira-Barral, I.; Ibeas, S.; Fernández-Muiño, M. A.; Sancho, M. T.; García, J. M.; Vallejos, S.

- Smart Sensory Polymer for Straightforward Zn(II) Detection in Pet Food Samples. *Spectrochim. Acta Part A Mol. Biomol. Spectrosc.* **2023**, *284*, 121820. <https://doi.org/10.1016/j.saa.2022.121820>.
- (33) Amidžić Klarić, D.; Klarić, I.; Mornar, A.; Velić, D.; Velić, N. Blackberry Wines Mineral and Heavy Metal Content Determination after Dry Ashing: Multivariate Data Analysis as a Tool for Fruit Wine Quality Control. *Int. J. Food Sci. Nutr.* **2016**, *67* (5), 514–523. <https://doi.org/10.1080/09637486.2016.1181159>.
- (34) Zengin, H. B.; Gürkan, R. Eco-Friendly Trace Analysis of Silver in Beer/Wine Samples Using a New Co-Polymeric Nanocomposite Based-Ultrasound Assisted-Cloud Point Extraction Combined with Spectrophotometry. *J. Food Compos. Anal.* **2021**, *98* (September 2020), 103814. <https://doi.org/10.1016/j.jfca.2021.103814>.
- (35) Alki;ş, I. M.; Öz, S.; Atakol, A.; Yi;lmaz, N.; Anlı, R. E.; Atakol, O. Investigation of Heavy Metal Concentrations in Some Turkish Wines. *J. Food Compos. Anal.* **2014**, *33* (1), 105–110. <https://doi.org/10.1016/j.jfca.2013.11.006>.
- (36) Arrowsmith, P. Laser Ablation of Solids for Elemental Analysis by Inductively Coupled Plasma Mass Spectrometry. *Anal. Chem.* **1987**, *59* (10), 1437–1444. <https://doi.org/10.1021/ac00137a014>.
- (37) Moreno, I. M.; González-Weller, D.; Gutierrez, V.; Marino, M.; Cameán, A. M.; González, A. G.; Hardisson, A. Determination of Al, Ba, Ca, Cu, Fe, K, Mg, Mn, Na, Sr and Zn in Red Wine Samples by Inductively Coupled Plasma Optical Emission Spectroscopy: Evaluation of Preliminary Sample Treatments. *Microchem. J.* **2008**, *88* (1), 56–61. <https://doi.org/10.1016/j.microc.2007.09.005>.
- (38) Lara, R.; Cerutti, S.; Salonia, J. A.; Olsina, R. A.; Martinez, L. D. Trace Element Determination of Argentine Wines Using ETAAS and USN-ICP-OES. *Food Chem. Toxicol.* **2005**, *43* (2), 293–297. <https://doi.org/10.1016/j.fct.2004.10.004>.
- (39) Latorre, M.; Herbello-Hermelo, P.; Peña-Farfal, C.; Neira, Y.; Bermejo-Barrera, P.; Moreda-Piñeiro, A. Size Exclusion Chromatography – Inductively Coupled Plasma – Mass Spectrometry for Determining Metal-Low Molecular Weight Compound Complexes in Natural Wines. *Talanta* **2019**, *195* (September 2018), 558–565. <https://doi.org/10.1016/j.talanta.2018.11.055>.
- (40) Gutierrez, M. C.; Gomez-Hens, A.; Valcarcel, M. Selective Kinetic Fluorimetric Determination of Copper at the Ng MI Level. *Talanta* **1986**, *33* (7), 567–570. [https://doi.org/10.1016/0039-9140\(86\)80131-X](https://doi.org/10.1016/0039-9140(86)80131-X).
- (41) Costa, M. H.; Ferreira, D. T. S.; Pádua, J. E. S.; Fernandes, J. P. A.; Santos, J. C. C.; Cunha, F. A. S.; Araujo, M. C. U. A Fast, Low-Cost, Sensitive, Selective, and Non-Laborious Method Based on Functionalized

- Magnetic Nanoparticles, Magnetic Solid-Phase Extraction, and Fluorescent Carbon Dots for the Fluorimetric Determination of Copper in Wines without Prior Sample Treatm. *Food Chem.* **2021**, *363*, 130248. <https://doi.org/10.1016/j.foodchem.2021.130248>.
- (42) Pessanha, S.; Carvalho, M. L.; Becker, M.; Von Bohlen, A. Quantitative Determination on Heavy Metals in Different Stages of Wine Production by Total Reflection X-Ray Fluorescence and Energy Dispersive X-Ray Fluorescence: Comparison on Two Vineyards. *Spectrochim. Acta - Part B At. Spectrosc.* **2010**, *65* (6), 504–507. <https://doi.org/10.1016/j.sab.2010.04.003>.
- (43) Kontoudakis, N.; Smith, M.; Smith, P. A.; Wilkes, E. N.; Clark, A. C. The Colorimetric Determination of Copper in Wine: Total Copper. *Aust. J. Grape Wine Res.* **2020**, *26* (2), 121–129. <https://doi.org/10.1111/ajgw.12425>.
- (44) Yin, K.; Li, B.; Wang, X.; Zhang, W.; Chen, L. Ultrasensitive Colorimetric Detection of Cu<sup>2+</sup> Ion Based on Catalytic Oxidation of L-Cysteine. *Biosens. Bioelectron.* **2015**, *64*, 81–87. <https://doi.org/10.1016/j.bios.2014.08.058>.
- (45) Zhang, C.; Wan, L. Y.; Wu, S.; Wu, D.; Qin, X.; Ko, F. A Reversible Colorimetric Chemosensor for Naked-Eye Detection of Copper Ions Using Poly (Aspartic Acid) Nanofibrous Hydrogel. *Dye. Pigment.* **2015**, *123*, 380–385. <https://doi.org/10.1016/j.dyepig.2015.07.028>.

*Smart sensory polymer for straightforward Zn(II) detection in pet food simples.*



## Smart sensory polymer for straightforward Zn(II) detection in pet food samples

José Carlos Guirado-Moreno,<sup>a</sup> Lara González-Ceballos,<sup>b</sup> Israel Carreira-Barral,<sup>a</sup> Saturnino Ibeas,<sup>a</sup> Miguel A. Fernández-Muiño,<sup>b</sup> M. Teresa Sancho,<sup>b</sup> José M. García,<sup>a,\*</sup> Saúl Vallejos<sup>a,\*</sup>

<sup>a</sup> Departamento de Química, Facultad de Ciencias, Universidad de Burgos, Plaza Misael Bañuelos s/n, 09001 Burgos, Spain

<sup>b</sup> Departamento de Biotecnología y Ciencia de los Alimentos, Universidad de Burgos, Plaza Misael Bañuelos s/n, 09001 Burgos, Spain

\* Corresponding author: Dr Vallejos ([svallejos@ubu.es](mailto:svallejos@ubu.es)), Prof. García ([jmiguel@ubu.es](mailto:jmiguel@ubu.es))

### Abstract

We report on an innovative method to measure the Zn(II) concentration in pet food commercial pet food samples, both wet and dry food. It is based on a colorimetric sensory polymer prepared from commercial monomers and 0.5% of a synthetic monomer having a quinoline sensory core (*N*-(8-(2-azidoacetamido)quinolin-5-yl)methacrylamide). We obtained the sensory polymer as crosslinked films by thermally initiated bulk radical polymerization of the monomers of 100 µm thickness, which we punched into Ø6mm sensory discs. The immersion of the discs in water solutions containing Zn(II) turned the fluorescence on, allowing for the titration of this cation using the G parameter of a digital picture taken to the discs. The limits of detection and quantification were 29 and 87 µg/L, respectively. Furthermore, we measured the concentration of Zn(II) even in the presence of other cations, detecting no significant interferences. Thus, in a further step, we obtained the concentration of Zn(II) from 15 commercial pet food, ranging from 19 to 198 mg/kg, following a simple extraction procedure and contacting the extractant with our sensory discs. These results were contrasted with that obtained by a reference method, ICP-MS.

**Keywords:** zinc detection; zinc in food; sensory polymers; fluorescent probes; RGB parameters.

*Spectrochimica Acta part A: Molecular and Biomolecular Spectroscopy, 2023,*  
284, 121820

## 1. Introduction

Zn(II) cation is an essential trace element for all living beings and is part of countless proteins where it acts as a catalytic, structural, or regulatory cofactor [1–3]. Despite its important role in life, it can be toxic in high concentrations, like all metals [4,5]. Excess of zinc in diet avoids the absorption of other essential elements, such as copper or iron, due to mere competition between cations [6]. Also, the assimilation of zinc by living organisms is inversely proportional to the consumed amount, so the zinc ingested in excess is excreted. And this is the leading environmental problem with zinc since manures contain high zinc concentrations that seep through soils into groundwater [7].

Generally speaking, environmental zinc contamination has three primary sources: leaching from galvanized steel (~30%), industrial point sources (10%), and others (60%), including agriculture and stockbreeding [7]. Animals ingest high amounts of Zn(II) as salts (zinc sulphate monohydrate, zinc chelate of amino acids hydrate, or zinc oxide) added in high quantities in the feed of all animals, especially on farms, as it favours the rapid growth of animals. This represents the main route of Zn(II) intake by humans through the food chain.

Given the concern about the environmental effect and the effect on people's health, countries such as China [8] and the European Union [7] have already established the maximum amount of zinc in animal feed at 150–250 mg/kg and 100–150 mg/kg, respectively. In addition, the most recent studies have shown that soil contamination with zinc leads to bacterial resistance to antibiotics, is phytotoxic, and drastically decreases microbiota activity [9]. However, the most significant risk is not associated with soil contamination but with contamination of groundwater, drainage, and zinc runoff from farmland to surface water [7].

Analysing a target's concentration in a given medium is an expensive and time-consuming procedure and is a task generally carried out by specialized personnel [10–12]. This is one of the big problems when talking about regulatory control compliance. In other words, more straightforward zinc detection methods

---

are still necessary [13,14], since traditional methods are difficult to apply *in situ*; they always require advanced equipment, and a specialist must carry them out.

In this study, we have designed and prepared a polymeric film for detecting Zn(II) in aqueous media that meets all these requirements. Thus, the equipment for the measurement is only a smartphone, and the procedure is as simple as dipping the sensory polymeric film, waiting, and photographing [15–17]. Furthermore, the new material and measuring method have been tested in real conditions, with water and pet food samples. The results have been compared and contrasted with a highly selective and sensitive method such as Inductively Coupled Plasma Mass Spectrometry (ICP-MS).

## 2. Experimental

### 2.1. Materials

All materials and solvents were commercially available and used as received unless otherwise indicated. The following materials and solvents were used: 1-vinyl-2-pyrrolidone (VP) (99%, Aldrich), methyl methacrylate (MMA) (99 %, Aldrich), ethylene glycol dimethacrylate (E) (97.5%, Aldrich), pH 4.66 Buffer (VWR), acetone (99%, VWR), potassium hydroxide (99%, VWR-Prolabo), methacrylic anhydride (94%, Alfa Aesar), hydrochloric acid (37%, VWR-Prolabo), trichloroacetic acid ( $\geq$ 99.99%, Sigma-Aldrich), 8-nitroquinoline (98%, Alfa Aesar), hydroxylamine hydrochloride (97%, TCI), ethanol ( $\geq$ 99.9%, VWR), methanol ( $\geq$ 99.8%, VWR), 1,4-dioxane ( $\geq$ 99.9%, VWR), ethyl acetate ( $\geq$ 99.9%, VWR), bromoacetyl bromide (98%, Alfa Aesar), sodium azide (99%, Alfa Aesar), dimethylsulfoxide-d<sub>6</sub> (99.9%, VWR), dimethylformamide (99.9%, Supelco).

Azo-bis-isobutyronitrile (AIBN, Aldrich, 98%) was recrystallized twice from methanol to provide the highest quality polymerization initiator.

Selectivity and interference study was performed with the following metallic salts: zinc (II) nitrate hexahydrate (98%, Sigma-Aldrich), iron(III) nitrate nonahydrate (99%, Sigma-Aldrich), manganese(II) nitrate hexahydrate (98+%, Alfa Aesar), cobalt(II) nitrate hexahydrate ( $\geq$ 99%, Labkem), calcium nitrate

tetrahydrate ( $\geq 99\%$ , Sigma-Aldrich), mercury(II) nitrate (98%, Alfa Aesar), cadmium nitrate tetrahydrate (98.5%, Alfa Aesar), potassium nitrate (99+%, Sigma-Aldrich), lead(II) nitrate ( $\geq 99\%$ , Fluka), iron(II) sulphate heptahydrate (99%, Sigma-Aldrich), magnesium nitrate hexahydrate ( $\geq 99\%$ , Labkem), copper(II) sulphate pentahydrate (98%, Sigma-Aldrich), nickel(II) nitrate hexahydrate (98.5%, Sigma-Aldrich), sodium nitrate (99%, LabKem), cesium(I) nitrate ( $\geq 99\%$ , Fluka), barium(II) chloride dihydrate (99%, Labkem), ammonium nitrate ( $\geq 98\%$ , Sigma-Aldrich), chromium(III) nitrate (98.5%, Alfa Aesar), rubidium(I) nitrate (99.95%, Sigma-Aldrich), dysprosium(III) nitrate (99.9%, Alfa Aesar), lithium chloride ( $\geq 99\%$ , Sigma-Aldrich), cerium(III) chloride tetrahydrate ( $\geq 99.99\%$ , Sigma-Aldrich), zirconium(IV) chloride (98%, Alfa Aesar), lanthanum(III) nitrate hexahydrate (99.9%, Alfa Aesar), samarium(III) nitrate (99.9%, Alfa Aesar), aluminium(III) nitrate ( $\geq 98.9\%$ , Sigma-Aldrich), silver(I) nitrate ( $\geq 99.9\%$ , Sigma-Aldrich), neodymium(III) nitrate (99.9%, Alfa Aesar), strontium(II) nitrate (99%, Sigma-Aldrich).

## 2.2. Instrumentation and methods

$^1\text{H}$  and  $^{13}\text{C}\{^1\text{H}\}$  NMR spectra (Advance III HD spectrometer, Bruker Corporation, Billerica, Massachusetts, USA) were recorded at 300.17 MHz for  $^1\text{H}$  and 75.38 MHz for  $^{13}\text{C}$  using deuterated dimethyl sulfoxide ( $\text{DMSO}-d_6$ ) as solvent. The experiments were acquired at 298 K with the standard pulse sequences from the Bruker library and processed with MestReNova software (v. 12.0, Mestrelab Research SL, Santiago de Compostela, Spain). The chemical shifts ( $\delta$ ) are reported in ppm relative to the solvent resonance as the internal standard ( $\text{DMSO}-d_6 = 2.51$  ppm).

The powder X-ray diffraction (PXRD) patterns were obtained using a diffractometer (D8 Discover Davinci design, Bruker Corporation, Billerica, Massachusetts, USA) operating at 40 kV, using  $\text{Cu}(\text{K}\alpha)$  as the radiation source, a scan step size of  $0.02^\circ$ , and a scan step time of 2 s. X-ray diffraction studies were conducted at 200 K on a Bruker D8 VENTURE diffractometer.

The polymers thermal and mechanical characterization was performed

---

by: a) thermogravimetric analysis (Q50 TGA analyser, TA Instruments, New Castle, DE, USA) with 10–15 mg of sample under synthetic air and nitrogen atmosphere at  $10^{\circ}\text{C}\cdot\text{min}^{-1}$ ; b) differential scanning calorimetry, with 10–15 mg of the sample under a nitrogen atmosphere at a heating rate of  $10^{\circ}\text{C min}^{-1}$  (Q200 DSC analyser, TA Instruments, New Castle, DE, USA), and c) Young's modulus analysis were calculated in tensile test of dried Film-Zn strips ( $5\times9.44\times0.122$  mm) performed at a rate of  $1\text{ mm}\cdot\text{min}^{-1}$  (Shimadzu EZ Test Compact Table-Top Universal Tester, Shimadzu, Kyoto, Japan).

Infrared spectra (FTIR) were recorded with an infrared spectrometer (FT/IR-4200, Jasco, Tokyo, Japan) with an ATR-PRO410-S single reflection accessory.

Solution fluorescence spectra were recorded using a F-7000 Hitachi Fluorescence spectrophotometer (Hitachi, Tokyo, Japan). Solution measurements for the interaction study were carried out in a conventional cuvette with no special procedures. A rectangular 10 mm cuvette was used for the fluorescence measurements, measuring all data at  $25^{\circ}\text{C} \pm 0.1^{\circ}\text{C}$ .

The weight percentage of water taken up by the films upon soaking in pure water at  $20^{\circ}\text{C}$  until reaching equilibrium (water-swelling percentage, WSP) was obtained from the weight of a dry sample film ( $\omega_d$ ) and its water-swelled weight ( $\omega_s$ ) using the following expression:  $\text{WSP} = 100 \times [(\omega_s - \omega_d)/\omega_d]$ .

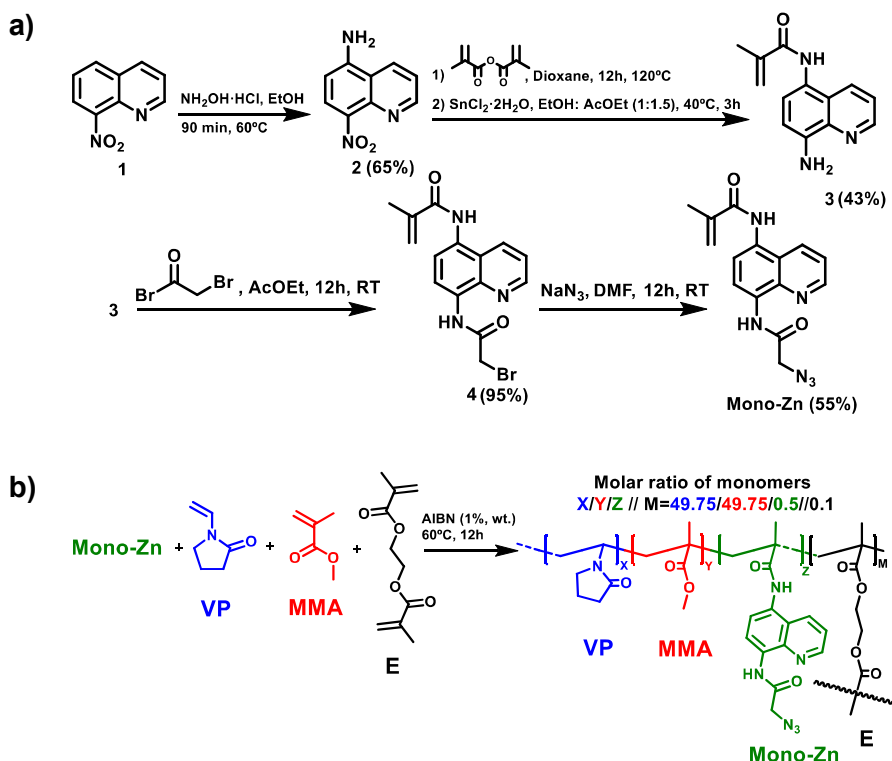
High-resolution electron-impact mass spectrometry (EI-HRMS) was carried out on a Micromass AutoSpect (Waters mass, Micromass Holdings Ltd., Cary, North Carolina), using ionisation energy of 70 eV, and a mass resolving power: >10,000. Inductively coupled plasma mass spectrometry (ICP-MS) measurements were recorded on an Agilent 7500 ICP-MS spectrometer (Agilent, Santa Clara, USA).

Digital photographs were taken with a Huawei p30 pro (Huawei, Shenzhen, China) in a dark room (distance to the object = 25 cm) under UV

radiation (365 nm lamp, 45° inclination). G parameter of digital photographs was extracted using the smartphone app “Colorimetric Titration” [18,19].

### 2.3. Synthesis of the sensory monomer **Mono-Zn**

We prepared the sensory monomer **Mono-Zn** following conventional organic reactions starting from 8-nitroquinoline. The preparation route is depicted in **Scheme 1**, and the detailed description of the synthesis steps and the characterisation of intermediates and **Mono-Zn** can be found in the Supporting Information (**SI-Section S1**).



**Scheme 1.** Synthetic route for: a) the sensory monomer **Mono-Zn**; and b) the sensory polymer **Film-Zn**.

### 2.4. Preparation of the sensory polymer synthesis **Film-Zn**

We prepared the sensory film **Film-Zn** by bulk thermally initiated bulk radical

polymerization [20]. Thus, two commercial monomers (**VP** and **MMA**), a crosslinker (ethylene glycol dimethacrylate, **E**), and the synthesised sensory monomer (**Mono-Zn**) were mixed in a molar ratio of 49.75/49.75/0.5/0.1 (VP/MMA/Mono-Zn/E). Additionally, we added AIBN (1%, wt.) radical thermal initiator. Then, we injected the mixture into a mould (100  $\mu\text{m}$  thickness) comprised of two sealed silanised glasses and heated it overnight at 60 °C, where the polymerization took place under an oxygen-free atmosphere. Finally, we washed the resultant material with water and acetone and punched it into Ø6 mm discs. The FTIR, TGA, DSC and PRXD, patterns can be found in the **SI-Section S2**.

### 2.5. Interference study

We carried out a preliminary experiment for testing the fluorimetric response of the synthesized sensory monomer with 29 different cations by preparing solutions of **Mono-Zn** ( $2.6 \times 10^{-3}$  M) and a cation ( $5 \times 10^{-3}$  M) in an aqueous:organic medium. All vials were photographed together (**SI-Section S3, Figure S6**) under 365 nm light irradiation.

In a second step, we conducted a more profound study with the identified potential interferents. Thus, for each interferent, we prepared the following tubes containing: a) Ø6mm disc of **Film-Zn**, 1 mL of 10 mg/L Zn(II) solution buffered at pH 4.66; and b) Ø6mm disc of **Film-Zn**, 1 mL of 10 mg/L Zn(II) and 10 mg/L cation solution buffered at pH 4.66. The films were dipped for 2 hours, washed in triplicate with water (10min each), and photographed under 365 nm light irradiation to obtain the G parameter.

### 2.6. Titration of **Mono-Zn** with Zn(II)

This study was carried out by adding  $\text{Zn}(\text{NO}_3)_2 \times 6\text{H}_2\text{O}$  to a **Mono-Zn** solution ( $1.02 \times 10^{-4}$  M) in buffered organic-aqueous media (pH 4.66 buffer:DMA at 50:50 ratio), in concentrations ranging from 0.2 ppm to 72 mg/L. The fluorescence spectra were recorded at  $= 25^\circ\text{C} \pm 0.1^\circ\text{C}$  using the following conditions: excitation slit = 10 nm; emission slit = 10 nm; excitation wavelength = 380 nm; scan speed = 1,200 nm/min; step = 0.5 nm.

---

### 2.7. Titration of **Film-Zn** with Zn(II)

We dipped Ø6mm **Film-Zn** discs for 2 hours in fully aqueous solutions with different Zn(II) concentrations (from 0.5 to 15 mg/L) buffered at pH 4.66. After that, the discs were extracted from solutions and photographed with the smartphone. Finally, we carried out the experiments in triplicate.

### 2.8. Detection and quantification of Zn(II) from pet food

We analysed 15 dry and wet commercial pet food from the retail market. The product/band is shown in the **SI-Section S4**) by the following procedure (we follow the extraction procedure described by Wang et al. with some modifications [21]): a) firstly, we mixed 2 g of wet or 1 g of dry food with 40 mL of trichloroacetic acid (TCA, 1%); b) secondly, the mixture was magnetically stirred for 5 min, centrifuged for 10 min at 11,000 rpm, and filtered off; c) finally, we measured the Zn(II) content of the extractant by two ways: by a reference method (quantitative ICP-MS, data are means of 5 replicates for each pet food) and using our sensory film **Film-Zn** (data are means of 2 replicates for each pet food).

For measuring the Zn(II) concentration with **Film-Zn**, we followed the following procedure: 1 mL of the extract was diluted with 1 mL of pH 4.66 acetate buffer, and then one disc of **Film-Zn** (Ø6mm) was dipped in the solution for 2 hours. Afterward, the disc was washed in triplicate with distilled water (10min each) and photographed with the smartphone. **Figure 1** shows this procedure schematically. G parameter was extracted from the digital photographs, and the results were correlated with the obtained ones from the quantitative ICP-MS measurements.

### 2.9. Limits of detection (LOD) and quantification (LOQ)

The limit of detection (LOD) and the limit of quantification (LOQ) of our sensory system was calculated by the following equations:  $LOD=3.3\times SD/s$  and  $LOQ=10\times SD/s$ , respectively, where “SD” is the standard deviation of the blank sample and “s” is the slope of a calibration curve in the region of low analyte content (below 1 mg/L) (more information in **SI-Section S5**) [22,23].

---

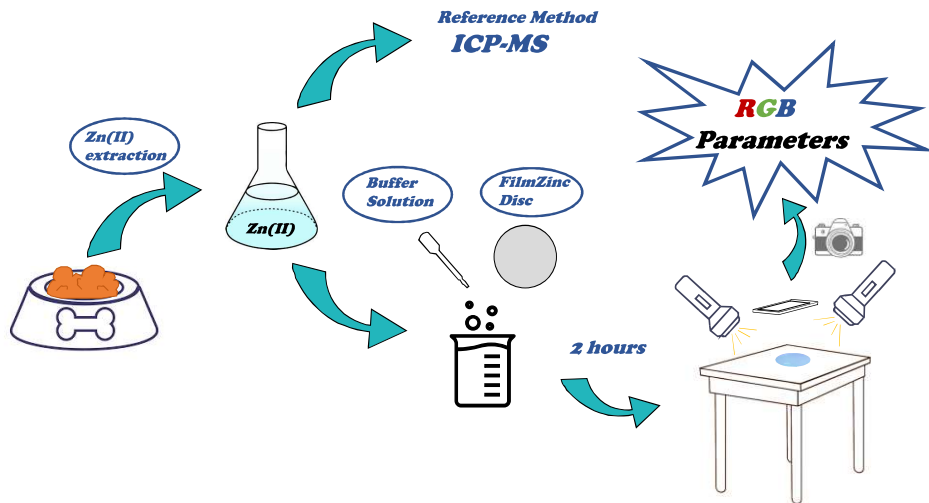


**Figure 1.** Representation of the procedures for the determination of Zn(II) content in pet food by a conventional method (ICP-MS) and by using the sensory polymer **Film-Zn**.

### 3. Results and discussion

We report in this work on film-shaped sensory materials useful for the selective detection and quantification of Zn(II) in water solution and on the application of this sensor to the quantification of Zn(II) in pet food samples. To explain the advantage and potential of detecting Zn(II) using our sensor, we will briefly describe the synthetic procedure for the preparation of the sensory films, the interaction of Zn(II) with the sensory material that gives rise to the *turn-on* of the fluorescence of the sensory films, responsible of the sensor phenomenon and, finally, the titration of water solutions of Zn(II) and the exploitation of the sensory materials for the determination of Zn(II) concentration in dry and wet pet commercial samples.

#### 3.1. Design of the material

For this kind of application, aimed at simple and direct use by non-skilled personnel, we opted for a manageable and resistant material appropriate for careless handling. For this a hydrophobic co-monomer providing rigidity to the

material is needed when dealing with polyacrylic materials. Accordingly, methylmethacrylate was used. However, this material must detect Zn(II) in water, and therefore a hydrophilic monomer is also necessary, which allows the target species (in this case, Zn(II)) to enter hydrated the three-dimensional polymeric network by diffusion, such as *N*-vinylpyrrolidone. Therefore, the molar ratio between the hydrophilic and the hydrophobic monomer (in our case 1) is key to obtaining a manageable material being, at the same time, able to swell in water. In addition, the material must be prepared with the sensory monomer **Mono-Zn**. As it is a synthetic monomer (not commercially available), the minimum ratio to other co-monomers was used to obtain an adequate visual response (0.5% mol).

The films were designed as thermostable materials crosslinked with ethyleneglycol dimethacrylate (**Scheme 1b**, the nominal crosslinking ratio was 1,000, i.e., the ratio of feed moles of co-monomers to the crosslinking agent), which gives rise to a water swelling percentage of 71%, and a Young's modulus of 974 MPa. As a result, the films had a glass transition temperature of 138 °C and thermal resistance, in terms of 5% and 10% weight loss, of 224 and 343 °C, respectively.

### 3.2. Study of the interaction of the sensory monomer **Mono-Zn** with Zn(II)

We initially envisaged that the interaction of Zn(II) with **Mono-Zn** would probably follow the previously described interaction of these cations with 1-(quinoline-8-yl)urea [24], which would give rise to a complex **Mono-Zn:Zn(II)** with a 1:1 stoichiometry. Thus, we analysed the complexation behaviour following the fluorescence *turn-on* associated with the formation of the complex **Mono-Zn:Zn(II)**, represented in **Figure 2a** as an increase and displacement of a fluorescence band centred at 497 nm. From the representation of fluorescence intensity against the concentration of Zn(II), we obtained the complex formation constant,  $1.6 \times 10^3$  M, and the Job's plot, which confirmed the 1:1 stoichiometry for the complex (**Figure 2b**). Additionally, **SI-Section S3** includes the three-dimensional fluorescence graphics, the species distribution diagram, and the

graphic representing the contribution of each species to the total fluorescence of the system.

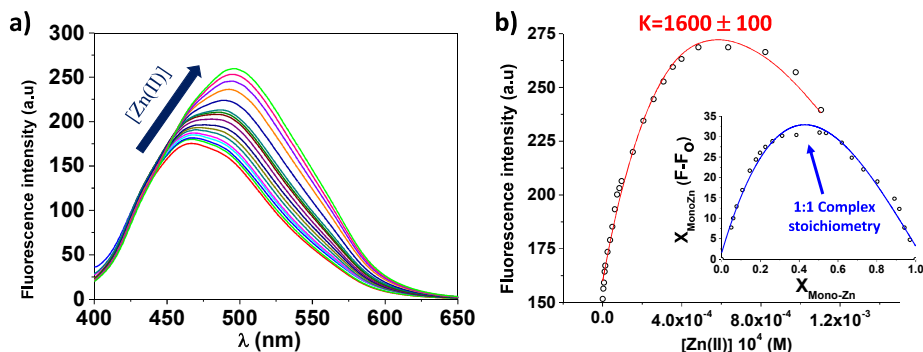


**Figure 2.** **a)** Titration of **Mono-Zn** with Zn(II) in buffered organic-aqueous media (pH 4.66:DMA at 50:50 ratio). The concentration of Zn(II) in the cuvette was increased from 0.2 to 72 mg/L (from  $3.1 \times 10^{-6}$  M to  $1.1 \times 10^{-3}$  M), and the initial concentration of **Mono-Zn** was 32 mg/L ( $1.02 \times 10^{-4}$  M). **b)** (In red) Representation of the fluorescence intensity at 497.6 nm versus Zn(II) Molarity. The fitted curve was used for the calculation of the complex formation constant; (in blue) Job's Plot diagram, which represents  $X_{\text{MonoZn}}(F-F_0)$  versus the molar fraction of **Mono-Zn**. Measuring conditions: excitation slit = 10 nm; emission slit = 10 nm; excitation wavelength = 380 nm; scan speed = 1,200 nm/min.

To proceed with the preparation of the sensory material, once described the efficient interaction of the sensory monomer with Zn(II), we first had to ensure the effectiveness of this interaction in terms of lack or controllable interferences. Therefore, we started with an overall study of **Mono-Zn** comparing the fluorescence response with 29 different cations, and we observed an only OFF-ON fluorescence process with Zn(II), but 4 ON-OFF fluorescence processes with Cu(II), Hg(II), Fe(III), Ni(II) and Cd(II). The image with all the studied cations can be found in **SI-Section S5 (Figure S6)**, where the interference effect can also be visually observed under 365 nm light irradiation.

Thus, after identifying potential interferents, we carried out the analysis with the sensory film **Film-Zn** and the above-mentioned cations in more realistic concentrations. **Figure 3a** shows the normalised G parameter ( $G_{\text{Zn(II)+Cation}}/G_{\text{Zn(II)}}$ ) extracted from the digital photographs. The results point out the validity of our

sensor in applications devoted to detecting and quantifying Zn(II) in commercial pet food. Additionally, Ni(II) and Co(II) are not relevant in pet food because they are usually in lower concentrations than Zn(II) [25–28]; Ni(II) can be even toxic for dogs [29], and these cations have not been indicated as additives in any commercial product.

Once we studied the sensory material's interaction with Zn(II) and disregarded the possible interferents, we carried out studies with **Film-Zn** in aqueous solutions with different Zn(II) concentrations, and a proof of concept with pet food samples, as reported on bellow.

### 3.2. Titration of **Film-Zn** in aqueous samples of Zn(II) with a smartphone

The titration curve was carried out by correlating the G parameter of the digital image with the concentration of Zn(II), as shown in **Figure 3b**. G parameter was chosen because after analysing all the coordinates of the colour space (R, G and B), we realised that it was the most variant parameter and that it followed a clear trend with the concentration of Zn(II) in the solutions.

Additionally, we performed a second experiment in the linearity zone at low concentrations of Zn(II) (from 0.15 to 0.75 mg/L). This assay allows the calculation of the detection and quantification limits of the system (LOD and LOQ). In our case, these limits are low enough (LOD = 29 µg/L; LOQ = 87 µg/L) to point out the validity of the prepared material for the application we have addressed, i.e., the determination of Zn(II) in commercial pet food. Table 1 shows a comparative study with the most used methodologies for determining zinc in terms of LOD, equipment required for the measurement, and validation for the proposed application.

### 3.3. Proof of Concept. Zn(II) detection in real samples

Once addressed the validity of our sensory system for the *in vitro* evaluation of Zn(II), even in the presence of other cations, our next step was evaluating the performance of the polymer sensor in determining the concentration of Zn(II) in commercial samples.

---

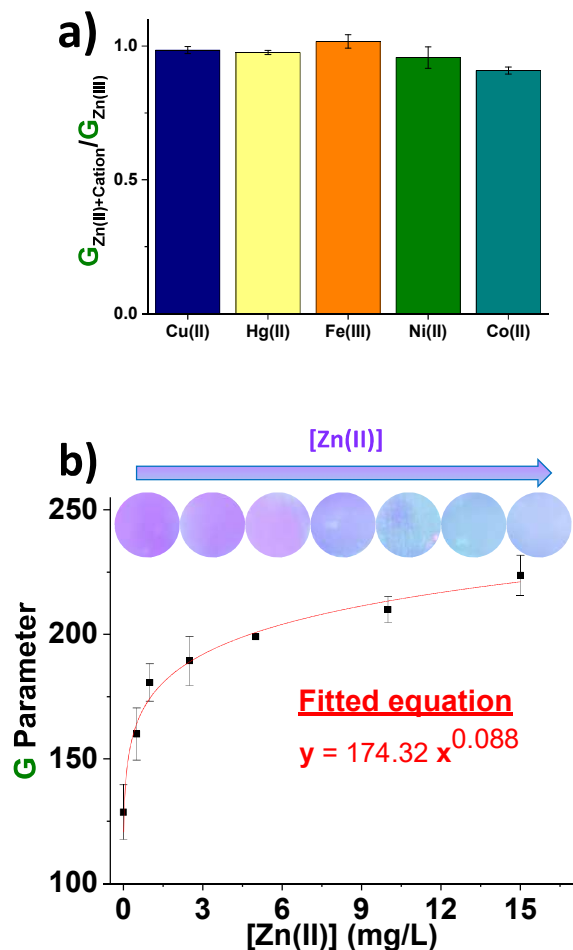


**Figure 3. a)** Interference study with metal cations that produce quenching of the fluorescence of the system, i.e., Cu(II), Hg(II), Fe(III), Ni(II), Co(II). Experimental procedure: a Ø6mm disc of **Film-Zn** was dipped in 1 mL of 10 mg/L Zn(II) solution buffered at pH 4.66, another disc in 1 mL of 10 mg/L Zn(II) and 10 mg/L cation solution buffered at pH 4.66. The films were dipped for 2 hours and photographed under 365 nm light irradiation to obtain the G parameter. A value of  $G_{\text{Zn(II)+Cation}} / G_{\text{Zn(II)}}$  equal to 1 means no interference. **b)** Graphical representation of the G parameter (mean ± standard error of 3 replicates) from the photographed discs vs Zn(II) concentration (fully aqueous solutions buffered at pH 4.66 with Zn(II) concentrations ranging from 0.5 to 15 mg/L).

**Table 1.** Figure of merits of **Film-Zn** based methodology in comparison with the most relevant method for the detection of Zn(II).

Detection method	Quantification in animal feed samples	Equipment required	LOD	Ref.
ICP-Mass	No	ICP-Mass spectrometer	2.0 µg/g	[30]
	Yes	ICP-Mass spectrometer	-	[31]
AAS (Atomic Absorption Spectrometry)	No	Atomic absorption spectrometer	0.01 µg/g	[32]
	Yes	Atomic absorption spectrometer	0.05 µg/L	[33]
Continuous wavelength transforms	No	UV/Vis spectrophotometer	0.9 µg/L	[34]
Fluorimetric probes in solution	Yes	Fluorimeter	1 µg/L	[35]
	No	Fluorimeter	0.2 µg/L	[36]
Colorimetric probes in solution	Yes	UV/Vis spectrophotometer	0.004 µg/mL	[21]
Poly (azomethine-urethane) as fluorescent probe	No	Fluorimeter	19.6 mg/L	[37]
Fluorometric film ( <b>Film-Zn</b> )	Yes	Smartphone	29 µg/L	This Work

After we measured the Zn(II) concentration in 15 commercial pet foods (see brand names in the **SI-Section S4**) by two different methods, as we depicted in the experimental section, we represented the concentration obtained by the reference method (ICP-MS) against G parameter (**Figure 4**). The fitted line in this representation should be visualised as a 15-point calibration line, which from now on, an end-user can utilise in the following way: 1) perform the extraction of Zn(II) from a pet food problem sample; 2) insert a Ø6mm disc of **Film-Zn** for 2 hours;

3) take a picture of the disk and extract the G parameter with the "Colorimetric titration" app; 4) enter the value G as the "x" in the fitted line and obtain the concentration of Zn(II).

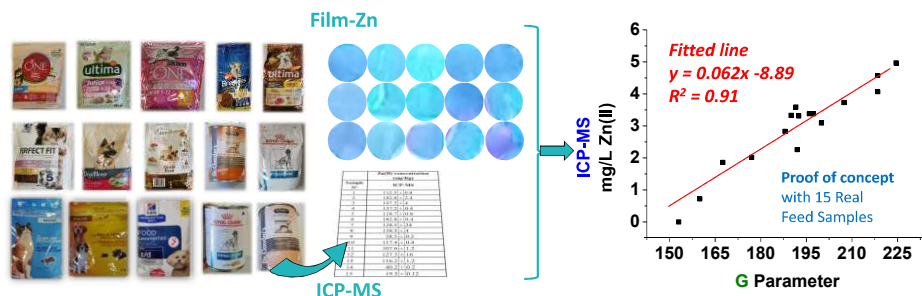


**Figure 4.** Graphical abstract of the proof of concept, including the representation of the Zn(II) concentration obtained by the reference method (ICP-MS, data are means  $\pm$  standard error of 5 replicates) against the G parameter obtained from the photographs (Film-Zn, data are means  $\pm$  standard error of 2 replicates).

Therefore, we have inserted the G data obtained for each pet food in this fitted equation ( $y = 0.062x - 8.89$ ), and analysed the results obtained in comparison with the reference method. The data shown in **Table 2** have been statistically analysed (**SI-Section S6**), and we can affirm that there are no significant differences between both methods.

In short, our method is a more innovative and costless alternative to any reference method, e.g., ICP-MS, since the analysis can be carried out *in situ* and without the concurrence of specialised personnel or scientific equipment, just a smartphone.

#### 4. Conclusions

The use of smart materials in different fields is opening new technological opportunities. Among them are the new analysis systems using sensory polymers, systems that in colorimetric sensory polymers allow the detection and quantification of chemical species of interest with the naked eye, and in a fine way using common tools, such as mobile phones. In addition, this analysis can

be carried out *in situ*, very cheaply, and by non-specialised personnel, which leads to the democratisation of analytical systems. In this framework, we have prepared a sensory system based on polymer sensors prepared in film form for visual evaluation and through a mobile application of Zn(II) in water and animal feed. Furthermore, we have verified the reliability and usability of this system through the alternative evaluation of the Zn(II) concentration with a proven technique, such as ICP-MS. The concentrations determined by both methods are coincident, in the range of mg/kg.

**Table 2.** Zn(II) concentration of measured pet foods obtained by the reference method (ICP-MS) and the proposed method, based on the use of Film-Zn and a smartphone. Zn(II) concentration data from reference and **Film-Zn** methods are means of  $\pm$  standard errors of 5 and 2 replicates, respectively.

Sample Nº	Zn(II) concentration (mg/kg)			
	Indicated by manufacturer*	ICP-MS	Film-Zn	
1	134	133.1 $\pm$ 0.7	112.5 $\pm$ 4.9	
2	54	182.9 $\pm$ 2.6	182.8 $\pm$ 6.2	
3	135	198.7 $\pm$ 5.2	197.5 $\pm$ 28.3	
4	80	123.6 $\pm$ 0.6	137.2 $\pm$ 27.1	
5	148	132.4 $\pm$ 0.9	118.7 $\pm$ 25.9	
6	42	162.6 $\pm$ 0.4	182.8 $\pm$ 13.6	
7	108	135.0 $\pm$ 26.0	130.6 $\pm$ 4.1	
8	82	149.1 $\pm$ 3.1	155.2 $\pm$ 17.7	
9	20	37.1 $\pm$ 0.1	28.5 $\pm$ 1.8	
10	154	90.4 $\pm$ 0.4	117.4 $\pm$ 4.9	
11	120	113.1 $\pm$ 1.3	107.6 $\pm$ 2.5	
12	86	134.9 $\pm$ 17.4	127.3 $\pm$ 2.5	
13	106	143.4 $\pm$ 1.3	116.2 $\pm$ 8.6	
14	36	40.5 $\pm$ 0.2	40.2 $\pm$ 2.5	
15	9	14.5 $\pm$ 0.1	19.3 $\pm$ 3.7	

\*Zn(II) content added by the manufacturer as an additive (it does not take into account the Zn(II) contained in the ingredients used in the manufacturing).

## Supporting Information

Synthesis and characterisation of **Mono-Zn** (including X-ray crystallographic data, CCDC 2180092); characterisation of the sensory polymer **Film-Zn**; fluorescence study; proof of concept; limit of detection (LOD) and limit of quantification (LOQ); statistical analysis.

The supporting information is available free of charge at:

<https://ars.els-cdn.com/content/image/1-s2.0-S1386142522009684-mmc1.pdf>

## Open Data

Open Data is available at <https://riubu.ubu.es/handle/10259/5684> under the name “Dataset of the work Smart sensory polymer for straightforward Zn(II) detection in pet food samples”.

## Conflicts of interest

The authors declare that they have no conflicts of interest.

## Acknowledgements

We gratefully acknowledge the financial support provided by the Spanish Agencia Estatal de Investigación (State Research Agency) (grant PID2020-113264RB-I00/AEI/10.13039/501100011033).

## References

- [1] V.J. Temple, A. Masta, Zinc in human health., P. N. G. Med. J. 47 (2004) 146–158. <https://doi.org/10.9790/0853-13721823>.
- [2] L. Rink, Zinc in human health., IOS Press, Amsterdam, 2011. <https://www.cabdirect.org/cabdirect/abstract/20123153476> (accessed April 5, 2022).
- [3] W. Maret, Zinc Biochemistry: From a Single Zinc Enzyme to a Key Element of Life, Adv. Nutr. 4 (2013) 82–91. <https://doi.org/10.3945/AN.112.003038>.
- [4] J. Lu, G.F. Combs, Effect of Excess Dietary Zinc on Pancreatic Exocrine Function in the Chick, J. Nutr. 118 (1988) 681–689.

- [https://doi.org/10.1093/JN/118.6.681.](https://doi.org/10.1093/JN/118.6.681)
- [5] J. Lu, G.F. Combs, J.C. Fleet, Time-Course Studies of Pancreatic Exocrine Damage Induced by Excess Dietary Zinc in the Chick, *J. Nutr.* 120 (1990) 389–397. <https://doi.org/10.1093/JN/120.4.389>.
  - [6] W. Maret, H.H. Sandstead, Zinc requirements and the risks and benefits of zinc supplementation, *J. Trace Elem. Med. Biol.* 20 (2006) 3–18. <https://doi.org/10.1016/J.JTEMB.2006.01.006>.
  - [7] European Food Safety Authority (EFSA), Scientific Opinion on the potential reduction of the currently authorised maximum zinc content in complete feed, *EFSA J.* 12 (2014) 3668. <https://doi.org/10.2903/j.efsa.2014.3668>.
  - [8] General Administration of Quality Supervision Inspection and Quarantine of the People's Republic of China-AQSIQ, Limited contents of zinc in feeds, GB 26419., 2010.
  - [9] S.C. Monteiro, S. Loft, A.B.A. Boxall, Pre-assessment of environmental impact of zinc and copper used in animal nutrition, *EFSA Support. Publ.* 7 (2010) 74E. <https://doi.org/10.2903/SP.EFSA.2010.EN-74>.
  - [10] G.W. Evans, P.E. Johnson, J.G. Brushmiller, R.W. Ames, Detection of Labile Zinc-Binding Ligands in Biological Fluids by Modified Gel Filtration Chromatography, *Anal. Chem.* 51 (1979) 839–843. <https://doi.org/10.1021/AC50043A016>.
  - [11] P. Carol, S. Sreejith, A. Ajayaghosh, Ratiometric and near-infrared molecular probes for the detection and imaging of zinc ions, *Chem. - An Asian J.* 2 (2007) 338–348. <https://doi.org/10.1002/ASIA.200600370>.
  - [12] P. Jiang, Z. Guo, Fluorescent detection of zinc in biological systems: Recent development on the design of chemosensors and biosensors, *Coord. Chem. Rev.* 248 (2004) 205–229. <https://doi.org/10.1016/J.CCT.2003.10.013>.
  - [13] M. Hanif, M. Rafiq, M. Mustaqeem, M.A. Shaheen, K.F.I. Qadri, I. Qadri, M. Saleem, Intracellular and Extracellular Zinc Detection by Organic Fluorescent Receptor, *Curr. Org. Chem.* 23 (2019) 2664–2678. <https://doi.org/10.2174/1385272823666191029114111>.
  - [14] Z. Wang, X. Wang, Q. Wang, X. Xiong, H. Luo, K. Huang, Recent developments in chemical vapor generation atomic spectrometry for zinc detection, *Microchem. J.* 149 (2019) 104052. <https://doi.org/10.1016/J.MICROC.2019.104052>.
  - [15] M. Guembe-García, V. Santaolalla-García, N. Moradillo-Renuncio, S. Ibeas, J.A. Reglero, F.C. García, J. Pacheco, S. Casado, J.M. García, S. Vallejos, Monitoring of the evolution of human chronic wounds using a ninhydrin-based sensory polymer and a smartphone, *Sensors Actuators, B Chem.* 335 (2021) 129688. <https://doi.org/10.1016/j.snb.2021.129688>.
-

- [16] M. Guembe-García, S. Vallejos, I. Carreira-Barral, S. Ibeas, F.C. García, V. Santaolalla-García, N. Moradillo-Renuncio, J.M. García, Zn(II) detection in biological samples with a smart sensory polymer, *React. Funct. Polym.* 154 (2020) 104685. <https://doi.org/10.1016/j.reactfunctpolym.2020.104685>.
- [17] S. Vallejos, E. Hernando, M. Trigo, F.C. García, M. García-Valverde, D. Iturbe, M.J. Cabero, R. Quesada, J.M. García, Polymeric chemosensor for the detection and quantification of chloride in human sweat. Application to the diagnosis of cystic fibrosis, *J. Mater. Chem. B* 6 (2018) 3735–3741. <https://doi.org/10.1039/c8tb00682b>.
- [18] S. Vallejos, M. Guembe García, J.M. García Pérez, C. Represa Pérez, F.C. García García, Colorimetric Titration on the App Store, (2021). <https://apps.apple.com/es/app/colorimetric-titration/id1533793244> (accessed August 7, 2021).
- [19] S. Vallejos, M. Guembe García, J.M. García Pérez, C. Represa Pérez, F.C. García García, Application for smartphones “Colorimetric Titration”. Software registration BU-122-20 (00/2021/568), (2021). <https://play.google.com/store/apps/details?id=es.inforapps.chameleon&hl=ES> (accessed August 7, 2021).
- [20] M. Trigo-íñez, A. Mu, S. Ibeas, F. Serna, F.C. García, J.M. García, Sensors and Actuators B: Chemical Colorimetric detection and determination of Fe ( III ), Co ( II ), Cu ( II ) and Sn ( II ) in aqueous media by acrylic polymers with pendant terpyridine motifs, *Sensors Actuators B Chem.* 226 (2016) 118–126. <https://doi.org/10.1016/j.snb.2015.11.116>.
- [21] J. Wang, Y. Niu, C. Zhang, Y. Chen, A micro-plate colorimetric assay for rapid determination of trace zinc in animal feed, pet food and drinking water by ion masking and statistical partitioning correction, *Food Chem.* 245 (2018) 337–345. <https://doi.org/10.1016/J.FOODCHEM.2017.10.054>.
- [22] D.A. Armbruster, T. Pry, Limit of Blank, Limit of Detection and Limit of Quantitation, *Clin. Biochem. Rev.* 29 (2008) S49.
- [23] D.W. Tholen, K. Linnet, M. Kondratovich, D.A. Armbruster, P.E. Garrett, R.L. Jones, M.H. Kroll, R.M. Lequin, T.J. Pankratz, G.A. Scassellati, H. Schimmel, J. Tsai, Protocols for determination of limits of detection and limits of quantitation; approved guideline, The National Committee for Clinical Laboratory Standards, 2004.
- [24] K. Boonkitpatarakul, A. Smata, K. Kongnukool, S. Srisurichan, K. Chainok, M. Sukwattanasinitt, An 8-aminoquinoline derivative as a molecular platform for fluorescent sensors for Zn(II) and Cd(II) ions, *J. Lumin.* 198 (2018) 59–67. <https://doi.org/10.1016/j.jlumin.2018.01.048>.
- [25] E. Panel, F. Chain, Scientific Opinion on the risks to animal and public health and the environment related to the presence of nickel in feed 1,

- EFSA J. 13 (2015) 4074. <https://doi.org/10.2903/j.efsa.2015.4074>.
- [26] M. Davies, R. Alborough, L. Jones, C. Davis, C. Williams, D.S. Gardner, Mineral analysis of complete dog and cat foods in the UK and compliance with European guidelines, Sci. Rep. 7 (2017) 17107. <https://doi.org/10.1038/s41598-017-17159-7>.
- [27] E.A.D.N. Fernandes, C. Elias, M.A. Bacchi, P. Bode, C. Elias, P. Bode, Trace element measurement for assessment of dog food safety, Environ. Sci. Pollut. Res. 25 (2018) 2045–2050. <https://doi.org/10.1007/s11356-017-8541-4>.
- [28] K. Kazimierska, W. Biel, R. Witkowicz, Mineral Composition of Cereal and Cereal-Free Dry Dog Foods versus Nutritional Guidelines, Molecules. 25 (2020) 5173. <https://doi.org/10.3390/molecules25215173>.
- [29] S. Sgorlon, M. Sandri, B. Stefanon, D. Licastro, Elemental composition in commercial dry extruded and moist canned dog foods, Anim. Feed Sci. Technol. 287 (2022) 115287. <https://doi.org/10.1016/j.anifeedsci.2022.115287>.
- [30] P. Arrowsmith, Laser Ablation of Solids for Elemental Analysis by Inductively Coupled Plasma Mass Spectrometry, Anal. Chem. 59 (1987) 1437–1444.
- [31] D.J. Lyons, K.P. Spann, R.L. Roofayel, Determination of total calcium, zinc, manganese, iron, magnesium and phosphorus in animal feeds and plant material using inductively coupled plasma emission spectrometry, Analyst. 110 (1985) 955–957. <https://doi.org/10.1039/AN9851000955>.
- [32] G.C. Brandao, R.M. de Jesus, E.G.P. da Silva, S.L.C. Ferreira, Use of slurry sampling for the direct determination of zinc in yogurt by high resolution-continuum source flame atomic absorption spectrometry, Talanta. 81 (2010) 1357–1359. <https://doi.org/10.1016/j.talanta.2010.02.033>.
- [33] M.A.D. Saleh, R. De Cássio Ferreira Neves, F.A. Silva, P.M. De Moraes, V.R. Loureiro, P. Dos Santos Roldan, P. De Magalhães Padilha, GFAAS determination of zinc in fish feed and feces using slurry sampling, Food Anal. Methods. 2 (2009) 162–168. <https://doi.org/10.1007/s12161-008-9053-0>.
- [34] A. Afkhami, T. Madrakian, M. Abbasi-Tarighat, Simultaneous determination of calcium, magnesium and zinc in different foodstuffs and pharmaceutical samples with continuous wavelet transforms, Food Chem. 109 (2008) 660–669. <https://doi.org/10.1016/j.foodchem.2007.12.078>.
- [35] R.C. Martins, A.M. Pereira, E. Matos, L. Barreiros, A.J.M. Fonseca, A.R.J. Cabrita, M.A. Segundo, Miniaturized Fluorimetric Method for Quantification of Zinc in Dry Dog Food, J. Anal. Methods Chem. 2020 (2020) 0–5. <https://doi.org/10.1155/2020/8821809>.

- [36] R. Compañó, R. Ferrer, J. Guiteras, M.D. Prat, Flow Injection Method for the Fluorimetric Determination of Zn with 8-(Benzenesulphonamido) Quinoline, *Mikrochim. Acta.* 124 (1996) 73–79. <https://doi.org/10.1007/bf01244959>.
- [37] M. Kamacı, İ. Kaya, The Novel Poly(azomethine-urethane): Synthesis, Morphological Properties and Application as a Fluorescent Probe for Detection of Zn<sup>2+</sup> Ions, *J. Inorg. Organomet. Polym. Mater.* 25 (2015) 1250–1259. <https://doi.org/10.1007/S10904-015-0234-1/FIGURES/10>.



# CONCLUSIONES Y PERSPECTIVAS

Durante la realización de esta tesis doctoral se ha demostrado la gran versatilidad que presentan los polímeros inteligentes. En este sentido, como conclusión general, el trabajo realizado ha permitido una mayor comprensión del comportamiento de los polímeros sensores, así como su diseño y obtención, además de cómo se pueden maximizar sus propiedades más relevantes según, la aplicación específica para la que se desarrolla el material.

Por otra parte, las conclusiones específicas son:

- Se ha desarrollado una metodología para el desarrollo de biosensores que pueden aplicarse en saliva u otros fluidos corporales para la detección de infecciones de virus o bacterias. Además, concretamente, se ha demostrado el funcionamiento de esta metodología a través del diseño, síntesis y caracterización de un recubrimiento polimérico con la capacidad de detectar de manera visual la infección causada en muestras de saliva del SARS-CoV-2.
- Se ha demostrado la posibilidad de utilizar recubrimientos poliméricos colorimétricos para el desarrollo de nuevas metodologías contra las falsificaciones y seguridad documental. Esta tecnología permite garantizar la autenticidad de documentos, etiquetas y productos de manera sencilla y económica utilizando únicamente una disolución reveladora y un teléfono móvil.
- Se ha desarrollado un polímero sensor de cobre que permite la detección y cuantificación de este elemento en muestras complejas como el vino y/o mosto sin la necesidad de equipamiento específico, ni personal cualificado.

- De manera análoga, se ha desarrollado un polímero sensor para la determinación del catión zinc (II) que permite su análisis en muestras de pienso animal de forma sencilla, rápida y económica.

Las conclusiones obtenidas en esta tesis doctoral abren un amplio abanico de posibilidades para los polímeros sensores. Su versatilidad ha quedado demostrada, lo que implica su posible aplicación en diversos campos. En particular, se destaca el desarrollo de biosensores poliméricos para la detección de distintas especies diana que provoquen una mejora en el diagnóstico de enfermedades. En resumen, los polímeros sensores representan una tecnología prometedora con un potencial significativo en distintos campos de relevancia, lo que justifica su investigación y estudio en el futuro próximo.

## CONCLUSIONS AND PERSPECTIVES

As a general conclusion, this research has enhanced understanding of the behaviour, design, and synthesis of sensory polymers, and how their key properties can be optimized according to their specific application.

Moreover, the specific conclusions can be summarized as follows:

- A methodology has been developed for the preparation of biosensors that can be applied in saliva or other bodily fluids for the detection of virus or bacteria infections. Specifically, the functioning of this methodology has been demonstrated through the design, synthesis, and characterization of a polymeric coating with the ability to visually detect the infection caused by the SARS-CoV-2 virus in saliva samples.
- The possibility of using colorimetric polymeric coatings for the development of new methodologies against counterfeiting and document security has been demonstrated. This technology allows for the simple

and cost-effective authentication of documents, labels, and products using only a revealing solution and a mobile phone.

- A copper sensory polymer has been developed that enables the detection and quantification of this element in complex samples such as wine and/or must, without the need for specific equipment or qualified personnel.
- Similarly, a sensory polymer for the determination of zinc (II) cation has been developed, allowing for its analysis in animal feed samples in a simple, fast, and economical manner.

The conclusions drawn in this doctoral thesis open up a wide range of possibilities for sensory polymers. Their versatility has been demonstrated, which implies their potential application in various fields. Particularly noteworthy is the development of polymeric biosensors for the detection of different target species, leading to an improvement in disease diagnosis. In summary, sensory polymers represent a promising technology with significant potential in various relevant fields, justifying further research and study in the near future.